

Institute for Laboratory Animal Pathology  
University of Veterinary Medicine Vienna  
(Head: Univ.-Prof. Dr. Lukas Kenner)

The Role of AP-1 Transcription Factor c-JUN in Prostate Cancer

Master thesis

University of Veterinary Medicine Vienna

submitted by  
Roman Ziegler

Vienna, June 2020

## **Acknowledgements**

I want to thank Lukas Kenner for giving me the opportunity to work on the c-JUN project and for allowing me to participate in his skilled research group. I want to thank my direct supervisor Christina Sternberg for her dedication in guiding me through this master's project and for all the time she spent in helping me to acquire the required skill set. For helping me to establish a c-JUN knockout cell line and for all her continued support throughout my master project, I want to thank Sabine Lagger.

I want to thank Michaela Schlederer for performing mouse genotyping and immunohistochemistry. I want to thank the VetMed Pathology Histology Team for processing formalin fixed samples to FFPE samples and Petra Kodajova for sectioning FFPE samples. I want to thank Sandra Högl for sharing her pathological experience when evaluating histological results. I want to thank Ursula Reichart for providing support in the quantification of immunohistochemistry.

I want to thank Tanja Limberger and Sabine Lagger for providing RNA sequencing data and Jan Oppelt for his support in bioinformatical analyses. I want to thank Monika Oberhuber for her advice on statistical evaluation of data and bioinformatical analysis.

I want to thank Olaf Merkel and Astrid Aufinger for providing me with TMA data from human patients.

Furthermore, I want to thank all my colleagues at the University of Veterinary Medicine Vienna and the Medical University of Vienna for helping me in various instances and for providing me with a friendly work environment. I want to thank the animal care taker team from the Center for Biomedical Research at the Medical University of Vienna for ensuring the health of our research animals.

Finally, I want to thank my family for giving me essential financial and emotional support from the very beginning of my education.

## Table of contents

Acknowledgements .....	2
Table of contents .....	3
Abstract .....	7
Zusammenfassung .....	8
List of Abbreviations .....	9
1 Introduction .....	12
1.1 Prostate Cancer .....	12
1.1.1 Prostate cancer development .....	12
1.1.2 Prostate cancer diagnostic tools .....	14
1.1.3 Hereditary risk factors and frequently mutated genes .....	14
1.1.4 Models in prostate cancer research .....	16
1.2 AP-1 transcription factors .....	17
1.3 AP-1 transcription factor c-JUN .....	17
1.3.1 c-JUN in cancer .....	19
1.4 Hallmarks of cancer .....	20
1.5 Aim of the thesis .....	23
2 Material and Methods .....	23
2.1 Ethics statement .....	23
2.2 Work with animals .....	23
2.2.1 Prostate cancer mouse model .....	23
2.2.2 Sacrificing animals and processing mouse tissue .....	25
2.3 Work with human cell lines .....	26
2.3.1 Cell line maintenance .....	26
2.3.2 Transfection of HEK239 FT cells .....	27
2.3.2.1 Transfection for lentivirus production .....	27

2.3.3 Transduction of PCa cell lines .....	28
2.3.4 Picking single clones .....	29
2.3.5 Proliferation experiments .....	29
2.3.5.1 Cell count-based proliferation analysis .....	29
2.3.5.2 Resazurin assay .....	29
2.4 Work with bacteria .....	30
2.4.1 Chemical transformation of competent Stbl3 .....	30
2.4.1.1 Mini Prep of transformed bacteria .....	31
2.4.1.2 Midi Prep of transformed bacteria .....	31
2.5 Work with DNA .....	32
2.5.1 Gel electrophoresis of DNA .....	32
2.5.2 Genotyping of mice .....	32
2.5.3 Genomic DNA extraction from cell pellets .....	34
2.5.4 Design of guide RNA for CRISPR KO of c-JUN .....	34
2.5.5 Cloning of c-JUN sgRNA into the lentiCRISPR v2 vector .....	36
2.5.6 T7 Endonuclease I Assay .....	36
2.5.7 Sequence validation by TIDE Assay .....	38
2.6 Work with RNA .....	39
2.6.1 Total RNA Isolation from prostate samples .....	39
2.6.2 RNA quality testing and cDNA synthesis .....	40
2.6.3 RT-qPCR .....	40
2.6.4 RNA sequencing .....	41
2.7 Immunochemistry and histological methods .....	43
2.7.1 Protein lysates from prostate tissue .....	43
2.7.2 Protein lysates from cell pellets by a freeze and thaw method .....	43
2.7.3 Bradford assay and dilution of protein lysates .....	44

2.7.4 SDS page and WB.....	44
2.7.4.1 Casting SDS page gels .....	44
2.7.4.2 Denaturation of lysates.....	45
2.7.4.3 SDS page and WB on conventional gels.....	45
2.7.4.4 SDS page and WB on TGX gels .....	47
2.6.4.5 List of WB antibodies .....	47
2.7.5 Immunohistochemistry.....	48
2.7.5.1 List of IHC antibodies.....	48
2.7.6 H&E staining.....	49
2.7.7 C <sub>12</sub> FDG staining based senescence FACS .....	49
2.8 Bioinformatics and statistical testing .....	51
2.8.1 Proliferation experiments on transduced human cell lines.....	51
2.8.2 RNA methods.....	51
2.8.2.1 RT-qPCR quantification.....	51
2.8.2.2 RNA-seq bioinformatics and software .....	52
2.8.3 Immunochemistry.....	52
2.8.3.1 WB quantification .....	52
2.8.3.2 Immunohistochemistry quantification.....	53
2.8.3.3 C <sub>12</sub> FDG FACS Gating strategy and calculation.....	54
2.8.5 Other software .....	57
3 Results .....	58
3.1 Low c-JUN expression correlates with bad prognosis in human PCa .....	58
3.2 Loss of c-Jun in a PCa <i>in-vivo</i> mouse model .....	60
3.3 Mouse model confirmation at the protein level .....	61
3.4 c-Jun deficient PCa mice develop aggressive tumors .....	64
3.5 c-Jun deficiency does not affect proliferation in a murine PCa model .....	66

3.6 c-Jun deficiency does not affect proliferation in a PCa *in-vitro* model..... 67

3.7 c-Jun deficiency does not affect CC3 mediated apoptosis in murine PCa model..... 74

3.8 Trend of increased senescence in response to c-Jun deficiency in the murine PCa model175

3.9 RNA-seq suggests an influence of c-Jun on PCa immunology and inflammation ..... 78

3.10 c-Jun regulates mRNA expression and activity of other transcription factors..... 80

3.11 Trend of deregulation of selected senescence related genes in response to c-Jun deficiency  
..... 82

4 Discussion ..... 83

4.1 c-JUN and its role in cancer ..... 83

4.2 Low c-JUN levels correlate with reduced progression free survival in human PCa patients  
..... 84

4.3 c-Jun deficiency leads to increased PCa aggressiveness in mice..... 85

4.4 c-JUN is not required for sustained proliferation of transformed prostate cells ..... 86

4.5 c-Jun does not regulate caspase 3 mediated apoptosis in murine prostate tumorigenesis87

4.6 c-Jun may be a weak regulator of senescence in murine prostate tumorigenesis ..... 89

4.7 c-Jun regulates immune response and inflammation ..... 90

4.8 c-JUN is a putative PCa biomarker with many faces..... 92

5 References ..... 93

## Abstract

Prostate cancer (PCa) is the second most common diagnosed cancer and the fifth leading cause of cancer related deaths in men. Therefore, PCa represents a significant public health issue. A common practice for early detection of PCa is the screening for prostate specific antigen (PSA) in healthy men. However, increased PSA levels are not specific to PCa and also result from benign tumors or inflammation. This frequently leads to overdiagnosis and overtreatment. As a consequence, more reliable biomarkers are required for improved diagnosis and treatment of PCa patients.

AP-1 transcription factors are upregulated in a variety of cancers and are historically considered as tumor-promoters. However, more recent studies showed that AP-1 transcription factors also act in a tumor-suppressive manner. For example, the JUN family member JUNB has been described as a tumor-suppressor in human PCa. We similarly found a correlation between low *c-JUN* mRNA levels and bad prognosis in publicly available RNA-seq datasets from human PCa patients. Such a potential tumor-suppressive function defies the stigma of c-JUN being a proto-oncogene. In this work, we address the question how c-JUN might suppress prostate tumorigenesis.

To investigate the molecular functions of c-Jun in PCa, we utilized an established *Pten* deficient PCa mouse model. By breeding floxed *c-Jun* alleles into this tumor model, we generated *Pten/c-Jun* double knockout (KO) mice. We detected increased tumor size and decreased overall survival in *Pten/c-Jun* KO compared to regular *Pten* KO mice supporting our hypothesis of c-Jun suppressing prostate tumorigenesis. Interestingly, in *Pten* KO mice c-Jun expression was upregulated compared to wild type mice pointing toward an important regulative role of c-Jun in *Pten*-loss mediated PCa. Our further research suggested that loss of c-JUN has no direct effect on classical cleaved-caspase 3 mediated apoptosis or proliferation. However, we detected a mild deregulation of cellular senescence which needs to be explored further beyond the scope of this thesis. Furthermore, our findings suggest that c-JUN regulates the immune response during prostate tumorigenesis. In summary, we propose that c-JUN is a tumor-suppressor of PCa and fulfills this role by regulation of multiple tumorigenesis related pathways.

## Zusammenfassung

Das Prostatakarzinom (PCa) ist die zweithäufigste Krebsart bei Männern und die fünft-häufigste krebsbedingte Todesart. Früherkennungstests sollten diesem Problem der öffentlichen Gesundheit entgegenwirken. Der Bluttest für das prostata-spezifische Antigen (PSA) wird routinemäßig bei Vorsorgeuntersuchungen von gesunden Männern eingesetzt. Da aber erhöhte PSA Werte auch bei Infekten und benignen Tumoren gemessen werden können, führt der PSA Test in vielen Fällen zu einer falsch positiven Diagnose und darauffolgend zu unnötigen Behandlungen. Dieses Problem verdeutlicht, dass die Erforschung neuer PCa Biomarker nötig ist, um PCa Diagnosis zu verbessern.

Obwohl die Familie der AP-1 Transkriptionsfaktoren durch ihre Hochregulierung in unterschiedlichen Krebserkrankungen häufig als Onkogene bezeichnet wurden, haben in vergangenen Jahren Studien zunehmend AP-1 Transkriptionsfaktoren auch mit tumorsuppressiven Eigenschaften in Verbindung gebracht. Zum Beispiel wurde JUNB als Tumorsuppressor in Prostatakrebs identifiziert. Durch Auswertung von öffentlich-zugänglichen RNA-seq Datensätzen konnten wir ebenfalls für c-JUN eine Korrelation zwischen niedriger mRNA Expression und verschlechterter Prognose von humanen Patienten feststellen. Historisch wurde c-JUN primär als Proto-Onkogen klassifiziert und derartige Regulative Eigenschaften auf Prostatakrebsentwicklung wurden bisher noch nicht beschrieben. In dieser Arbeit möchten wir die Mechanismen behandeln durch die c-JUN diese Regulation bewirkt.

Um den Einfluss von c-Jun auf Prostatakrebsentwicklung zu testen, kreuzten wir einen Mausstamm mit gefloxtem c-Jun Allel mit einem *Pten* defizienten (KO) Prostatakrebsmausmodell. *Pten/c-Jun* KO-Mäuse zeigten verglichen mit regulären *Pten* KO-Mäusen signifikant vergrößerte Prostatatumore und eine signifikant verkürzte durchschnittliche Lebensspanne. Diese Ergebnisse lassen drauf schließen, dass c-Jun sich in murinem PCa als Tumorsuppressor verhält. Außerdem deutet erhöhte c-Jun Expression in *Pten* KO-Mäusen verglichen mit Wildtypmäusen auf eine erhöhte Aktivierung von c-Jun in Prostatatumoren hin. Unsere Experimente konnten eine Regulation von traditioneller Caspase 3 vermittelter Apoptose durch c-JUN ausschließen. Wir beobachteten eine milde Deregulation von Seneszenz in *Pten/c-Jun* KO-Mäusen, dieser regulative Effekt muss aber noch weiter untersucht werden. Zusätzlich konnten wir einen regulativen Effekt von c-JUN auf die Krebs-Immunantwort feststellen. Wir möchten hiermit c-JUN als Prostatakrebs Tumorsuppressor vorstellen, der fähig ist eine Vielzahl von Krebs-signalwegen zu regulieren.

## List of Abbreviations

AKT	protein kinase B
APS	ammonium persulfate
AR	androgen receptor
BCP	1-bromo-3-chloropropane
BrdU	bromodeoxyuridine
BSA	bovine serum albumin
C <sub>12</sub> FDG	5-dodecanoylamino fluorescein di-β-D-galactopyranoside
CAM	cell adhesion molecule
CC3	cleaved-caspase 3
CC7	cleaved-caspase 7
CDK	cyclin depended kinases
CKI	cyclin depended kinase inhibitors
CMV	cytomegalovirus
cPPT	central polypurine tract
CRPC	castration resistant prostate cancer
CTL	cytotoxic t lymphocytes
CTS	circulating tumor cells
DDR	DNA damage repair
DE	differentially expressed
DHT	5α-dihydrotestosterone
DMEM	Dulbecco's Modified Eagle Medium
DMSO	dimethyl sulfoxide
DPBS	Dulbecco's phosphate-buffered saline
DRE	digital rectal examination
EFS	elongation factor 1α short promoter
EMT	epithelial to mesenchymal transition
EtOH	ethanol
eV	empty vector
FACS	fluorescence-activated cell sorting
FBS	fetal bovine serum
FIU	fluorescence intensity units
FSC-A	forward scatter area
FSC-H	forward scatter height

Fw	forward
GFP	fluorescence protein
GGG	five-tier Gleason group grading
GM-CSF	granulocyte and monocyte colony stimulating factor
GPCR	G-protein-coupled receptors
GSEA	gene set enrichment analysis
H&E	hematoxylin and eosin
HPN	housekeeping protein normalization
IFN $\alpha$	Interferon alpha
IGF-1	insulin-like growth factor-1
IHC	immunohistochemistry
IL-6	interleukin 6
InDel	insertion-deletion
JNK	c-JUN N-terminal kinase
KGF	keratinocyte growth factor
KO	knockout
LB	lysogeny broth
LTR	long terminal repeats
MSigDB	molecular signature database
NES	normalized enrichment score
NGS	next-generation sequencing
NK-cell	natural killer cell
P2A	2A self-cleaving peptide
p-Akt	phospho-Akt
PAM	Protospacer Adjacent Motif
PB	probasin
PBS	Phosphate-Buffered Saline
PCA	principal component analysis
PCa	prostate cancer
p-c-Jun	phospho-c-Jun
p-c-JUN	phospho-c-JUN
PI3K	phosphoinositide-3-kinase
PIN	prostatic intraepithelial neoplasia
PIP3	phosphatidylinositol-3,4,5-triphosphatase
PSA	prostate specific antigen

psi+	packaging signal
PTEN	phosphatase and tensin homolog
RB	retinoblastoma
RNA-seq	RNA sequencing
RPMI	Roswell Park Memorial Institute
RRE	HIV-1 Rev response element
RT	room temperature
RTK	receptor tyrosine kinase
RT-qPCR	quantitative real-time PCR
Rv	reverse
SAPK	stress-activated protein kinase
SASP	senescence-associated secretory phenotype
SCPC	small-cell prostate carcinoma
SDS	sodium dodecyl sulfate
sgRNA	single guide RNA
siRNA	short interference RNA
TGF- $\beta$	transforming growth factor $\beta$
TIDE	Tracking of Indels by Decomposition
TMA	tissue microarray
TNF- $\alpha$	tumor necrosis factor- $\alpha$
TPBS	Tween PBS solution
TPN	total protein normalization
WB	western blot
WPRE	posttranscriptional regulatory element
X-gal	5-bromo-4-chloro-3-indolyl $\beta$ -D-galactoside
$\beta$ -Act	$\beta$ -Actin
$\beta$ -Tub	$\beta$ -Tubulin

# 1 Introduction

## 1.1 Prostate Cancer

Prostate cancer (PCa) is the second most common cancer and fifth leading cause of cancer related deaths in men (Ferlay et al. 2015). PCa incidence rates have gradually increased over the past decades (Rawla 2019). This incidence rate increase is partially explained by an increase in population age and environmental factors such as diet and UV radiation (Wong et al. 2016). PCa risk starts to rise drastically in the mid-fifties and peaks between 70 and 74 years of age (Ferrís-I-Tortajada et al. 2011). Further environmental factors which have been linked to PCa development include smoking, infectious diseases and exposure to herbicides or pesticides. Due to modern screening methods, more PCa cases are detected raising the incidence rate especially in Western countries (Ferlay et al. 2015). These methods include screening for prostate specific antigen (PSA) in healthy men which is common practice for early detection of PCa (Ilic et al. 2013; Gann 2002). However, elevated blood PSA levels can also be induced by urogenital infections and benign tumors. This includes indolent PCa which is characterized by slow tumor growth and results in a lifelong asymptomatic disease (Esserman et al. 2014). Indolent PCa has been observed in 50 % of elderly men. This oversensitivity of PSA often leads to overdiagnosis and unnecessary cancer treatment in patients who would never develop symptomatic disease. Previously used diagnostic tools such as PSA screening are nowadays gradually supplemented with modern imaging techniques and testing of newly discovered molecular biomarkers (Litwin and Tan 2017).

### 1.1.1 Prostate cancer development

Most PCa initiate with the histological phenotype prostatic intraepithelial neoplasia (PIN) (Figure I1) (Shen and Abate-Shen 2010). This phenotype is characterized by intraluminal hyperplasia of epithelial cells, nuclear enlargement, nuclear atypia and reduction of basal cells. Progression to PCa is associated with the absence of basal cells. The most common type of PCa with over 95 % of cases being reported is adenocarcinoma. With a prevalence of 0.5 % to 2 % of cases, the neuroendocrine small-cell prostate carcinoma (SCPC) is the second most common type of PCa (Hoof et al. 2016). SCPC is a rare but clinically aggressive form of PCa with ~75 % of diagnosed patients suffering from advanced stages of the disease. Prostate adenocarcinoma is generally multifocal which means that multiple independent transformation events happen and lead to genetically different foci throughout the prostate (Shen and Abate-Shen 2010).

In many cases, these foci only lead to latent asymptomatic adenocarcinoma (Jahn, Giovannucci, and Stampfer 2015; Yatani et al. 1989). Latent adenocarcinoma which never develops into symptomatic disease is called indolent PCa (Shen and Abate-Shen 2010). However, both latent and clinical adenocarcinoma are characterized by disruption of the basal lamina and distinguishing latent disease from early stage clinical PCa is difficult on a histological basis (Figure I1) (Hegarty and Hegarty 2013; Shen and Abate-Shen 2010). Cribriform (sieve-like) glands are characteristic for adenocarcinoma and late stage prostate cancer is often accompanied by a cribriform pattern which resembles renal glomeruli (Figure I2) (Kryvenko and Epstein 2016; Epstein 2018; Parker et al. 2015). Furthermore, clinical adenocarcinoma can be accompanied by an intraluminal necrosis called comedonecrosis (Madan et al. 2019). Adenocarcinoma progresses into metastatic prostate cancer after dissemination of cancer cells into distant organs (Figure I1) (Gandaglia et al. 2014; Shen and Abate-Shen 2010). In metastatic prostate cancer cribriform glands are increasingly replaced by undefinable tissue sheets, single cells or cell cords (Figure I2) (Kryvenko and Epstein 2016; Epstein 2018; Gandaglia et al. 2014). The most common site for metastasis is bone marrow, found in over 80 % metastatic PCa patients. Around 20 % of PCa patients who undergo clinical treatment will develop a more aggressive PCa subtype called castration-resistant prostate cancer (CRPC) within 5 years and over 80 % of these patients will progress to metastatic CRPC (mCRPC) (Crawford, Petrylak, and Sartor 2017; Albala 2017).

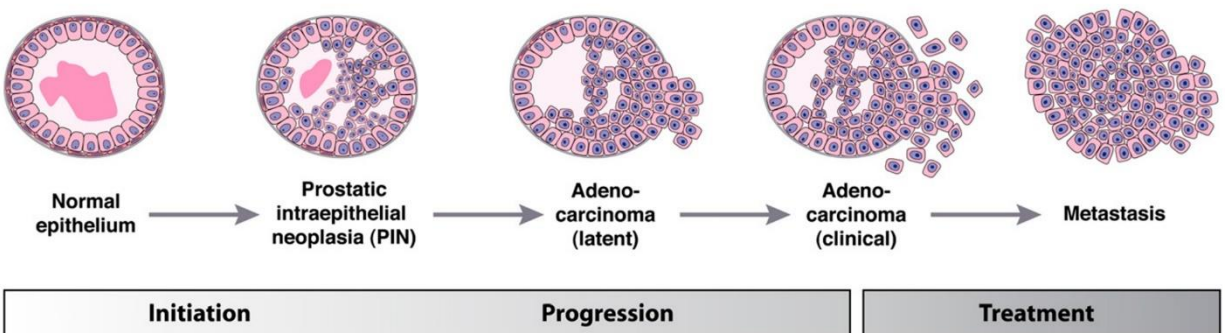


**Figure I1. Overview on histological prostate cancer progression.** Histological progression of normal prostate epithelium into invasive prostate cancer. Normal epithelium progresses to prostatic intraepithelial neoplasia (PIN) which is histologically indistinguishable from adenoma. A progressive loss of basal cells leads to invasive adenocarcinoma. Clinical adenocarcinoma is characterized by aggressive growth but early clinical stages are difficult to distinguish from latent disease. Prostate cancer cells disseminate into bone marrow, distant lymph nodes, liver or thorax and form metastasis. Image adapted from (Shen and Abate-Shen 2010).

### 1.1.2 Prostate cancer diagnostic tools

For early detection of PCa, the most frequently used methods are PSA screening, digital rectal examination (DRE) and prostate biopsy (Philip et al. 2005; George 2010). Mandatory for comprehensive diagnosis and risk assessment is the classification of PCa by histological analysis of tumor biopsies and prostatectomy (Kryvenko and Epstein 2016). In 1966 Donald Gleason described a scoring system allowing for comprehensive histological assessment of prostate sections (Gleason 1966). This Gleason score system was gradually improved over time and is still used for prostate diagnostics nowadays (Epstein 2018). A certain Gleason score is calculated by assessing two histological patterns within a prostate section and combining the values of the patterns (Figure 12) (Kryvenko and Epstein 2016; Epstein 2018).

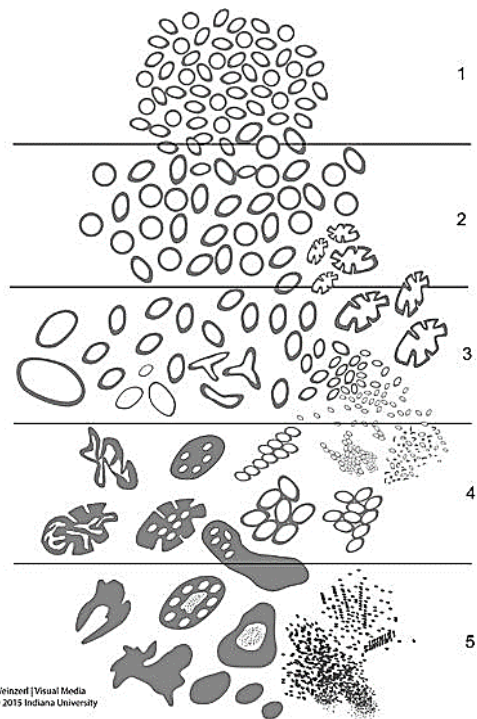


**Figure 12. Classification of histological architecture into five Gleason patterns.** WHO revised guidance diagram for Gleason scoring as of 2016 adapted from (Epstein 2018). Gleason patterns 1 and 2 are characterized by various shaped hyperplastic glands which are indistinguishable from benign adenoma. Gleason pattern 3 features large often misshaped glands with hyperplastic cells and well-circumscribed cribriform glands. Gleason pattern 4 is defined by cribriform glands which often resemble renal glomeruli. Gleason pattern 5 features large masses of cribriform glands, undefinable tissue sheets, single cells or cords of cells and is often accompanied with intraluminal comedonecrosis.

### 1.1.3 Hereditary risk factors and frequently mutated genes

Hereditary factors play an important role in prostate cancer risk (Bratt et al. 2016). The relative risk is increased by two- to five-fold when close relatives are diagnosed with PCa. Germline mutations in DNA damage repair (DDR) genes such as *BRCA2* were identified previously as hereditary risk factors for PCa, which also links increased hereditary PCa risk to hereditary breast and ovarian cancer (Pilié et al. 2017). However, *BRCA2* mutations only explain less than 10 % of hereditary PCa cases and the full extent of PCa inheritance has yet to be explored (Guy et al. 2009).

The most frequent somatic mutations found in prostate adenocarcinoma include *TP53*, *FOXA1*, *SPOP*, *PTEN* and *KMT2C* (Figure I3) (Abida et al. 2019; Nguyen et al. 2020). The phosphatase and tensin homolog (PTEN) has been describes as an important suppressor of prostate tumorigenesis (S. Wang et al. 2003). PTEN is directly counteracting the signaling pathway of phosphoinositide-3-kinase (PI3K) and protein kinase B (AKT) (Carnero and Paramio 2014; Switlyk et al. 2019). The PI3K-AKT pathway promotes proliferation and survival of cells and acts downstream of receptor tyrosine kinases (RTK) which are activated by growth factors. PTEN is a phosphatase which dephosphorylates phosphatidylinositol-3,4,5-triphosphate (PIP3) activated by PI3K. Inhibition of PTEN leads to constitutively activated PI3K-AKT signaling which increases proliferation and thus favors tumorigenesis.

The most frequent somatic mutations found mCRPC include *TP53*, *TTN*, *MUC16*, *AR* and *SYNE1* (Figure I3) (Abida et al. 2019; Nguyen et al. 2020). Enabling mutations in the androgen receptor (AR) are observed more frequently in mCRPC than in prostate adenocarcinoma (Gaddipati et al. 1994). Androgen receptor (AR) signaling takes up a key role in prostate cell growth and differentiation by enabling cellular response to steroid hormones such as testosterone (Tan et al. 2015). AR is an

### Frequently mutated genes in Prostate Cancer

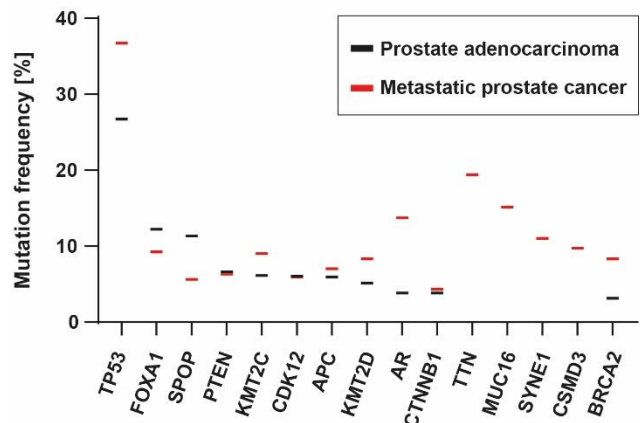


**Figure I3. Frequently mutated genes in prostate cancer.** Analysis on publicly available RNA-seq data of top 10 frequently mutated genes in prostate adenocarcinoma (Nguyen et al. 2020) and metastatic castration-resistant prostate cancer (Abida et al. 2019). Data was acquired from cBioPortal at “www.cbioportal.org”.

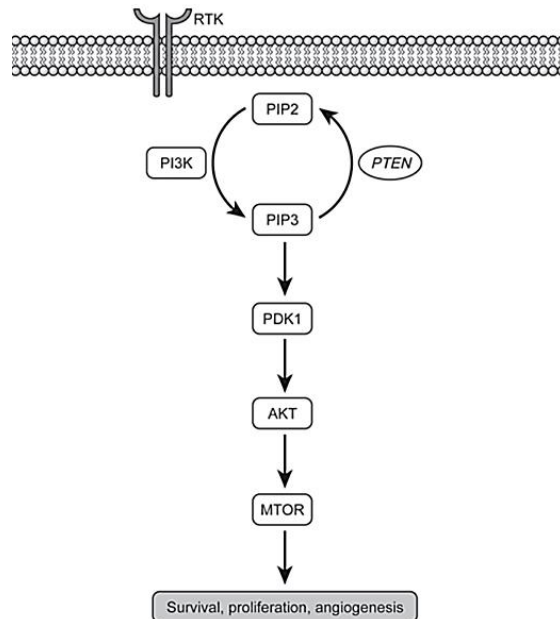


**Figure I4. PI3K-AKT signaling pathway.** Simplified scheme of the PI3K-AKT signaling pathway. Adapted from (Switlyk et al. 2019). Phosphoinositide-3-kinase (PI3K) is activated through receptor tyrosine kinases which are activated by their ligand growth factors. PI3K phosphorylates phosphatidylinositol-4,5-bisphosphate (PIP2) to phosphatidylinositol-3,4,5-triphosphate (PIP3) which then activates kinase B (AKT). AKT then activates mTOR, a regulator for proliferation, survival and angiogenesis.

intracellular androgen receptor and ligand binding results in translocation to the nucleus where it forms a transcription factor complex. This complex then activates target genes of androgen signaling such as *PSA*, *TMPRSS2* and other genes stimulating growth and survival. AR signaling is not only essential for growth and survival of homeostatic prostate cells but also for PCa cells (Fujita and Nonomura 2019). Anti-AR drugs utilize this dependence by targeting the receptor ligand binding domain of the AR and block interaction with testosterone. In 80 % of patients anti-AR drug treatment leads to a reduction of tumor burden but the majority of patients suffer from refraction when tumor cell growth becomes independent from androgen signaling (Gaddipati et al. 1994). Somatic mutations in the *AR* gene have been described to promote progression to CRPC by enabling androgen independent signaling of AR. Other frequently mutated genes in PCa include the tumor-suppressor *ERK* and the proto-oncogenes *MYC* and *RAS* (Dong 2006; Taylor et al. 2010).

#### **1.1.4 Models in prostate cancer research**

Human cell lines are the most frequently used *in-vitro* models for PCa research (Cunningham and You 2015). These cell lines are either derived from tumorigenic origin such as primary tumors and metastases or from non-tumorigenic prostate epithelial cells. DU145, PC-3 and LNCaP are commonly used cell lines derived from metastatic cancer tissue. PC-3 is derived from a bone metastasis (Kaighn et al. 1979), DU145 originates from a brain metastasis (Stone et al. 1978) and the LNCaP line from a metastasized lymph node (Horoszewicz et al. 1980). Xenografts of human cell lines in immunodeficient mice are a popular model used to study the tumorigenic potential of PCa cells in an *in-vivo* setting (Lange et al. 2012). This combination of *in-vitro* and *in-vivo* model is used to research metastatic properties of PCa cells. For studying PCa in an *in-vivo* setting, transgenic mouse models are frequently in use (Xinyu Wu et al. 2013). Tumor-suppressor gene KO mouse models for PCa research include *p53* (Vinall et al. 2012), Retinoblastoma (*Rb*) (Hill et al. 2005) and *Pten* (Di Cristofano et al. 1998; S. Wang et al. 2003) deficient mouse models. The probasin (PB) Cre-loxP system is commonly used to achieve a prostate cell specific knockout (KO) of these tumor-suppressor genes (Xiantuo Wu et al. 2001). In this system, expression of the Cre recombinase is under control of the PB promoter specifically expressed in prostate epithelial cells of sexually mature animals. The murine *Pten* KO model is commonly used in PCa research (S. Wang et al. 2003). This model has high translational value as *PTEN* is frequently mutated in human PCa patients and the mouse model mimics human disease progression.

## 1.2 AP-1 transcription factors

AP-1 are a family of dimeric transcription factor complexes formed by members of the subfamilies ATF, FOS, JUN and MAF (Eferl and Wagner 2003). Helical monomers of these families form homodimers or heterodimers resulting in an active transcription factor with leucine-zipper structure that directly bind DNA (Karin 1996). While ATF and JUN family members mainly form homodimers, FOS family members strictly form heterodimers (Kappelmann, Bosserhoff, and Kuphal 2014). AP-1 transcription factors show preferences in binding sites depending on the dimerization partners thereby allowing for a fine-tuning of transcriptional activity of AP-1 target genes (Van Dam and Castellazzi 2001). All of the AP-1 transcription factors share binding affinity for a common “AP-1 consensus sequence motif” (TGACTCA) (Ryseck and Bravo 2014). Another common binding motif is the CRE motif (TGACGTCA). The FOS family binds to a broad array of JUN family members and JUN-FOS heterodimers appear to have higher binding affinity than JUN homodimers. Functionally, AP-1 transcription factors are activators of gene expression and regulators of proliferation, apoptosis, differentiation and survival (Garces de Los Fayos Alonso et al. 2018).

## 1.3 AP-1 transcription factor c-JUN

c-JUN is a member of the JUN AP-1 family known for regulation of differentiation and cellular growth (Hess, Angel, and Schorpp-Kistner 2004). c-Jun is not required for *in-vitro* proliferation and differentiation in embryonic stem cells however, global loss of *c-Jun* is lethal during embryogenesis and appears to be essential for liver development (Hilberg et al. 1993). c-JUN fulfills a major role in proliferation of somatic hepatocytes through positive regulation of the cell cycle gene *CCND1* which encodes cyclin D1 (Behrens et al. 2002). This protein activates the cyclin dependent kinases (CDK) 4 and 6 which stimulate cell cycle progression. Furthermore, c-JUN has been described to promote transcription of keratinocyte growth factor (KGF) and granulocyte and monocyte colony stimulating factor (GM-CSF) (Szabowski et al. 2000). c-JUN mediated increased expression of KGF, GM-CSF and insulin-like growth factor-1 (IGF-1) in prostate stroma cells have been reported to promote proliferation of prostate epithelial cells through paracrine signaling (W. Li et al. 2007). This regulative property was suggested to enhance formation of benign hyperplasia. c-Jun was reported to suppress transcriptional activity of the tumor-suppressor p53 in mouse fibroblast (Schreiber et al. 1999). This regulation results in sustained proliferation and attenuated

apoptosis. Furthermore, c-Jun was observed to suppress apoptotic cell death through suppression of the Fas death receptor (Ivanov, Krasilnikov, and Ronai 2002).

The transcription factor function of c-JUN is regulated by the c-JUN N terminal kinase (JNK) which phosphorylates c-JUN at serine 63 and 73 (Shaullian 2010; L. Li, Feng, and Porter 2004). However, JNK has been reported to activate various other AP-1 transcription factors such as ATF-2 or JUNB and furthermore non-AP-1 nuclear substrates such as MYC or ELK1 (Bubici and Papa 2014; Zeke et al. 2016). There are three distinct JNKs including JNK1, 2 and 3. JNK3 is specifically expressed in brain, heart and testes while JNK1 and JNK2 are expressed in all tissues. JNK is a mitogen-activated protein kinase (MAPK) and participates in the MAPK signaling pathway (Figure I5) (H. F. Zhao, Wang, and To 2015). Receptors of the MAPK pathway include

G-protein-coupled receptors (GPCR), receptor tyrosine kinases and cytokine receptors. These receptors are activated through a vast array of extracellular signaling molecules including growth factors and cytokines (Karin 1996; H. F. Zhao, Wang, and To 2015). Active MAPK signaling controls cellular events such as inflammation, differentiation, proliferation and apoptosis. Furthermore, JNK has been reported as a signaling molecule in response to cellular stress and JNK is often referred to as stress-activated protein kinase (SAPK) (Mehan et al. 2011). The JNK stress response is activated through replicative or genotoxic stressors and facilitates tumor-

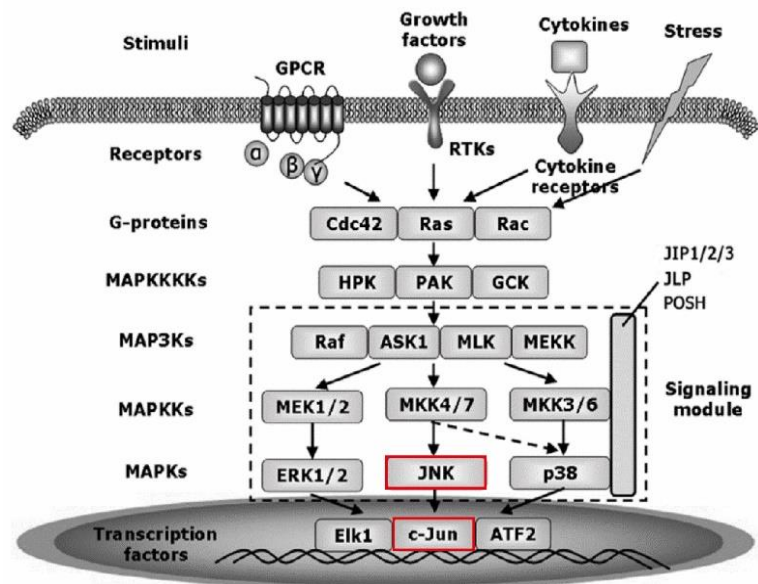


**Figure I5. MAPK pathway.** Simplified scheme of the MAPK pathway involved in the activation of c-JUN. Adapted from (H. F. Zhao, Wang, and To 2015). Mitogen activated protein kinase (MAPK) pathway stimuli are ligands of G-protein-coupled receptors (GPCR), RTKs or cytokine receptors but they can also be stressors which are detected by cell internal sensors. The signal is transduced from the activated receptors to the MAPK cascade through G-proteins. The MAPK signaling cascade consist of multiple levels of kinases and their activating paramount kinases. c-JUN N-terminal kinase (JNK) is the primary activating kinase of c-JUN and phosphorylates c-JUN at Ser-63 and Ser-73. Phosphorylation greatly enhances the transcription factor activity of c-JUN.

suppressive effects such as apoptosis (Potapova et al. 2000; H. F. Zhao, Wang, and To 2015). c-JUN has been reported to participate in regulating this tumor-suppressive effect.

### 1.3.1 c-JUN in cancer

c-JUN was originally believed to exclusively act as an oncogene as c-JUN's basic function includes promoting cell proliferation and overexpression of c-JUN was found in multiple cancers (Eferl and Wagner 2003; Shaulian 2010). This was also promoted by the fact that c-JUN was first discovered as a homolog to the viral v-Jun oncogene. In growth factor independent breast cancer cells, c-JUN and the FOS family member FRA-1 promote cell invasiveness and as a result metastatic behavior (C. Zhao et al. 2014). c-JUN-FRA-1 dimers are suspected to reduce levels of the cell adhesion protein E-cadherin and to promote epithelial to mesenchymal transition (EMT) by transcriptional activation of the E-cadherin repressor gene *ZEB2*. In an intestinal cancer mouse model at late disease stages c-Jun was suggested to beneficially interact with the pro-proliferative Wnt/ $\beta$ -catenin signaling pathway by forming ternary complex with  $\beta$ -catenin and the transcription factor Tcf4 (Nateri, Spencer-Dene, and Behrens 2005; Hasselblatt et al. 2008). Furthermore, c-JUN was observed to act as a major anti-apoptotic factor in liver cancer through suppression of transcriptional activity of p53 (Eferl et al. 2003).

However, recent findings suggest a more ambiguous role of c-JUN in tumorigenesis as it was suggested to act as a tumor-suppressor in certain cases (Shaulian 2010). In a human breast cancer cell line genotoxic stress induced by chemical agents resulted in increased binding of c-JUN to DNA repair genes (Hayakawa et al. 2004). Similarly, the c-JUN activating kinase JNK has been described as a promotor of the DNA damage response (Picco and Pagès 2013). Experiments on human and murine cell lines indicate that JNK signaling promotes apoptosis of UV irradiated cells (Shaulian et al. 2000; Le, Connors, and Maroney 2001; Fan et al. 2001). Stress induced JNK signaling appears to predominantly act tumor-suppressive.

In a murine *Pten/Jnk* KO mouse model it was shown that *Jnk* deficiency would lead to increased invasiveness of PCa which, drastically reduced the survival of *Pten/Jnk* double KO mice (Hübner et al. 2012). JNK also activates ATF family members and other JUN members such as JUNB or JUND and therefore the tumor-suppressive properties of JNK can also be linked to these AP-1 transcription factors (Gazon et al. 2018). In previous studies JunB was suggested to act as a tumor-suppressor for PCa and JunB deficiency led to increased invasiveness of prostate epithelial cells (Thomsen et al. 2015). How Jnk activated c-Jun influences PCa tumorigenesis has yet to be

fully explored. However, in neuronal cells the phosphorylation of c-Jun has been described to be of significant importance for stress induced apoptosis mediated by Jnk, which directly links the tumor-suppressive properties of JNK to c-JUN (Behrens, Sibia, and Wagner 1999; Davies and Tournier 2012).

Another role of c-JUN in PCa tumorigenesis appears to be the modulation of AR signaling (Hsu and Hu 2013). Comparable to healthy cells, PCa cells in early non-CRPC stages of tumorigenesis rely on the growth promoting signaling of the AR. c-Jun was shown to compete with AR at the promotor region of target genes therefore reducing transcriptional activity. However, the influence of c-Jun on AR signaling remains controversial because c-Jun has additionally been identified as a coactivator of AR (Bubulya et al. 2001; Cai, Hsieh, and Shemshedini 2007). In summary, there are several open questions challenging the importance of c-JUN in prostate tumorigenesis.

#### 1.4 Hallmarks of cancer

The term “hallmarks of cancer” was introduced to describe essential characteristics of most cancers to breach natural anti-tumorigenic barriers thereby ensuring malignant growth and tumor progression (Hanahan and Weinberg 2000). The original hallmarks of cancer consisted of six categories including evasion of apoptosis, self-sufficiency in growth signaling, insensitivity toward anti-growth signaling, angiogenesis induction, invasion and metastasis and enabling replicative immortality. New insights into the immunology of cancer prompted the update of the original hallmarks with four more hallmarks including avoidance of immune destruction, pro-tumorigenic inflammation, genome instability and deregulation of cellular metabolisms (Figure 16) (Hanahan and Weinberg 2011).

Hyperproliferation is an important characteristic of most

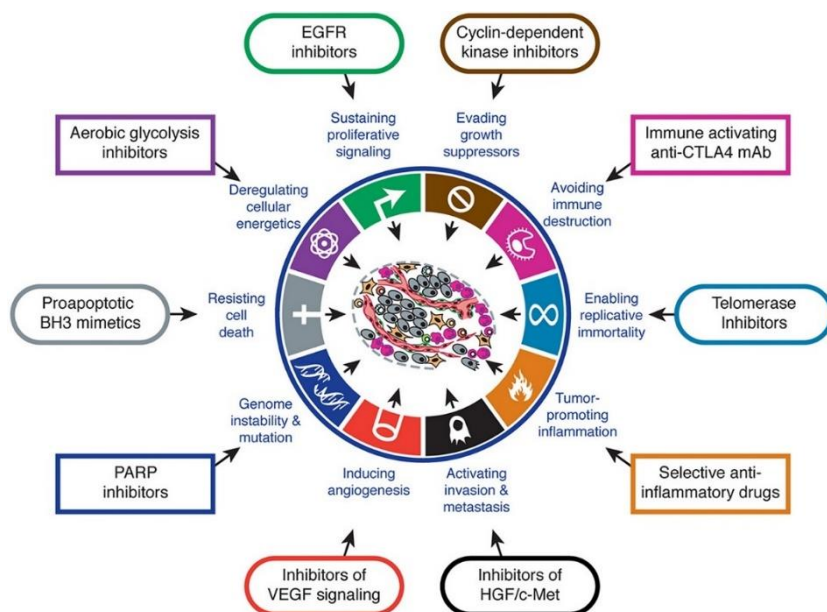


**Figure 16. Overview on the next generation Hallmarks of Cancer.** Image shows cancer hallmarks which promote tumor development and gives an overview on therapeutically used drugs targeting the hallmarks. Image was adapted from (Hanahan and Weinberg 2011).

cancer cells and this is mostly achieved by the hallmarks of sustained proliferation and avoidance of growth suppressors (Figure I6) (Hanahan and Weinberg 2011). Proliferation is characterized by fluctuating activity of cell cycle regulators throughout cell cycle phases (Vermeulen, Van Bockstaele, and Berneman 2003; Barnum and O'Connell 2014). CDKs promote cell cycle progression and negative regulators of these checkpoints are cyclin dependent kinase inhibitors (CKI) and their upstream activators which includes p21 activated by p53. Disabling mutations in these tumor-suppressor genes are essential for sustained proliferation in cancer cells. Furthermore, sustained proliferation is achieved in tumorigenesis by enabling mutations in pro-proliferative pathways and paracrine or autocrine stimulation through growth factors such as tumor necrosis factor- $\alpha$  (TNF- $\alpha$ ) (Aaronson 1991; Bast et al. 1993; Oberholzer et al. 2012). c-JUN is linked to the hallmark of sustained proliferative signaling as a downstream signaling molecule of growth factors (H. F. Zhao, Wang, and To 2015). For example, c-JUN activity was reported to promote sustained proliferative signaling in liver and breast cancer (Hui et al. 2007; Vleugel et al. 2006).

Closely related to the proliferation hallmark is the hallmark of evading growth suppressors (Figure I6) (Hanahan and Weinberg 2011). This includes evasion of senescence which is described as an irreversible cell cycle arrest (Shay and Wright 2000; Hayflick and Moorhead 1961). It was first discovered in association with aging of cells by *Hayflick & Moorhead* who identified a natural limit of cell divisions. Senescence requires a robust cell cycle arrest through continuous signaling of cell cycle inhibitors such as CKIs (Gorgoulis et al. 2019). Therefore, the cell cycle exit of senescent cells is distinctively different from that of quiescent G0 phase cells. External signaling molecules, mutations in tumor-suppressor genes and chemically or physically induced DNA damage are triggers of senescence (Figure I7) (Muñoz-Espín and Serrano 2014). Tumor cells ultimately need to avoid senescence to ensure sustained growth (S. Lee and Schmitt 2019). However, senescence has been reported to promote tumorigenesis by establishing a favorable tumor microenvironment through the senescence-associated secretory phenotype (SASP) (Schosserer, Grillari, and Breitenbach 2017). Senescent cells which adopt this phenotype release molecules which attract pro-inflammatory immune cells and induce senescence in a paracrine and autocrine manner. Furthermore, senescence is known to protect cells from apoptotic cell death (Gorgoulis et al. 2019; Sagiv et al. 2013). c-Jun was previously described as a suppressor of p53-p21 mediated senescence in mouse fibroblasts (Shaulian et al. 2000; Wada et al. 2004). This senescence suppression was suggested to promote the apoptotic clearance of UV-damaged cells.

Therefore c-JUN is linked to regulation of the cancer hallmark of resisting cell death (Figure I6) (Hanahan and Weinberg 2011).

Apoptosis describes the regulated non-inflammatory death of cells and is the primary mechanism to maintain a population of homeostatic cells by eliminating dysfunctional cells (Elmore 2007). The extrinsic and intrinsic pathways are the two major modes for activation of apoptosis and they utilize distinct initiator caspases but lead to a conjoint executioner caspase pathway. The extrinsic pathway requires activity of membrane bound death receptors such as Fas (Budihardjo et al. 1999). Cell internal apoptotic stimuli are recognized by tumor-suppressors such as p53 (Elmore 2007; Zimmermann and Green 2001; Kasibhatla and Tseng 2003). Accumulation of mutations in cell death receptor genes and intrinsic effectors has been reported to enable the cancer hallmark of resisting cell death (Takayama et al. 2002).

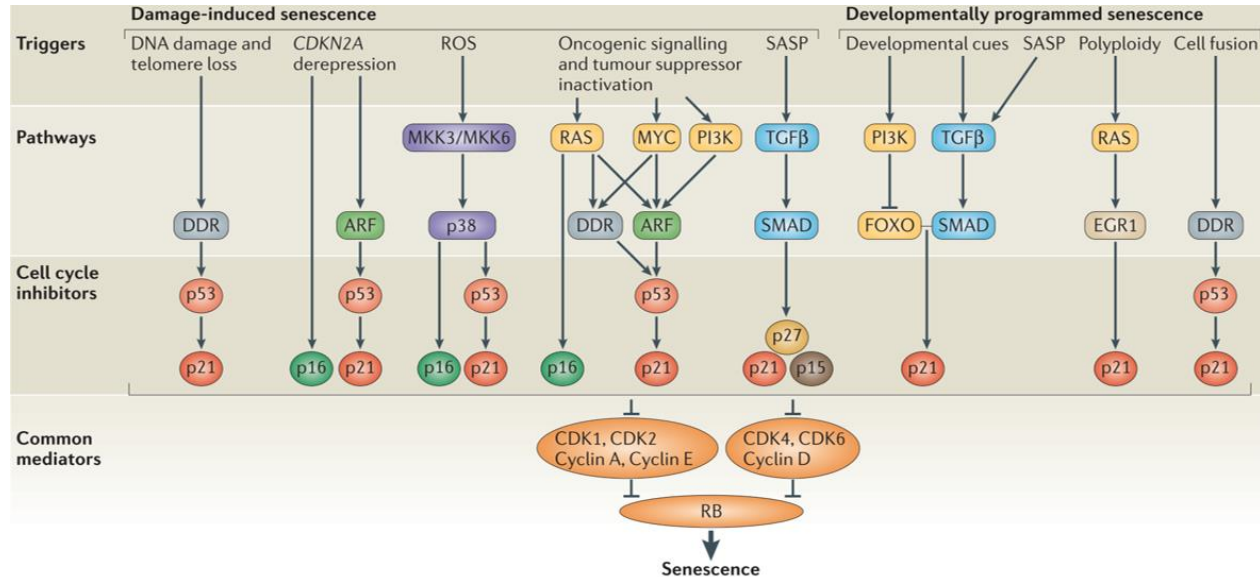


**Figure 17. Senescence pathways.** Overview on known molecular mechanisms that lead to cellular senescence (Muñoz-Espín and Serrano 2014). Senescence is driven by a multitude of triggers such as reactive oxygen species (ROS), extracellular signaling molecules and a vast array of oncogenic stressors including DNA damage, telomere loss, loss of tumor-suppressors, cell fusion or polyploidy. Oncogenic stressors usually lead to the activation of the DNA damage response (DDR). Cells which are activated through paracrine signaling molecules of the senescence associated secretory phenotype (SASP) use a distinct mechanism to mediate senescence. All pathways utilize cell cycle inhibitors and tumor-suppressors such as p53, p16, p21, p27 or p15 to inhibit the activity of cyclin dependent kinases (CDK). This releases the master mediator of senescence retinoblastoma (RB).

## 1.5 Aim of the thesis

In this project we addressed c-JUNs ambiguous role in cancer regulation and we aimed to determine whether c-JUN acts as a tumor-suppressor or an oncogene in PCa. To address this question, we analyzed publicly available RNA-seq datasets of human patients and performed survival experiments in a *c-Jun* deficient PCa mouse model. We used immunohistochemistry and Real time quantitative PCR to unveil putative regulatory effects of c-Jun on cancer hallmarks. Furthermore, we performed next generation sequencing for transcriptomic analysis of the *c-Jun* deficient PCa mouse model.

## 2 Material and Methods

### 2.1 Ethics statement

All animal experiments were conducted according to the Austrian Animal Testing Law (BGBI. I No. 114/2012) and approved by the Austrian Federal Ministry of Education, Science and Research under the licenses “BMWFV-66.009/0144-WF/II/3b/2014”, “BMWFV-66.009/0137-WF/V/3b/2017” and the amendment “BMBFW-66.009/0359- V/3b/2019”.

Experiments on histological sections of human PCa patients were approved by the Ethics Committee of the Medical University of Vienna under the application number “EK No.: 1877/2016 Version 5”.

### 2.2 Work with animals

#### 2.2.1 Prostate cancer mouse model

To establish the mouse model used for this study, we crossbred a *Pten* knockout (KO) prostate cancer mouse strain (Birbach et al. 2011) with a *c-Jun*-floxed mouse strain (Behrens et al. 2002) (Figure M1B). The *Pten* KO mouse strain was originally established (Birbach et al. 2011) by crossing *Pten*<sup>Ex4/Ex5</sup>-floxed mice (Suzuki et al. 2001) and heterozygous transgenic *Probasin* (*PB*)-*Cre4* mice (Xiantuo Wu et al. 2001) (Figure M1A). *PB-Cre4* transgenic mice express the Cre4 recombinase under the *PB* promoter. *PB* expression is restricted to prostate epithelial cells of sexually mature mice allowing prostate specific KO of floxed genes (Xiantuo Wu et al. 2001).

Inheritance of *PB-Cre4* through the maternal line could lead to unexpected recombination events and therefore only *PB-Cre4<sup>tg/+</sup>* males were used for breeding (A. J. Song and Palmiter 2018) (Figure M1A-M1B) (see table below for genotypes used for breeding and experiments). To minimize tumor burden on breeding animals, only heterozygous *Pten<sup>Δ/+</sup>* males were used for breeding. The generated groups of experimental genotypes included all possible genotypes: *PB-Cre4<sup>+/+</sup>* animals (*Control*), expressing no *PB-Cre4* and therefore expected to display a wild type phenotype; *PB-Cre4<sup>tg/+</sup>;c-Jun<sup>fl/fl</sup>* animals (*c-Jun<sup>Δ/Δ</sup>*); *PB-Cre4<sup>tg/+</sup>;Pten<sup>fl/fl</sup>* animals (*Pten<sup>Δ/Δ</sup>*); *PB-Cre4<sup>tg/+</sup>;Pten<sup>fl/fl</sup>;c-Jun<sup>fl/fl</sup>* animals (*Pten<sup>Δ/Δ</sup>;c-Jun<sup>Δ/Δ</sup>*) (Figure M1C).

Genotypes may also be referred to as *c-Jun* KO for *c-Jun<sup>Δ/Δ</sup>*, *Pten* KO for *Pten<sup>Δ/Δ</sup>* and *Pten;c-Jun* KO for *Pten<sup>Δ/Δ</sup>;c-Jun<sup>Δ/Δ</sup>*. The breeding strategy also resulted in heterozygous variations of the *Pten* and *c-Jun* KO, but no heterozygous animals were used for experiments. For identification and genotyping of animals an ear-punching method was used at the age between two to three weeks. Skin removed by punching was used for genotyping of the animals and tail tissue was used to re-genotype after sacrificing the animals.

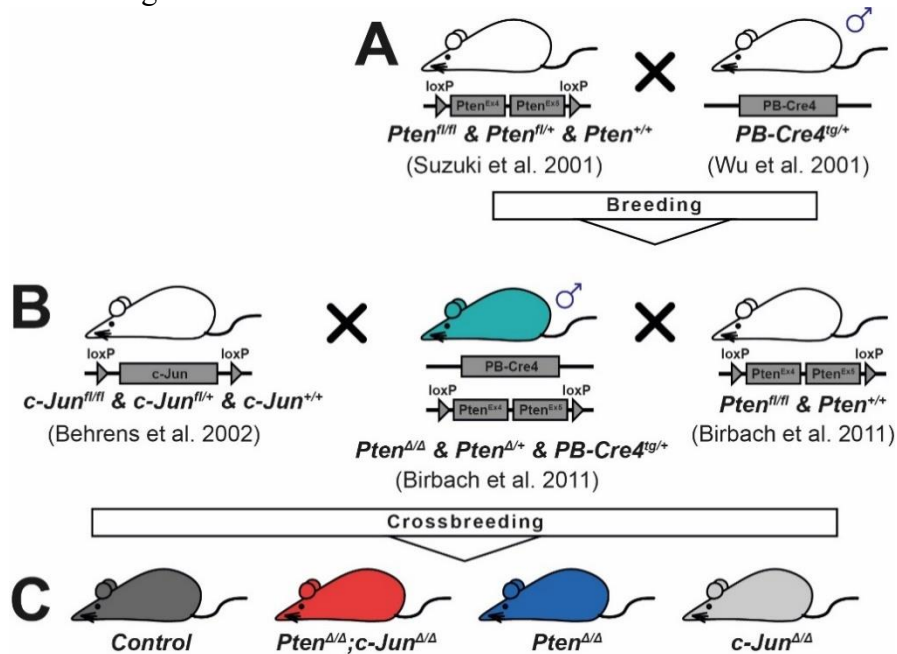


**Figure M1. Mouse model to investigate effects of *c-Jun* deficiency in PCa.** Breeding scheme leading to the four genotypes of interest used in the project. The *PB-Cre4* was exclusively inherited paternally. (A) First breeding step to generate *Pten* KO mice from *Pten* floxed mice and *Probasin Cre-recombinase 4 (PB-Cre4)* transgenic mice (Birbach et al. 2011). (B) Second breeding step of *c-Jun* floxed mice with *Pten* KO mice that led to generation of the *Pten/c-Jun* KO mouse model. (C) The four genotypes of interest used in experiments included *Control* mice with wild type phenotype, *Pten/c-Jun* KO mice, *Pten* KO mice and *c-Jun* KO mice.

**List of breeding genotypes and genotypes of offspring**

♀ breeding genotypes	♂ breeding genotypes	Offspring genotypes (♀/♂)*
<i>PB-Cre4<sup>+/+</sup>;Pten<sup>fl/fl</sup>;c-Jun<sup>+/+</sup></i>	<i>PB-Cre4<sup>tg/+</sup>;Pten<sup>fl/+</sup>;c-Jun<sup>+/+</sup></i>	<i>PB-Cre4<sup>tg/+</sup>;Pten<sup>fl/fl</sup>;c-Jun<sup>+/+</sup></i> ( <i>Pten<sup>Δ/Δ</sup></i> )
<i>PB-Cre4<sup>+/+</sup>;Pten<sup>+/+</sup>;c-Jun<sup>fl/fl</sup></i>	<i>PB-Cre4<sup>tg/+</sup>;Pten<sup>+/+</sup>;c-Jun<sup>fl/fl</sup></i>	<i>PB-Cre4<sup>tg/+</sup>;Pten<sup>+/+</sup>;c-Jun<sup>fl/fl</sup></i> ( <i>c-Jun<sup>Δ/Δ</sup></i> )
<i>PB-Cre4<sup>+/+</sup>;Pten<sup>fl/fl</sup>;c-Jun<sup>fl/fl</sup></i>	<i>PB-Cre4<sup>tg/+</sup>;Pten<sup>fl/+</sup>;c-Jun<sup>fl/fl</sup></i>	<i>PB-Cre4<sup>tg/+</sup>;Pten<sup>fl/fl</sup>;c-Jun<sup>fl/fl</sup></i> ( <i>Pten<sup>Δ/Δ</sup>;c-Jun<sup>Δ/Δ</sup></i> )
		<i>PB-Cre4<sup>tg/+</sup>;Pten<sup>fl/+</sup>;c-Jun<sup>+/+</sup></i> (breeding only)
		<i>PB-Cre4<sup>tg/+</sup>;Pten<sup>fl/+</sup>;c-Jun<sup>fl/fl</sup></i> (breeding only)
		<i>PB-Cre4<sup>+/+</sup>;Pten<sup>fl/fl</sup>;c-Jun<sup>+/+</sup></i> (Control)
		<i>PB-Cre4<sup>+/+</sup>;Pten<sup>+/+</sup>;c-Jun<sup>fl/fl</sup></i> (Control)
		<i>PB-Cre4<sup>+/+</sup>;Pten<sup>fl/fl</sup>;c-Jun<sup>fl/fl</sup></i> (Control)
		<i>PB-Cre4<sup>+/+</sup>;Pten<sup>fl/+</sup>;c-Jun<sup>+/+</sup></i> (Control)
		<i>PB-Cre4<sup>+/+</sup>;Pten<sup>fl/+</sup>;c-Jun<sup>fl/fl</sup></i> (Control)

\*use of male genotypes in “()”. Female *PB-Cre4<sup>tg/+</sup>* offspring was not used for breeding.

**2.2.2 Sacrificing animals and processing mouse tissue**

Male experimental animals were sacrificed at 19 weeks of age by cervical dislocation. Samples taken for formalin fixing and paraffin embedding (FFPE samples) included prostate, lymph nodes, liver, spleen, kidney, heart, lung, brain and femur. Samples were fixed overnight in 4 % formaldehyde in PBS solution (100496; Merck, DE) at 4 °C. Fixed samples were transferred into 70% ethanol (EtOH) (Pharmacy VetMed) and stored at 4 °C for up to 48 h until the dehydration procedure. Femur samples were decalcified in 8 % EDTA solution (A1104; AppliChem, DE) for about 1 week at room temperature (RT) before transfer into 70 % EtOH. The automated device Tissue-Tek VIP 6 AI (6042; Sakura Finetek, JP) was used to dehydrate samples. Dehydrated samples were paraffin embedded as blocks by the VetMed Pathology Histology Team. FFPE samples were used for experiments involving immunohistochemistry and hematoxylin and eosin (H&E) staining. For DNA and protein techniques, prostate, liver and spleen samples were snap-frozen in liquid nitrogen and stored at -80°C. For RNA isolation, prostate samples were treated with RNAlater Stabilization Solution (AM7020; Thermo Fisher Scientific, USA) overnight at 4 °C. Samples were washed in Dulbecco's phosphate-buffered saline (DPBS) (14190250; Thermo Fisher Scientific) and transferred into a fresh reaction tube. Finally, samples were snap-frozen in liquid nitrogen and stored at -80 °C.

## **2.3 Work with human cell lines**

### **2.3.1 Cell line maintenance**

#### **Expansion and splitting**

HEK239 FT (DuBridge et al. 1987), DU145 (Stone et al. 1978) and PC-3 (Kaighn et al. 1979) cell lines were used for experiments. HEK239 FT cells were cultivated in Dulbecco's Modified Eagle Medium (DMEM) (21969-035; Thermo Fisher Scientific) supplemented with 10 % Fetal Bovine Serum (FBS) (10500-064; Thermo Fisher Scientific), 1 U/ml of Penicillin-Streptomycin solution (15140122; Thermo Fisher Scientific) and 2 mM L-Glutamine (25030024; Thermo Fisher Scientific). PC-3 and DU145 cells were cultivated in Roswell Park Memorial Institute (RPMI) (31870-025; Thermo Fisher Scientific) medium supplemented with 10 % FBS, 1 U/ml of Penicillin-Streptomycin solution, 2 mM L-Glutamine and 2.5 mM HEPES (15630080; Thermo Fisher Scientific). Cells were split at a ratio of 1:3 to 1:10 after reaching >80 % confluency. Cells were detached from culture dishes using Trypsin-EDTA phenol red solution (25300054; Thermo Fisher Scientific) and the reaction was stopped using FBS containing media.

#### **Freezing of cells**

To freeze cells, dishes/flasks were trypsinized and cells were pelleted at  $1200 \times g$  at RT. After removing the supernatant, cells were resuspended in medium supplemented with 10% dimethyl sulfoxide (DMSO) (15303671; Thermo Fisher Scientific). 1 ml suspension was transferred into a cryo tube and frozen at  $-80^{\circ}\text{C}$  using a CoolCell cell freezing container (210005; Biozym Biotech Trading, DE).

#### **Harvesting of cell pellets**

To harvest cell pellets dishes/flasks were trypsinized, pelleted at  $1200 \times g$  at RT, resuspended in DPBS, transferred into 1.5 ml reagent tubes and re-pelleted at  $1200 \times g$  at RT. After fully removing the supernatant via pipetting cell pellets were snap-frozen in liquid nitrogen and stored at  $-80^{\circ}\text{C}$  until further use.

#### **Cell counting**

For experiments requiring the measurement of total cell counts in cell suspensions a LUNA-II Automated Cell Counter device (L40001; Logos Biosystems, KOR) and LUNA Cell Counting Slides (L12001; Logos Biosystems) were used. Cell suspension was mixed 1:1 with 0.4% Trypan Blue Stain (T13001; Logos Biosystems) to measure the cell viability ratio and calculate the live cell fraction.

### 2.3.2 Transfection of HEK239 FT cells

HEK293 FT cells were transfected with lentiCRISPR v2-sgRNA vectors which were cloned with the sgRNAs Guide 1 (G1), Guide 12 (G12) and Guide 14 (G14). As control, HEK293 FT cells were transfected with lentiCRISPRv2 empty vector (eV). To assess transfection efficiency by fluorescence microscopy, HEK293 cells were transfected with pLKO.1 CMV GFP vector which was kindly provided by Michael Kothmayer (Figure M2). The vector was constructed from the pLKO.1 puro vector which was a gift from Bob Weinberg (Addgene plasmid # 8453 ; <http://n2t.net/addgene:8453> ; RRID:Addgene\_8453) (Stewart et al. 2003). For each transfection 7.5  $\mu$ l of Lipofectamine 2000 (11668030; Thermo Fisher Scientific) was mixed with 150  $\mu$ l of Opti-MEM (31985062; Thermo Fisher Scientific) by flicking the tube and incubated at RT for 5 min. 0.5  $\mu$ g of GFP plasmid or 2  $\mu$ g of lentiCRISPR v2 plasmid was mixed with 150  $\mu$ l of Opti-MEM.

Plasmid and lipofectamine solution were mixed and incubated at RT for 25 min. For each transfection 1 ml of Penicillin-Streptomycin-free DMEM medium was pipetted into a well of a 6-well plate. Lipofectamine-plasmid mix was added dropwise to the well. 1 ml of HEK239 FT cell suspension in Penicillin-Streptomycin-free DMEM with a concentration of  $1.5 \times 10^6$  cells/ml was added to each well. After overnight incubation at 37 °C medium was exchanged with DMEM containing 1 U/ml of Penicillin-Streptomycin.

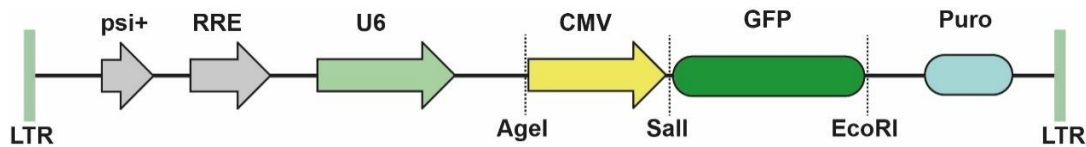


**Figure M2. Schematic image of pLKO.1 CMV GFP.** This image shows all major components of the pLKO.1 vector (Stewart et al. 2003). The cytomegalovirus (CMV) promoter region and the sequence which encodes green fluorescent protein (GFP) was inserted into this vector (Michael Kothmayer). The vector is flanked by long terminal repeats (LTR). The vector contains target sites for the restriction enzymes AgeI, Sall and EcoRI. Puromycin resistance gene (*Puro*) is encoded by the vector. The vector contains the U6 promoter region. The vector also contains psi packaging signal (psi+) and HIV-1 Rev response element (RRE). An Ampicillin resistance gene for selection in bacteria is also part of the vector to but not shown in this scheme.

#### 2.3.2.1 Transfection for lentivirus production

Lentivirus for transduction was produced in HEK239 FT cells. 36  $\mu$ l of Lipofectamine 2000 was mixed with 1.5 ml of Opti-MEM and incubated at RT for 5 min. In a second reaction tube 4.6  $\mu$ g of psPAX2, 2.8  $\mu$ g of pMD2.G (lentiviral packaging plasmids) and 7.5  $\mu$ g of GFP plasmid or

lentiCRISPRv2 containing the sgRNA was mixed with 1.5 ml of Opti-MEM. Both solutions were mixed and incubated at RT for 25 min. The psPAX2 and pMD2.G vectors were gifts from Didier Trono (Addgene plasmid # 12260 ; <http://n2t.net/addgene:12260> ; RRID:Addgene\_12260) (Addgene plasmid # 12259 ; <http://n2t.net/addgene:12259> ; RRID:Addgene\_12259) (unpublished) (Figure M3). HEK239 FT cells were trypsinized and diluted to a concentration of  $1.2 \times 10^6$  cells/ml. 1 ml of Penicillin-Streptomycin free DMEM medium was pipetted into a well of a 10 cm  $\phi$  dish and 3 ml of Lipofectamine-plasmid mix was added dropwise. 5 ml of HEK239 FT cell suspension were added, followed by overnight incubation at 37 °C. On day one after transfection medium was exchanged for regular DMEM medium containing antibiotics. Day three after transfection lentivirus was harvested by transferring medium supernatant into a 15 ml reaction tube and centrifuging cell debris at 5000 rpm for 15 min at RT.

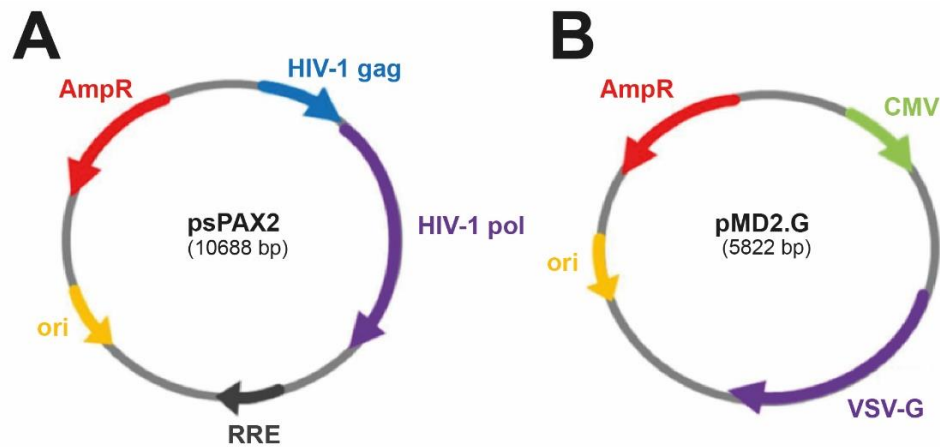


**Figure M3. Plasmid maps of psPAX2 and pMD2.G.** This image shows all major components of the packaging plasmids psPAX2 and pMD2.G (image adapted from Michael Kothmayer). (A) The psPAX2 plasmid contains the DNA template of the viral proteins HIV-1 gag and HIV-1 pol. The vector also contains HIV-1 Rev response element (RRE) and an Ampicillin resistance gene (*AmpR*). (B) The pMD2.G plasmid contains a cytomegalovirus (CMV) promoter region and the DNA template of the viral protein vesicular stomatitis virus G glycoprotein (VSV-G). The vector also contains an *AmpR* gene.

Supernatant was transferred into a fresh 15 ml reaction tube and 2.5 ml of PEG solution from the PEG virus precipitation Kit (K904-50; BioVision, USA) were mixed with the supernatant by inverting. After overnight incubation at 4 °C the solution was centrifuged at  $3200 \times g$  for 30 minutes to precipitate the viral particles. Supernatant was removed and the pellet was resuspended in 400  $\mu$ l of resuspension buffer, 30  $\mu$ l-aliquoted and stored at -80 °C until used for transduction.

### 2.3.3 Transduction of PCa cell lines

For transduction PC-3 and DU145 cells were trypsinized and diluted to a concentration of  $2.5 \times 10^5$  cells/ml. Per ml cell suspension 10  $\mu$ g of polybrene (107689-10G; Merck) were added to

the cell suspension. Per transduction reaction, 2 ml of the cell suspension were added to a 6-well plate. Virus was quickly thawed in a water bath and 30  $\mu$ l were added, followed by a 72-h incubation at 37 °C. After incubation medium was exchanged with Puromycin (J593-25MG; VWR International, USA) containing RPMI medium. For Puromycin selection of DU145 cell lines 2  $\mu$ g/ml of Puromycin RPMI medium were used, for selection of PC-3 cell lines 2.5  $\mu$ g/ml of Puromycin RPMI medium were used. The untransduced DU145 and PC-3 cell lines were used as positive controls for Puromycin selection. 48 h after Puromycin selection the medium was exchanged with Puromycin-free RPMI. Puromycin selection was repeated prior to experiments.

#### **2.3.4 Picking single clones**

Single clones were picked by passaging 10 cm  $\varnothing$  dishes of transduced cell lines at a rate of 1:1000 to 1:5000 into fresh 10 cm  $\varnothing$  dishes. Cells were incubated at 37 °C until single colonies became macroscopically visible. Plates were washed with DPBS and single clones were picked by pipetting 20  $\mu$ l of trypsin directly on colonies and repeated up and down pipetting. Single clones were expanded on a 24-well plate and were gradually moved to larger culture dishes after each splitting.

#### **2.3.5 Proliferation experiments**

Validated transduced PC-3 and DU145 bulk cultures and single clone cell lines were used for proliferation experiments. Proliferation experiments were based either on cell count-based proliferation analysis or a resazurin assay.

##### **2.3.5.1 Cell count-based proliferation analysis**

Cells from one 10 cm  $\varnothing$  dish were trypsinized with 1 ml of trypsin and suspended in 5 ml of standard RPMI medium. To measure cell density in the suspension the LUNA-II Automated Cell Counter device was used. 4 ml of cell suspension equivalent to 25000 viable DU145 cells were pipetted into a 6-well plate for each replicate. 4 ml of cell suspension equivalent to 90000 viable PC-3 cells were pipetted on a 6-well plate for each replicate. Plates were incubated at 37 °C and cell counts were measured at multiple time points using the LUNA-II Automated Cell Counter device. Bulk cultures were measured at days 2, 4, 6 and 8 after seeding. DU145 single clones were measured on days 1, 2, 4, 6 and 8. PC-3 single clones were measured on days 2, 4, 6 and 8.

##### **2.3.5.2 Resazurin assay**

The resazurin assay is based on the metabolization of resazurin into a fluorescent product by viable cells (O'Brien et al. 2000). Therefore, the viable cell density is directly proportional to the

metabolization rate of resazurin. Cells from one 10 cm  $\varnothing$  dish were trypsinized with 1 ml of trypsin and suspended in 5 ml of standard RPMI medium. For each replicate a cell suspension equivalent to 2000 viable cells for DU145 and 5000 viable cells for PC-3 were seeded per well on a 96-well plate in 200  $\mu$ l of total volume. 0.15 mg/ml of resazurin (R7017; Merck) dissolved in PBS was prepared, single-use-aliquoted and stored at  $-20^{\circ}\text{C}$  until used for measurements. At specific time points the medium was removed from wells by pipetting without disturbing the cell layer and 120  $\mu$ l of thawed resazurin solution were pipetted into each well. In addition, blanks were included by pipetting 120  $\mu$ l of resazurin solution into an empty well. After 2 h incubation at  $37^{\circ}\text{C}$ , 100  $\mu$ l of each well were transferred into a 96-well optical-bottom plate (165305; Thermo Fisher Scientific).

Plates were analyzed using a Synergy HT-I device (7091000; BioTek Instruments, USA). The detection method was end point fluorescence measurement at an excitation wavelength of  $530\pm 25$  nm and an emission wavelength of  $590\pm 35$  nm. The first measurement was taken after overnight incubation of cells and regarded as day 0. Follow-up measurements were performed on days 2, 4 and 6 after the first measurement.

## **2.4 Work with bacteria**

### **2.4.1 Chemical transformation of competent Stbl3**

The cloned vector was transformed into chemically competent Stbl3 bacteria (C737303; Thermo Fisher Scientific). 50  $\mu$ l of suspension from competent Stbl3 bacteria were mixed with 4  $\mu$ l of ligation product of the prior lentiCRISPR v2 cloning step. In addition, 50  $\mu$ l of suspension were mixed with 2  $\mu$ l of undigested lentiCRISPR v2 plasmid to gain a transformation positive control. After 25 min incubation on ice, a 45 sec heat-shock treatment at  $42^{\circ}\text{C}$  followed. Reaction tubes were immediately chilled on ice for 2 min and 150  $\mu$ l of  $30^{\circ}\text{C}$  prewarmed SOC medium (15544034; Thermo Fisher Scientific) were added to the tube. Incubation for 1.5 h at  $30^{\circ}\text{C}$  shaking at 350 rpm on a thermo shaker followed. 100  $\mu$ l of suspension were plated on a lysogeny broth (LB)-agar plate supplemented with 100  $\mu\text{g}/\text{ml}$  of Ampicillin (K029.1; Carl Roth, DE) and incubated overnight at  $30^{\circ}\text{C}$ . For each type of lentiCRISPRv2-sgRNA vector three single colonies were picked, suspended in 3 ml LB-medium supplemented with 50  $\mu\text{g}/\text{ml}$  of Ampicillin and incubated overnight at  $30^{\circ}\text{C}$  shaking. 1.5 ml of this cell suspension were used to produce plasmids using the ZR Plasmid Mini Prep Kit (D4015; Zymo Research Corporation, USA) according to manufacturer's recommendations. From the remaining cell suspension glycerol stocks were

produced and stored at  $-80\text{ }^{\circ}\text{C}$ . Introduction of sgRNA was confirmed by Sanger sequencing performed by Microsynth. Plasmids of sequence confirmed vectors were produced from glycerol stocks by extraction from 100 ml overnight culture using the HiSpeed Plasmid Midi Kit (12643; QIAGEN N.V., DE) and following the product manual.

### LB-agar and medium

	final concentration (f. conc.)
Tryptone (8952.1; Carl Roth)	1 %
NaCl	0.5 %
Yeast extract (2363.2; Carl Roth)	0.5 %
mili-q H <sub>2</sub> O	
Agarose* (AGA500-BCAT; BioCat, DE)	1.5 %

\*not included in LB-medium

### Sequencing primers

Primer name	Sequence
pLKO1_U6_Seq_fw	TTTGCTGTA CTTTCTATAGTG
LKO1_seq	GACTATCATATGCTTACCGT

#### 2.4.1.1 Mini Prep of transformed bacteria

Single colonies of transformed Stb13 were scratched from LB-agar plates using a pipette tip and the tip was plunged into an incubation vial containing 3 ml LB-medium supplemented with 50  $\mu\text{g/ml}$  of Ampicillin. The suspension was incubated overnight at  $30\text{ }^{\circ}\text{C}$  shaking and 1.5 ml of cell suspension were transferred to a fresh reaction tube. Cells were pelleted at  $21000 \times g$  at RT and supernatant was removed. Plasmids were extracted from the cell pellet using the ZR Plasmid Mini Prep Kit (D4015; Zymo Research Corporation, USA) following the product manual.

#### 2.4.1.2 Midi Prep of transformed bacteria

Transformed Stb13 were scratched from the glycerol stock using a pipette tip and the tip was plunged into an incubation flask containing 100 ml LB-medium supplemented with 50  $\mu\text{g/ml}$  of Ampicillin. The suspension was incubated overnight at  $30\text{ }^{\circ}\text{C}$  shaking and cell suspension was split equally to two fresh 50 ml Falcon tubes. Cells were pelleted at  $6000 \times g$  at  $4\text{ }^{\circ}\text{C}$  and supernatant was removed. Plasmids were extracted from the cell pellets using the HiSpeed Plasmid Midi Kit (12643; QIAGEN N.V., DE) following the product manual. Both cell pellets of one sample were united at the resuspension step of the product manual.

## 2.5 Work with DNA

### 2.5.1 Gel electrophoresis of DNA

PCR amplicons were mixed with 6 × Orange loading dye (R0631; Thermo Fisher Scientific) and transferred on an agarose gel supplemented with 1 × ROTI GelStain (3865.1; Carl Roth). For <500 bp amplicons a 2 % agarose gel, for 500-1000 bp amplicons a 1.5 % agarose gel and for >1000 bp amplicons a 0.8 % agarose gel was prepared. Gel electrophoreses was performed at 90 V for 45 min using a Bio-Rad PowerPac Basic (1645050; Bio-Rad Laboratories) and a Bio-Rad Sub-Cell (17044; Bio-Rad Laboratories).

### 2.5.2 Genotyping of mice

#### Proteinase K digestion of ear and tail samples

Ear punch samples for genotyping and tail samples for re-genotyping of experimental animals were proteinase K digested to extract DNA for genotyping. 400 µl of lysis buffer were added to the tissue sample. 15 µl of 10 mg/ml Proteinase K solution (BP1700-500; Thermo Fisher Scientific) were added and mixed by vortexing. Samples were incubated overnight at 55 °C shaking at 350 rpm. This lysate was directly used for genotyping.

#### Genotyping PCR and gel electrophoresis

Primers for the *PB-Cre4<sup>tg/+</sup>*, *Pten* flox, *Pten* delta, *c-Jun* flox and *c-Jun* deltax were used for genotyping PCR. *PB-Cre4<sup>tg/+</sup>* primers do not produce amplicons in *PB-Cre4<sup>+/+</sup>* mice and delta allele primers do not produce amplicons for the floxed or wild type alleles. A positive control was included for this genotyping. *Pten* flox and *c-Jun* flox primers produce amplicons of different length for floxed and wild type alleles. Master mix and proteinase K digestion product were mixed and PCR was performed. PCR products were mixed with loading dye and used for gel electrophoresis.

#### Lysis buffer (pH 8.0)

	final concentration (f. conc.)
Tris (R5429.5; Carl Roth)	100 mM
EDTA	0.5 mM
NaCl	200 mM
10% SDS (R1057.1; Carl Roth)	0.1 %
mili-q H <sub>2</sub> O	

**Genotyping primers**

Primer name	Sequence	Expected amplicon length
Cre Fw	CGGTTCGATGCAACGAGTGATGAGG	700 bp (Cre+)
Cre Rv	CCAGAGACGGAAATCCATCGCTCG	
Pten fl Fw	CTCCTCTACTCCATTCTTCCC	209 bp (Pten wt); 335 bp (Pten fl)
Pten fl Rv	ACTCCCACCAATGAACAAAC	
Pten Δ Fw	GTCACCAGGATGCTTCTGAC	850 bp (Pten Δ)
Pten Δ Rv	ACTATTGAACAGAATCAACCC	
cJun fl Fw	CCGCTAGCACTCACGTTGGTAGGC	300 bp (cJun fl); 350 bp (cJun fl)
cJun fl Rv	CTCATACCAGTTCGCACAGGCGGC	
cJun Δ Fw	CAGGGCGTTGTGTCAGTCTGAGCT	600 bp (cJun Δ)
cJun Δ Rv	CTCATACCAGTTCGCACAGGCGGC	

Desalted primers were ordered from Microsynth.

**PCR Master Mix (Cre & Pten fl & c-Jun fl, Δ)**

	f.conc.
10 × Dream Taq buffer (EP0701; Thermo Fisher Scientific)	1 ×
DMSO	10 %
10 mM dNTPs (10319879; Thermo Fisher Scientific)	0.2 mM
10 μM primer mix	0.4 μM
Nuclease-free water (10977-035; Thermo Fisher Scientific)	
Dream Taq DNA Polymerase (EP0701; Thermo Fisher Scientific)	0.04 U/μl
Template DNA	variable (2 μl)

**PCR Master Mix (Pten Δ)**

	f.conc.
5 × One Taq buffer (M0481S; New England Biolabs)	1 ×
10 mM dNTPs	0.2 mM
10 μM primer mix	0.4 μM
Nuclease-free water	
One Taq DNA Polymerase (M0481S; New England Biolabs)	0.025 U/μl
Template DNA	variable (2 μl)

**PCR- program (Cre & Pten fl, Δ)**

Step	Temperature	Time
Denaturation	94 °C	2 min
Cycle 40 ×	94 °C	2 sec
	55 °C	30 sec
	72 °C	2 min
Elongation	72 °C	10 min
Hold	22 °C	∞

**PCR- program (c-Jun fl, Δ)**

Step	Temperature	Time
Denaturation	94 °C	2 min
Cycle 40 ×	94 °C	30 sec
	60 °C	40 sec
	65 °C	90 sec
Elongation	65 °C	5 min
Hold	12 °C	∞

### 2.5.3 Genomic DNA extraction from cell pellets

Cell pellets from transfected cell lines were suspended in 500  $\mu\text{l}$  of freshly prepared DNA extraction buffer. 20  $\mu\text{l}$  of 10 mg/ml Proteinase K solution were added and mixed by vortexing. Incubation at 55 °C and 450 rpm on a thermo shaker was performed overnight. 700  $\mu\text{l}$  of Phenol Chloroform Isoamyl ethanol (P2069; Merck) were added to the reaction tube and solutions were mixed by vortexing for 1 min. Solution was transferred into Phasemaker tubes (A33248; Thermo Fisher Scientific) and centrifugation at 14000 rpm for 5 min at RT was performed. The aqueous supernatant was transferred into a fresh reaction tube and mixed with 500  $\mu\text{l}$  of isopropanol (131090.1212; VWR International) and 100  $\mu\text{l}$  of 3 M sodium acetate solution (S2889-250G; Merck) by vortexing. Centrifugation at 14000 rpm for 4 min at RT was performed. Supernatant was removed and the pellet was washed in 1 ml of 70 % EtOH, followed by centrifugation at 14000 rpm for 5 min at RT. Supernatant was removed completely by pipetting and the DNA pellet was resuspended depending on pellet size in 150-300  $\mu\text{l}$ . 1  $\mu\text{l}$  of RNAase A (10 mg/ml) (10753721; Thermo Fisher Scientific) was added to the reaction tube followed by 20 min incubation at 55 °C. DNA concentration was measured using a nanophotometer (P330; Implen, DE) and samples were stored at 20 °C until further use.

#### DNA extraction buffer

	f. conc.
Guanidine thiocyanate (G9277; Merck)	0.8 M
EDTA	10 mM
Tween 20 (9127.1; Carl Roth)	5 %
Triton X-100 (R3051.3; Carl Roth)	0.5 %
0.5 M HEPES pH 5.3	50 mM
mili-q H <sub>2</sub> O	

### 2.5.4 Design of guide RNA for CRISPR KO of c-JUN

Guide RNAs targeting Exon 1 of *c-JUN* were designed using the CRISPR/Cas9 single guide RNA (sgRNA) design web tool at [www.crispr.mit.edu](http://www.crispr.mit.edu) using the *c-JUN* reference sequence “ENST00000371222.3” (Figure M4). Targeted *c-JUN* sequences are flanked by a Protospacer Adjacent Motif (PAM) which is required for the binding of Cas9 to the target site. An additional G-base was added to the designed oligo if the target sequence lacked a 5'-end G-base. This improves transcription mediated by the U6 promotor (Lone et al. 2018). Desalted oligos were ordered from Microsynth (Microsynth, CHE).

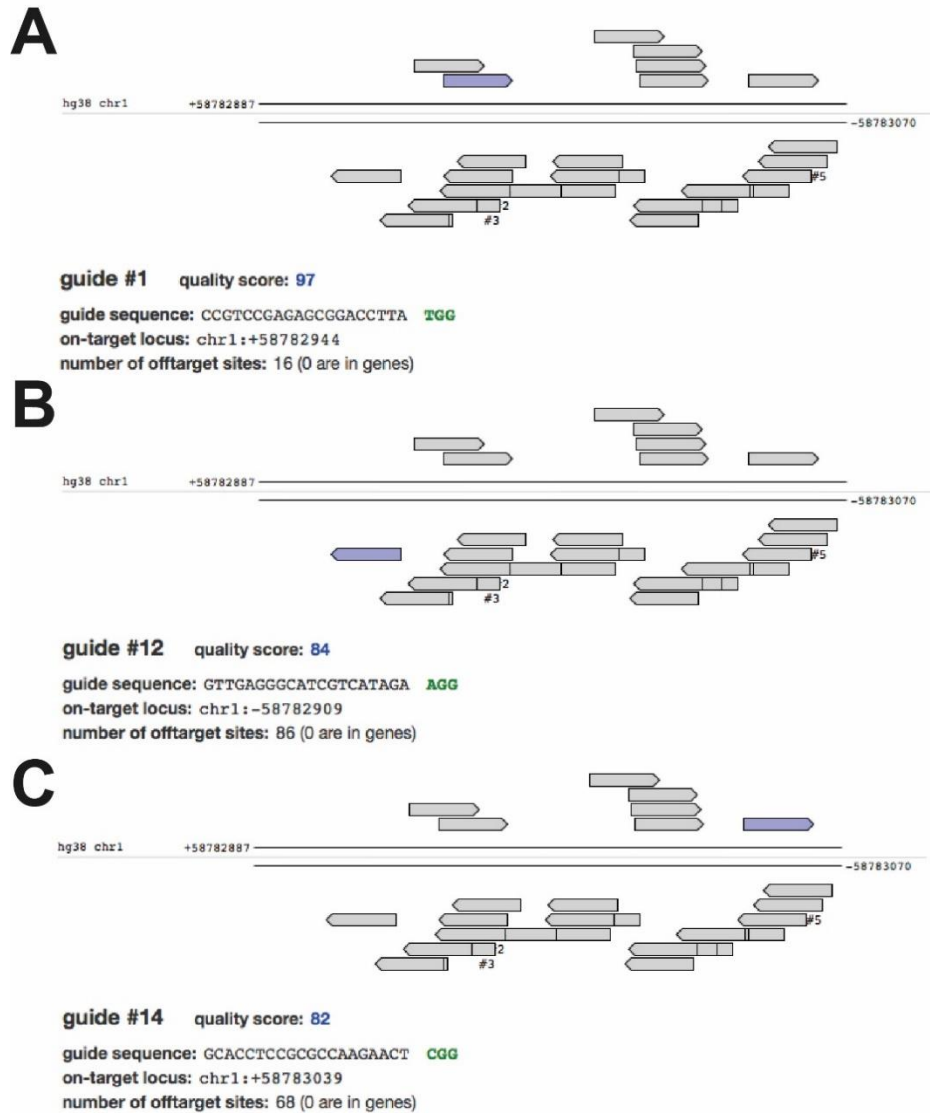


**Figure M4. CRISPR sgRNA design for KO of *c-JUN*.** Overview on sgRNA designs and locations on the *c-JUN* cDNA suggested by design tool. Blue arrows represent the binding region of selected oligo within the exon. Grey arrows represent the target sites of all possible sgRNAs. Tables show sgRNA sequence, target loci and number of off targets. Designs for G1 (A), G12 (B) and G14 (C) are shown. Protospacer Adjacent Motif (PAM) of Cas9 on the *c-JUN* sequence is highlighted in green.

sgRNA description	Sequence Forward Oligo	Sequence Reverse Oligo
Guide 1 (G1)	CACCGCCGTCCGAGAGCGGACCTTA	AAACTAAGGTCCGCTCTCGGACGGC
Guide 12 (G12)	CACCGTTGAGGGCATCGTCATAGA	AAACTCTATGACGATGCCCTCAAC
Guide 14 (G14)	CACCGCACCTCCGCGCCAAGAACT	AAACAGTTCTTGGCGCGGAGGTGC
	(target sequence) (overhang necessary to clone target sequence into vector)	
	(G:C base-pair added to target sequence to improve U6 promoted transcription)	

### 2.5.5 Cloning of *c-JUN* sgRNA into the lentiCRISPR v2 vector

For cloning of sgRNAs the ZhangLab protocol “Target Guide Sequence Cloning Protocol” (Shalem et al. 2014; Sanjana, Shalem, and Zhang 2014) available from Addgene was followed. *c-JUN* guide RNAs were cloned into the lentiCRISPR v2 vector. lentiCRISPR v2 was a gift from Feng Zhang (Addgene plasmid # 52961 ; <http://n2t.net/addgene:52961> ; RRID:Addgene\_52961) (Sanjana, Shalem, and Zhang 2014) (Figure M5). The vector was digested with BsmBI (R0739; New England Biolabs, USA) and the digested vector was separated from the filler by gel electrophoresis. The digested vector was purified from the gel using the NEB DNA gel extraction kit (T1020S; New England Biolabs). Finally, the vector was ligated with annealed and phosphorylated oligos using the NEB Quick Ligation Kit (M2200; New England Biolabs).

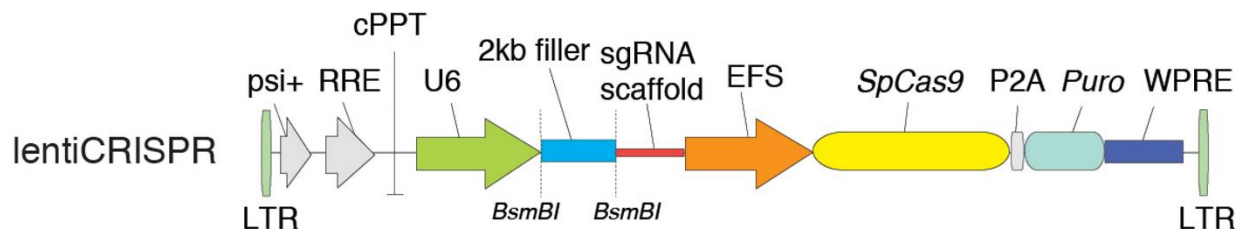


**Figure M5. Schematic image of the cloning vector lentiCRISPR v2.** This image shows all major components of the lentiCRISPR v2 vector (Shalem et al. 2014; Sanjana, Shalem, and Zhang 2014). The vector is flanked by long terminal repeats (LTR) and contains a 2 kb filler fragment which is replaced by *c-JUN*-targeting sgRNA during the cloning process. The vector is digested with the restriction enzyme BsmBI and oligos were designed with overhangs specific to the overhang produced by digestion. Transcription of a sgRNA scaffold sequence is required for the binding to SpCas9. The *SpCas9* and a Puromycin resistance gene (*Puro*) are encoded by the vector. The vector contains the U6 and elongation factor-1 $\alpha$  short promoter (EFS) promoter regions. The vector also contains psi packaging signal (psi+), HIV-1 Rev response element (RRE), central polypurine tract (cPPT), 2A self-cleaving peptide (P2A) and a posttranscriptional regulatory element (WPRE). An Ampicillin resistance gene for selection in bacteria is also part of the vector but not shown in this scheme.

### 2.5.6 T7 Endonuclease I Assay

A T7 Endonuclease I assay was performed to confirm whether transfection of lentiCRISPRv2-sgRNA vectors into HEK239 FT cells would disrupt the *c-JUN* gene. CRISPR/Cas9 introduces double strand breaks at the target locus of the sgRNA and these double strand breaks are repaired by nonhomologous end-joining (NHEJ). However, DNA repair by NHEJ is not fully efficient and base-pairs can be mismatched. The T7 endonuclease cuts DNA at mismatched base-pairs and can therefore be used to verify the disruption of genes by CRIPR/Cas9. Primers were designed to produce a 961 bp amplicon flanking the target sites of the sgRNAs G1, G12 and G14. 200 ng DNA from transfected HEK239 FT cells was used to amplify the *c-Jun* allele using Q5 High-Fidelity

DNA Polymerase (M0491; New England Biolabs). To confirm successful amplification 5  $\mu$ l of each reaction were used for a gel electrophoresis prior to the T7 digestion. 5  $\mu$ l of NEBuffer 2 (B7002; New England Biolabs) were added to the remaining PCR product and a thermocycling program allowing heteroduplex formation was applied. 25  $\mu$ l of each reaction were either mixed with 1  $\mu$ l of T7 Endonuclease I (E3321 New England Biolabs) or 1  $\mu$ l of nuclease free water as control. Samples were incubated at 37 °C for 30 min. Samples were mixed with loading dye and gel electrophoresis was performed on a 1.5 % agarose gel.

### Primers used for T7 assay PCR

Primer name	Sequence	Target gene	Amplicon length	Reference sequence
c-JUN_T7 Fw	GGAGACAAGTGGCAGAGTCC	<i>c-JUN</i>	961 bp	ENSG00000177606
c-JUN_T7 Rv	GAAGCCCTCCTGCTCATCT			

### PCR Master Mix

	f.conc.
5 $\times$ Q5 Reaction Buffer (M0491S; New England Biolabs)	1 $\times$
10 mM dNTPs	200 $\mu$ M
10 $\mu$ M c-JUN_T7 Fw	0.5 $\mu$ M
10 $\mu$ M c-JUN_T7 Rv	0.5 $\mu$ M
Template DNA	~200 ng
Q5 HF DNA Polymerase (M0491S; New England Biolabs)	0.02 U/ $\mu$ l
Nuclease-free water	

### PCR- program

Step	Temperature	Time
Denaturation	98 °C	30 sec
Cycle 35 $\times$	98 °C	10 sec
	68 °C	15 sec
	72 °C	30 sec
Elongation	72 °C	2 min
Hold	4 °C	$\infty$

### T7 heteroduplex formation thermocycling

Step	Temperature	Time
Denaturation	95 °C	10 minutes
Heteroduplex formation	85 °C	ramp rate 0.1 °C/sec
	75 °C	ramp rate 0.1 °C/sec
	65 °C	ramp rate 0.1 °C/sec
	55 °C	ramp rate 0.1 °C/sec
	45 °C	ramp rate 0.1 °C/sec
	35 °C	ramp rate 0.1 °C/sec
	25 °C	ramp rate 0.1 °C/sec
Hold	4 °C	10 min
Hold	10 °C	$\infty$

### 2.5.7 Sequence validation by TIDE Assay

The clonality of single clones of transduced cell lines was validated by Tracking of Indels by DEcomposition (TIDE) assay. The TIDE assay was used to analyze the editing efficacy of the CRISPR/Cas9 KO and to determine predominant insertions and deletions from Sanger sequencing data (Brinkman et al. 2014). For sequencing, a region between 500 and 1500 bp surrounding the sgRNA target site has to be amplified. Sequencing primers should be placed ~200 bp downstream of the sgRNA target site. Amplification primers and sequencing primers were designed according to these guidelines. 200 ng extracted DNA were used to amplify the *c-JUN* allele using Q5 High-Fidelity DNA Polymerase. The TIDE assay amplification primers “c-JUN\_amp” forward (Fw) and reverse (Rv) flanking the sgRNA target sites on the *c-JUN* allele were used for amplification. To confirm amplification 5 µl of each reaction were used for gel electrophoresis. The remaining reaction was cleaned up using the Monarch PCR & DNA Cleanup Kit (5 µg) (T10305; New England Biolabs) according to the manual. Cleaned up amplicons were Sanger sequenced using two different sequencing primers, one primer for TIDE assay of sgRNA G1 and G12 transduced cell lines (c-JUN\_seq Fw5) and one primer for sgRNA G14 transduced cell lines (c-JUN\_seq Fw6). To obtain control sequences for TIDE analysis, empty vector control single clones were sequenced using both sequencing primers in two separate sequencing reactions. Prepared sequencing reactions were sent to Microsynth for Sanger sequencing. For TIDE analysis the TIDE Web tool at “www.tide.deskgen.com” was used (Brinkman et al. 2014).

#### Primers used for PCR

Primer name	Sequence	Target gene	Amplicon length	Reference sequence
c-JUN_amp Fw	AGTGAGTGACCGCGACTTTT	<i>c-JUN</i>	968 bp	ENSG00000177606
c-JUN_amp Rv	GTCTGAGGCTCCTCCTTCAG			
c-JUN_seq Fw5	CGCGAGTCGACAAGTAAGAG	<i>c-JUN</i>	na.	ENSG00000177606
c-JUN_seq Rv6	GTGTCCCCCGCTTGC	<i>c-JUN</i>	na.	ENSG00000177606

#### c-JUN amplification PCR Master Mix

	f.conc.
5 × Q5 Reaction Buffer (M0491S; New England Biolabs)	1 ×
10 mM dNTPs	200 µM
10 µM c-JUN_amp Fw	0.5 µM
10 µM c-JUN_amp Rv	0.5 µM
Template DNA	~200 ng
Q5 HF DNA Polymerase (M0491S; New England Biolabs)	0.02 U/µl
Nuclease-free water	

**PCR- program**

Step	Temperature	Time
Denaturation	98 °C	30 sec
Cycle 35 ×	98 °C	10 sec
	68 °C	15 sec
	72 °C	30 sec
Elongation	72 °C	2 min
Hold	4 °C	∞

**2.6 Work with RNA****2.6.1 Total RNA Isolation from prostate samples**

For total RNA isolation from *in-vivo* prostate samples, the ReliaPrep RNA Tissue Miniprep System (Z6111; Promega Corporation, USA) was used. Prior to the experiment RNase AWAY (10666421; Thermo Fisher Scientific) was used to clean all the work benches and devices used. ~25 mg of RNAlater treated snap-frozen prostate tissue were homogenized in 300 µl of TRI Reagent Solution (T9424 Merck) with the tissue homogenizer IKA T10 standard (IKA\_3002; IKA Werke, DE). The tissue homogenizer head was cleaned with milli-q H2O, 70% EtOH and 1 × PBS in this order between sample processing steps. 700 µl of TRI Reagent Solution were added and homogenized samples were incubated at RT for 5 min. After adding 100 µl 1-bromo-3-chloropropane (BCP) (B9673; Merck), reaction tubes were vortexed thoroughly. Samples were centrifuged at 21000 × g for 30 min at 4 °C after incubation at RT for 15 min. The aqueous supernatant was transferred to a fresh 2 ml reaction tube and 70% EtOH equivalent to 1.5 × the supernatant volume was mixed with the sample by vortexing. 700 µl of this suspension were transferred to a ReliaPrep Minicolumn mounted into a collection tube and column was centrifuged at 14000 × g for 1 minute at RT. The flow through was discarded. This step was repeated until the entire suspension volume had been transferred over the column. 500µl of RNA Wash Solution were added to the column and the column was centrifuged at 14000 × g for 30 seconds at RT. Flow-through was discarded. DNAase I incubation mix was prepared by mixing 24 µl of Yellow Core Buffer, 3 µl of 0.09M MnCl<sub>2</sub> and 3 µl of DNase I enzyme. Reagents were mixed by pipetting. 30 µl of DNAase I incubation mix were directly pipetted to the membrane of the column. After 15 min of incubation at RT, 200 µl of column wash solution were added to the column and the column was centrifuged at 14000 × g for 30 seconds at RT. 500 µl of RNA Wash Solution were added to the column and the centrifugation step was repeated. After transferring the column into a fresh collection tube 300 µl of RNA Wash Solution were added to the column and the column was

centrifuged at  $21000 \times g$  for 2 min at RT. The column was transferred to a 1.5 ml safe seal reaction tube and 25  $\mu$ l of nuclease-free water were directly pipetted to the membrane of the column. After incubation at RT for 1 min, the column was centrifuged at  $14000 \times g$  for 1 min at RT. The flow through was transferred back into the column and the centrifugation step was repeated. Samples were stored at  $-80 \text{ }^{\circ}\text{C}$  until further use.

### 2.6.2 RNA quality testing and cDNA synthesis

RNA concentration was measured using a DeNovix DS-11 FX+ nanophotometer (31DS-11FXPLUS DeNovix, USA). The Agilent 4200 TapeStation system (G2991AA; Agilent Technologies, USA) was used to determine quality of RNA measured in RNA integrity number values (RIN values). 1  $\mu$ l of sample was diluted to a concentration between 100 to 300 ng/ $\mu$ l. 1  $\mu$ l of diluted sample was mixed with 5  $\mu$ l of RNA ScreenTape Sample Buffer (5067-5577; Agilent Technologies) by vortexing for 1 min. After 3 min incubation at  $72 \text{ }^{\circ}\text{C}$ , samples were incubated on ice for 2 min. Samples were analyzed in the TapeStation system using RNA ScreenTape (5067-5576; Agilent Technologies). All samples with a RIN value below 6 were excluded from further steps. 1  $\mu$ g of RNA was converted into cDNA using the iScript cDNA Synthesis Kit (1708890; Bio-Rad Laboratories). 4  $\mu$ l of  $5 \times$  iScript buffer, 1  $\mu$ l of reverse transcriptase and 1  $\mu$ g of RNA sample were pipetted into a PCR reaction tube. The reaction was filled to a volume of 20  $\mu$ l with nuclease-free water. The tube was gently mixed by flicking the tube. cDNA synthesis was performed using a Master Cycler Pro Device (EPPE6324000.516; Eppendorf, DE). The reaction product was diluted five-fold with nuclease-free water and cDNA samples were stored at  $-20 \text{ }^{\circ}\text{C}$  until further use.

#### Thermo cycle for iScript cDNA synthesis

Step	Temperature	Time
Priming	$25 \text{ }^{\circ}\text{C}$	5 min
DNA synthesis	$46 \text{ }^{\circ}\text{C}$	20 min
Enzyme inactivation	$95 \text{ }^{\circ}\text{C}$	1 min
Hold	$4 \text{ }^{\circ}\text{C}$	$\infty$

### 2.6.3 RT-qPCR

Prostate cDNA samples were used for quantitative real-time PCR (RT-qPCR) experiments. Standards were produced by pooling the entire set of samples and generating dilutions of 1:2, 1:4, 1:8, 1:16 and 1:32 using nuclease free water. 100  $\mu$ M primer stock solution of Fw and Rv primer were mixed in equal amounts and diluted 1:5 with nuclease free water to produce a 10  $\mu$ M primer

mix working solution. Samples, standards and water control were pipetted in duplicates on a 384-well plate at a volume of 2.5  $\mu$ l/per reaction. 10  $\mu$ l of master mix were added to each well. PCR was performed on a ViiA 7 Real-Time PCR System (4453536; Thermo Fisher Scientific).

### Primers used for RT-qPCR

Primer name	Sequence	Target gene	Amplicon length	Reference sequence
mRT Jun FW	TTGAAAGCGCAAACTCCGA	c-Jun	116 bp	ENSG00000177606
mRT Jun RV	GTTAGCATGAGTTGGCACCC			
mPtenEx5_fw	TGGGGAAGTAAGGACCAGAG	Pten	191 bp	ENSMUSG00000013663
mPtenEx5_rv	GGCAGACCACAACTGAGGA			
mRT p16 FW	CCGCTGCAGACAGACTGG	p16 <sup>INK4a</sup>	132 bp	ENSG00000147889
mRT p16 FV	CCATCATCATCACCTGAATCG			

### RT-qPCR Master Mix

	f.conc.
2 $\times$ Biozym Blue S'Green qPCR Kit Master Mix (331416S; Biozym Biotech Trading)	1 $\times$
10 $\mu$ M Fw & Rv primer mix	0.77 $\mu$ M
Nuclease free water	

### PCR- program for RT-qPCR

Step	Temperature	Time
Denaturation	95 $^{\circ}$ C	2 min
Cycle 40 $\times$	95 $^{\circ}$ C	5 sec
	60 $^{\circ}$ C	30 sec
Melt curve	95 $^{\circ}$ C	ramp rate 0.05 $^{\circ}$ C/sec

### 2.6.4 RNA sequencing

Sample collection, MACS and Library preparation for the RNA-seq experiments was performed by Tanja Limberger and Sabine Lagger.

#### Single cell preparation and MACS sorting

For RNA sequencing five animals of each *Control*, *Pten<sup>Δ/Δ</sup>* and *Pten<sup>Δ/Δ</sup>;c-Jun<sup>Δ/Δ</sup>* were used as biological replicates. ~150 mg of prostate tissue were cut into pieces in a small cell culture dish filled with PBS. Samples were transferred into a 15 ml reaction tube followed by centrifugation at 150  $\times$  g for 5 min. Supernatant was removed and pellet resuspended in 1 ml of advanced DMEM (adDMEM) (12634010; Thermo Fisher Scientific) supplemented with 5 mg/ml of collagenase II (17101015; Thermo Fisher Scientific) and 10  $\mu$ M Y-27632 (HY-10583; MedChemexpress, USA) in a 1.5 ml reaction tube. Digestion was performed for 2 h at 37  $^{\circ}$ C shaking at 800 rpm with repeated dissociation by pipetting every 20 min. Centrifugation at 150  $\times$  g for 5 min followed. Supernatant was removed and the pellet was dissolved in 1 ml of TrypLE (12605010; Thermo Fisher Scientific)

supplemented with 10  $\mu$ M Y-27632 followed by incubation at 37 °C for 15 min shaking at 800 rpm. Suspension was passed through a 40  $\mu$ m cell strainer followed by washing twice with 2 ml of MACS buffer consisting of 1  $\times$  PBS and 2 mM EDTA and 2 % FBS.

The suspension was then centrifuged at 150  $\times$  g for 5 min, the supernatant was discarded and the pellet was resuspended in 1 ml MACS buffer. This suspension was passed 5 times through a 27G syringe followed by centrifugation at 150  $\times$  g for 5 min and resuspension of the pellet in 200  $\mu$ l MACS buffer in a fresh 1.5 ml reaction tube. 100 mg of anti-mouse CD326 (EpCAM) antibody (13-5791-82; Thermo Fisher Scientific) were added and pulse vortexed five times followed by RT incubation for 10 min. 1 ml of MACS buffer was added and centrifugation at 300  $\times$  g for 5 min and discarding of supernatant, resuspension in 200  $\mu$ l MACS buffer and transfer into a 12  $\times$  75 mm FACS tube followed. 60  $\mu$ l of positive selection bead solution (MSPB-6003-71; Thermo Fisher Scientific) were mixed with the suspension by vortex pulsing five times. An incubation at RT for 10 min was followed by washing with 2.5 ml of MACS buffer and mixing by pipetting. The tube was inserted into a magnetic tube holder and incubated for 5 min at RT. The unbound fraction was discarded and the bound fraction was washed by resuspending in 5 ml of MACS buffer pelleting at 300  $\times$  g for 5 min followed by resuspension in 100  $\mu$ l of MACS buffer. 5  $\mu$ l of this epithelial cell suspension were removed for FACS quality control. The remaining suspension was pelleted at 300  $\times$  g for 5 min and frozen in liquid nitrogen.

### **RNA isolation and Library Preparation**

RNA isolation was performed by extraction with TRI Reagent Solution (T9424 Merck) and using the ReliaPrep RNA Tissue Miniprep System (Z6111; Promega Corporation) according to manufacturer's instructions. 250 ng of total RNA were used for library preparation with the NEBNext Ultra II Directional RNA Library Prep Kit for Illumina (E7765; New England Biolabs) according to manufacturer's instructions. mRNA enrichment was performed by selection with OligoDT beads. (E7490; New England Biolabs). Libraries were barcoded with dual indexing primers for Illumina (E7600; New England Biolabs) and 11 PCR cycles were used to amplify libraries. Library size was analyzed on the Agilent Tape station or the Bioanalyser DNA 1000 chip (G2938-90014; Agilent Technologies). The quality-controlled libraries were quantified, multiplexed and 75 bp single end reads were generated on three High Seq lanes at the CEITEC Institute of Masaryk University (CZ).

## 2.7 Immunochemistry and histological methods

### 2.7.1 Protein lysates from prostate tissue

All steps were performed on ice. To prepare lysis buffer 1 ml of RIPA buffer (R0288; Merck) was mixed with 10  $\mu$ l of 100x PMSF (100 mM), 20  $\mu$ l of 50  $\times$  cOmplete Mini Protease Inhibitor (11836153001; Roche) and 50  $\mu$ l of 20  $\times$  PhosSTOP (4906845001; Roche). For each prepared sample 250  $\mu$ l of lysis buffer were pipetted into a 2 ml reagent tube. 50-80 mg of prostate tissue were suspended in 250  $\mu$ l of lysis buffer using a tissue homogenizer IKA T10 standard. Tissue was homogenized for 30-90 seconds. Homogenizer was cleaned in between samples by rinsing with milli-q H<sub>2</sub>O, 70% EtOH and 1  $\times$  PBS, in this order. Foam was cleared by short centrifugation and suspension was transferred to a fresh 1.5 ml reaction tube. Samples were centrifuged at 21000  $\times$  g for 30 minutes at 4°C. Aqueous supernatant was transferred into a new 1.5 ml reaction tube, not disrupting the pellet or the fat layer on top. The centrifugation step was repeated and supernatant was again transferred into a new 1.5 ml reaction tube. The protein lysates were stored at -80°C until further use.

### 2.7.2 Protein lysates from cell pellets by a freeze and thaw method

All steps were performed on ice. 1 ml of Hunt Buffer was mixed with 10  $\mu$ l of saturated phenylmethylsulfonylfluoride (PMSF) solution (A0999; AppliChem), 20  $\mu$ l of 50  $\times$  cOmplete Mini Protease Inhibitor (11836153001; Roche) and 50  $\mu$ l of 20  $\times$  PhosSTOP (4906845001; Roche). 50  $\mu$ l of Hunt buffer were added to snap frozen cell pellets. After resuspension, samples were snap-frozen in liquid nitrogen. After thawing on ice, samples were again snap-frozen in liquid nitrogen and re-thawed at 37 °C on a thermo shaker. After a third snap-freezing step, samples were centrifuged for 30 min at 21000  $\times$  g at 4 °C. The supernatant was transferred into a new 1.5 ml reaction tube. The protein lysates were stored at -80°C until further use.

### Hunt Buffer p.8.0

	f. conc.
1 M Tris-HCL pH 8.0	20 mM
5 M NaCl	100 mM
0.5 M EDTA	1 mM
NP-40	0.5 %

### 2.7.3 Bradford assay and dilution of protein lysates

Bradford solution was prepared by mixing Protein Assay Dye Reagent Concentrate (500-0006; Bio-Rad Laboratories, USA) in a 1:5 dilution with milli-q H<sub>2</sub>O. For each sample 1 ml of Bradford solution was mixed with 1 µl of protein lysate. A blank was prepared by mixing 1 µl of lysis buffer with 1 ml of Bradford solution. After incubation for 5 min at RT the Bradford solution/lysate-mix was transferred into a plastic cuvette and absorbance was measured at a wavelength of 595 nm using a nanophotometer (P330; Implen). The absorbance value was multiplied by 10 to get a relative protein concentration value in µg/µl.

### 2.7.4 SDS page and WB

#### 2.7.4.1 Casting SDS page gels

##### Conventional SDS gels

Gels were cast in Bio-Rad Mini-Protean cassettes (1653308, 1653311; Bio-Rad Laboratories). First the resolving gel was prepared and pipetted into the cassettes. The resolving gel was overlaid with 70% EtOH and after solidification of the gel (20-30 min), the EtOH was removed completely. A stacking gel was prepared and cast. To generate wells either a 15-well comb or 10-well comb was used. After solidification of stacking gel, the gel was stored wrapped in a wet paper towel at 4 °C for up to 2 weeks until use.

##### **Gel for conventional SDS page of prostate lysates**

	Stacker:	f. conc.	Resolver:	f. conc.
30% acrylamide/bis (1610158; Bio-Rad Laboratories)		4 %		16 %
0.5 M Tris-HCL, pH 6.8		125 mM		
1.5 M Tris-HCL, pH 8.8				375 mM
10% SDS		0.1 %		0.1 %
milli-q H <sub>2</sub> O				
TEMED (161-0800; Bio-Rad Laboratories)		~1:1000*		~1:2000*
10% APS (161-0700; Bio-Rad Laboratories)		0.05 %		0.05 %

\*Dilution of reagent

##### **Gel for conventional SDS page of cell pellet lysates**

	Stacker:	f. conc.	Resolver:	f. conc.
30% acrylamide/bis		4 %		10 %
0.5 M Tris-HCL, pH 6.8		125 mM		
1.5 M Tris-HCL, pH 8.8				375 mM
10% SDS		0.1 %		0.1 %
milli-q H <sub>2</sub> O				
TEMED		~1:1000*		~1:2000*
10% APS		0.05 %		0.05 %

\*Dilution of reagent

**TGX gels**

For total protein normalization the TGX technology was used. A TGX FastCast Acrylamide Kit, 10% (1610173; Bio-Rad Laboratories) was used to cast gels following the product manual.

**Gel for TGX based SDS page of prostate lysates (1 Gel)**

	Stacker:	f. conc.	Resolver:	f. conc.
Resolver A				1 ×
Resolver B				1 ×
Stacker A		1 ×		
Stacker B		1 ×		
TEMED		~1:1000*		~1:2000*
10% APS		0.05 %		0.05 %

\*Dilution of reagent

**2.7.4.2 Denaturation of lysates**

Protein lysates were mixed with 4 × SDS sample buffer in a 1.5 ml safe seal reaction tube and proteins were denatured at 95°C for 3 min on a thermo shaker. After denaturation, samples were immediately transferred to ice.

**4 × SDS sample buffer**

	f. conc.
1 M Tris-HCL, pH 6.8	100 mM
Glycerol (G6279; Merck)	20 %
Bromphenolblue (T116.1; Carl Roth)	0.01 %
β-Mercaptoethanol	0.5 %
20 % SDS	5 %

**2.7.4.3 SDS page and WB on conventional gels**

For SDS page gel cassettes were mounted into a Mini-PROTEAN Tetra System chamber (1658005EDU; Bio-Rad Laboratories). The chamber was filled with 1 × SDS running buffer. The comb of the gel was removed and lysates mixed with 4 × SDS sample buffer were loaded on the gel. For cell pellet lysates a volume equivalent to 20 µg of protein was loaded. For prostate lysates a volume equivalent to 40 µg of protein was loaded. As a protein ladder, 3 µl of Color Prestained Protein Standard, Broad Range (P7712; New England Biolabs) were loaded on gels. The chamber was plugged to a Bio-Rad PowerPac power supply and electrophoresis was performed at constant 25 mA per gel until the loading dye front ran out of the gel chamber (30 to 50 min). After SDS page, gels were removed from the gel chambers. Gel and a nitrocellulose membrane (10600002; General Electric Company, USA) were wet with transfer buffer and sandwiched between two layers of two wet 3 MM filter papers. This sandwich was mounted into the wet transfer system of

the Mini-PROTEAN Tetra System chamber filled with transfer buffer. A cool pack was mounted into the chamber to minimize heat development during transfer. Wet transfer was performed at a constant 100 V for 45 min using a PowerPac HC Power Supply (1645052; Bio-Rad Laboratories). Membranes were incubated with Ponceau S solution (P7170; Merck) for 5 min rocking on a shaker and excess staining solution was removed by shaking the membranes in milli-q H<sub>2</sub>O for about 1 min before imaging with the ChemiDoc XRS+ (1708265; Bio-Rad Laboratories). Ponceau S stain images were produced using the “colorimetric” imaging protocol of the ChemiDoc XRS+ software. Membranes were blocked in 5 % Bovine serum albumin (BSA) blocking solution for 30 min shaking at RT. After rinsing with western wash buffer, membranes were incubated overnight with primary antibody rolling in a 50 ml reaction tube at 4 °C. Primary antibodies were either diluted in 5 % BSA blocking solution or 5 % milk blocking solution according to data sheet. After primary antibody incubation membranes were washed three times shaking in western wash buffer for 10 min. Membranes were incubated in 10 ml of secondary antibody solution for 1 h shaking at RT. Secondary antibody solution was prepared by 1:10000 dilution of secondary antibody with western wash buffer. When using primary antibodies of mouse origin, an anti-mouse secondary antibody (7074; Cell Signaling Technology, UK) was used, when using primary antibodies of rabbit origin, an anti-rabbit secondary antibody (MA1-191-D488; Thermo Fisher Scientific) was used. Secondary antibody solution was discarded and membranes were washed 3 × 10 min in western wash buffer. Membranes were developed for 5 min at RT using Clarity Western ECL Substrate (1705061; Bio-Rad Laboratories) according to manufacturer’s instructions. Western blot (WB) images were produced using the “Chemi” blot protocol of the ChemiDoc XRS+ software. If signal intensity was low, membranes were developed 1 min at RT using Clarity Max Western ECL Substrate (1705062; Bio-Rad Laboratories).

### **Buffers and blocking solutions**

#### **1 × SDS running buffer**

	f. conc.
Glycine (3790.1; Carl Roth)	192 mM
Tris	25 mM
20 % SDS	0.1 %
mili-q H <sub>2</sub> O	

**Transfer buffer**

	f. conc.
Glycine	192 mM
Tris	25 mM
Methanol	10 %
mili-q H <sub>2</sub> O	

**Western wash buffer**

	f. conc.
10 × PBS	1 ×
Tween 20	0.01 %
mili-q H <sub>2</sub> O	

**5 % BSA solution**

	f. conc.
BSA (8076.4; Carl Roth)	5 %
10 × TBS	1 ×
Tween 20	0.1 %
Sodium azide	0.01 %
mili-q H <sub>2</sub> O	

**5 % milk solution**

	f. conc.
BSA	5 %
10 × TBS	1 ×
Tween 20	0.1 %
Sodium azide	0.01 %
mili-q H <sub>2</sub> O	

**2.7.4.4 SDS page and WB on TGX gels**

SDS page and WB on TGX gels were performed following the protocol for conventional gels except for additional TGX specific imaging steps. TGX stain free images were produced from the SDS gel using the “stain free gel” imaging protocol of the ChemiDoc XRS+ software before using the gel for wet transfer. After wet transfer, TGX stain free images were produced from the WB membrane using the “stain free blot” imaging protocol of the ChemiDoc XRS+ software.

**2.6.4.5 List of WB antibodies**

Target protein	Antibody type	Source	Dilution	BSA/milk blocking	Company and CAT No.	Size (kDa)
β- Act	pAb	rabbit	1:1000	BSA	CST 4967	45
β- Tub	mAb	rabbit	1:1000	milk	CST 2128	55
Akt	mAb	rabbit	1:1000	BSA	CST 4691	60
p-Akt	mAb	rabbit	1:2000	BSA	CST 4060	60
c-Jun	mAb	rabbit	1:1000	milk	CST 9165	43.5
p-c-Jun	mAb	rabbit	1:1000	BSA	CST 9165	43.5
p16 <sup>INK4a</sup>	mAb	rabbit	1:2000	BSA	ab 211542	16

### 2.7.5 Immunohistochemistry

Prostate FFPE samples were sectioned at 10  $\mu\text{m}$  using a microtome and fixed on Superfrost slides by Petra Kodajova. Immunohistochemistry (IHC) staining was performed by Michaela Schleder. Slides were incubated in an incubator at 56°C for ~1.5 h to melt the paraffin. Paraffin was removed and sections were re-hydrated by rinsing 2  $\times$  in xylene, 4  $\times$  in 100 % EtOH, 1  $\times$  96% EtOH, 1  $\times$  70% EtOH, 1  $\times$  5 % EtOH and 2  $\times$  distilled H<sub>2</sub>O in this order. Antibody retrieval was performed using pH 6.1 citrate buffer (S169984-2; Agilent Technologies, USA) and incubating at 121 °C for 40 min in an autoclave or using pH 9.0 Tris/EDTA (S236784-2; Agilent Technologies) and incubating at ~100 °C for 1 h in a steaming device. After letting the slides cool for ~30 min, slides were washed 3-5  $\times$  in 0.25 % Tween PBS solution (TPBS) while shaking. Liquid blocker was applied to the slides. All blocking and incubations steps were performed using a humid chamber to keep slides from drying out. Endogenous peroxidase was blocked by incubating with 80-120  $\mu\text{l}$  of 3 % H<sub>2</sub>O<sub>2</sub> solution for 10 min at RT. Slides were washed 3-5  $\times$  in TPBS solution. Endogenous biotin was blocked with 80-120  $\mu\text{l}$  of avidin solution from Avidin/Biotin Blocking Kit (SP-2001; Maravai Life Sciences, USA) for 10 min at RT. Slides were washed 3-5  $\times$  in TPBS solution. Samples were blocked for 7 min at RT with 80-120  $\mu\text{l}$  of superbloc (IDST1007; ID Labs, CA). Slides were washed 3-5  $\times$  in TPBS solution. After blocking at RT for 1 h in 80-120  $\mu\text{l}$  of mouse block (MKB-2213; Maravai Life Sciences), samples were washed 3-5  $\times$  in TPBS solution. Samples were incubated overnight at 4 °C with 80-120  $\mu\text{l}$  of primary antibody diluted in 1 % BSA PBS solution. Slides were washed 3-5  $\times$  in TPBS solution. After 10 min of incubation at RT in 80-120  $\mu\text{l}$  of secondary antibody (IDST1007; ID Labs), slides were washed 3-5  $\times$  in TPBS solution. Slides were incubated with 80-120  $\mu\text{l}$  of HRP enzyme complex (IDST1007; ID Labs) for 10 min at RT and then washed 3-5  $\times$  in TPBS solution. Slides were developed using 80-120  $\mu\text{l}$  of HRP of the AEC substrate KIT (SK-4200; Maravai Life Sciences). The reaction was stopped in tap water. Counterstaining was performed for 30-60 sec in hematoxylin solution. Slides were washed 3-5 times in tap water and then embedded using Aquatex mounting medium (108562; Merck).

#### 2.7.5.1 List of IHC antibodies

Target protein	Antibody type	Source	Dilution	Company and CAT No.
c-Jun	mAb	rabbit	1:300	CST 9165
Ki67	mAb	rabbit	1:400	CST 9129
CC3	pAb	rabbit	1:200	CST 9661

### 2.7.6 H&E staining

FFPE samples were sectioned at 10  $\mu\text{m}$  using a microtome and fixed on slides by Petra Kodajova. Slides were incubated in an incubator at 60°C for about 30 min to melt the paraffin. Paraffin was removed by 10 min incubation in 96 % Limonene (ORT-5000-96-1; SAV Liquid Production, DE). Slides were rinsed 3  $\times$  in 100 % EtOH and 2  $\times$  in 96 % EtOH, tap water and mili-q H<sub>2</sub>O. After 10 min incubation in hematoxylin solution, slides were rinsed 1  $\times$  in tap water and 3  $\times$  in HCL-ethanol solution. Samples were washed under running tap water for 10 min and then rinsed with mili-q H<sub>2</sub>O. Slides were rinsed 3  $\times$  in eosin solution and then rinsed in tap water. After dehydration by rinsing 1  $\times$  in 96 % EtOH, 2  $\times$  in 100 % EtOH and 5 min incubation in 96 % Limonene, slides were mounted using Eukitt Quick-hardening mounting medium (03989; Merck).

#### Hematoxylin solution

	f.conc.
Hematoxylin	0.65 %
Potassium aluminium sulfate	0.95 %
Glycerol	~ 1:3 diluted
96 % EtOH	~ 1:3 diluted
mili-q H <sub>2</sub> O	
100 % Acetic acid	3.23 %

Solution was matured at RT in the dark for about 6 months

#### Eosin solution

	f.conc.
Eosin G	1 %
70 % EtOH	70 %
100 % Acetic acid	0.33 %

#### HCL-Ethanol solution

	f.conc.
70 % EtOH	70 %
37 % HCL	1 %

### 2.7.7 C<sub>12</sub>FDG staining based senescence FACS

Sample preparation, C<sub>12</sub>FDG staining, antibody staining and senescence FACS experiment were performed by Christina Sternberg.

#### Preparation of single cell suspension

For this experiment prostate samples from ~19 week old animals of the genotypes *Control*, *c-Jun <sup>$\Delta/\Delta$</sup>* , *Pten <sup>$\Delta/\Delta$</sup>*  and *Pten <sup>$\Delta/\Delta$</sup> ;c-Jun <sup>$\Delta/\Delta$</sup>*  were used. ~30  $\mu\text{g}$  of fresh prostate sample were cut into pieces in 3 ml of 1  $\times$  PBS. Prostate pieces in PBS were transferred into a 15 ml reaction tube.

The tube was centrifuged at  $150 \times g$  for 5 min and the supernatant was discarded. 500  $\mu$ l of adDMEM supplemented with 10 mM HEPES (15630056; Thermo Fisher Scientific), 1  $\times$  Penicillin-Streptomycin solution (15140122; Thermo Fisher Scientific), 1  $\times$  GlutaMAX Supplement (35050061; Thermo Fisher Scientific), 5 mg/ml of collagenase II (17101015; Thermo Fisher Scientific) and 10  $\mu$ M Y-27632 (HY-10583; MedChemexpress) were used to resuspend the pellet. Suspension was transferred into a 1.5 ml reaction tube and incubated at 37  $^{\circ}$ C for 2 h shaking. During incubation suspension was mixed every 30 min. Suspension was centrifuged at  $300 \times g$  for 5 min and supernatant was discarded. Pellet was resuspended in 500  $\mu$ l of TrypLE (12605010; Thermo Fisher Scientific) supplemented with 10  $\mu$ M Y-27632. Suspension was incubated at 37  $^{\circ}$ C for 15 min shaking. Solution was passed through a 40  $\mu$ m cell strainer (CLS431750; Merck) into a 50 ml reaction tube and the strainer was rinsed two times with 2 ml PBS. Solution was transferred into a 15 ml reaction tube. After centrifugation at  $150 \times g$  for 5 min, the supernatant was discarded. Pellet was resuspended in 500  $\mu$ l of PBS and the solution was passed five times through a 27G syringe needle. 2  $\mu$ l of suspension were used for cell counting in a CASY Cell Counter & Analyzer (5651736; Omni Life Science, DE).

### **C<sub>12</sub>FDG staining**

A cell suspension equivalent to  $2 \times 10^6$  cells was transferred into a fresh 1.5 ml reaction tube and centrifuged at  $300 \times g$  for 5 min. Supernatant was discarded and the pellet was resuspended in 500  $\mu$ l of adDMEM supplemented with 100 nM Bafilomycin A1 (B1793; Merck), 1 mM Nicotinamide (N0636; Merck), 1.25 mM N acetylcysteine (A9165; Merck), 1 nM DHT (A8380; Merck), 200 nM A 83-01 (2939; Tocris Bioscience, GB), 500 ng/ml hEGF (100-15; PeproTech, USA), 1  $\times$  B27 (17504044; Thermo Fisher Scientific) and 10  $\mu$ M Y-27632. This adDMEM solution was also used to dilute a 20 nM C<sub>12</sub>FDG (D2893; Thermo Fisher Scientific) in DMSO stock solution to a 2 mM solution. Suspension was transferred into a 24-well plate and incubated for 2 h at 37  $^{\circ}$ C. Cells were resuspended every 30 min during incubation. 8.3  $\mu$ l of 2 mM C<sub>12</sub>FDG solution was added to reach an end concentration of  $\sim 33 \mu$ M C<sub>12</sub>FDG. Suspension was transferred into a fresh 1.5 ml reaction tube and centrifuged at  $300 \times g$  for 5 min at 4  $^{\circ}$ C. Supernatant was removed and pellet was resuspended in FACS buffer consisting of 1  $\times$  PBS supplemented with 2 mM EDTA and 2 % FBS. The centrifugation step was repeated.

### **Antibody staining and FACS**

Supernatant was removed and the pellet was resuspended in 100  $\mu$ l FACS buffer supplemented with 1.25 ng/ml anti-mouse PE labeled EpCAM antibody (12-5791-82; Thermo Fisher Scientific) and 3  $\mu$ g/ml of anti-mouse APC labeled CD45 antibody (130-102-544; Miltenyi Biotec, DE). This suspension was incubated for 30 min at 4 °C in the dark. 1 ml of FACS buffer was added and centrifugation at  $300 \times g$  for 5 min at 4 °C followed. Supernatant was discarded and pellet was resuspended in 500  $\mu$ l of FACS buffer and transferred into a FACS tube. This suspension was supplemented with DAPI in PBS solution to a final concentration of 1  $\mu$ g/ml (D9542; Merck) and used for flow cytometry.

## **2.8 Bioinformatics and statistical testing**

### **2.8.1 Proliferation experiments on transduced human cell lines**

G1, G12 and G14 replicates were considered as the *c-JUN* KO group while eV replicates were the control group. The mean viable cell count for each group was calculated for all time-points. The mean viable cell count at the first measurement time point was set to 1 and mean viable cell counts of later time-points were calculated as fold-changes of this value. Resazurin assay proliferation curves were produced by plotting fold-changes of mean fluorescence intensity units (FIU). The FIU mean of the first time point set to 1 and all following time points were plotted as fold-changes to this value. For both proliferation experiments, *c-JUN* KO and control group fold-changes were compared by an unpaired t-test conducted with GraphPad Prism 8 (version 8.1.1; GraphPad Software, USA).

### **2.8.2 RNA methods**

#### **2.8.2.1 RT-qPCR quantification**

The threshold cycle (cT) of the standard dilutions 1:2, 1:4, 1:8, 1:16 and 1:32 was correlated with arbitrary copy numbers of 1000, 500, 250, 125 and 62.5 total cDNA copies. The mean cT value was calculated from duplicates and cT values were plotted corresponding to the arbitrary copy number assigned to each dilution to produce a standard curve. The curve function of the standard curve was then used to calculate copy numbers for each sample according to the mean cT of duplicates. Calculated copy numbers of target genes were divided by copy numbers of *18S rRNA* or *CypA* for normalization to a house keeping gene.

Relative mRNA expression was determined by setting the normalized mean copy number of the *Control* group to 1 and calculating fold-changes to this value for the other genotypes. The mean normalized copy number of *Pten<sup>Δ/Δ</sup>* group was set as 1 instead if the relative mean copy number of *Control* group was low. After calculating relative mRNA expression values, the results from individual experiments were combined. For group comparison an unpaired t-test was performed using GraphPad Prism 8.

### **2.8.2.2 RNA-seq bioinformatics and software**

Bioinformatic processing of RNA-seq raw data was performed by Jan Oppelt, CEITEC Institute of Masaryk University, using R packages. Quality control was performed with the packages FastQC, MultiQC, minion and swan. Data was pre-processed using the packages setqk, Trimmomatic, FastQC and MultiQC. Read mapping was performed with the packages STAR, Samtools and MultiQC. Mapping was performed using the reference genome “Ensembl GRCm38” with the gene annotation of “Ensembl v91”. Mapped reads were counted using the package featureCounts. Differential gene expression analysis and normalization were performed using edgeR and DESeq2. The significance cut-off for differentially expressed (DE) genes was set at an adjusted p-value of 0.05 for further analyses which used edgeR and DESeq2 data. Gene set enrichment analysis (GSEA) was performed by Monika Oberhuber using R packages. For GSEA the Molecular signature database (MSigDB) gene set collections “Kegg” (Subramanian et al. 2005) “Hallmark” (Liberzon et al. 2015) and “transcription factor target” (Yevshin et al. 2019) were used. The MSigDB can be accessed at “[www.gsea-msigdb.org/gsea/msigdb/index.jsp](http://www.gsea-msigdb.org/gsea/msigdb/index.jsp)”. The significance cut-off for GSEA was set at an adjusted p-value of 0.05.

### **2.8.3 Immunochemistry**

#### **2.8.3.1 WB quantification**

The ChemiDoc XRS+ compatible software Biorad Image Lab (version 6.0.1; Bio-Rad Laboratories) was used to analyze WB images. The “create multichannel image” function of the software was used to overlay images of normalization and target protein WB (Figure M6). For WB of human cell line lysates, housekeeping protein normalization (HPN) was chosen. The normalization image was a WB picture of the housekeeping protein  $\beta$ -TUB. For WB of mouse prostate samples, the normalization method total protein normalization (TPN) was chosen. For TPN images of TGX stain free blots or Ponceau S blots were used.

The first lane of the normalization image was specified as the normalization lane to calculate the normalization factor relative to this lane. The software is able to calculate normalized band intensity values for each replicate using this normalization factor. Relative protein levels were calculated by setting the mean band intensity value of the *Control* group to 1 and calculating fold-changes to this value. The mean band intensity value of *Pten<sup>Δ/Δ</sup>* group was set as 1 if the *Control* group showed no visible protein expression. To calculate relative protein levels in human cell lines, mean band intensity values of eV replicates were set to 1. An unpaired t-test was performed using GraphPad Prism 8 for comparison of genotype groups.

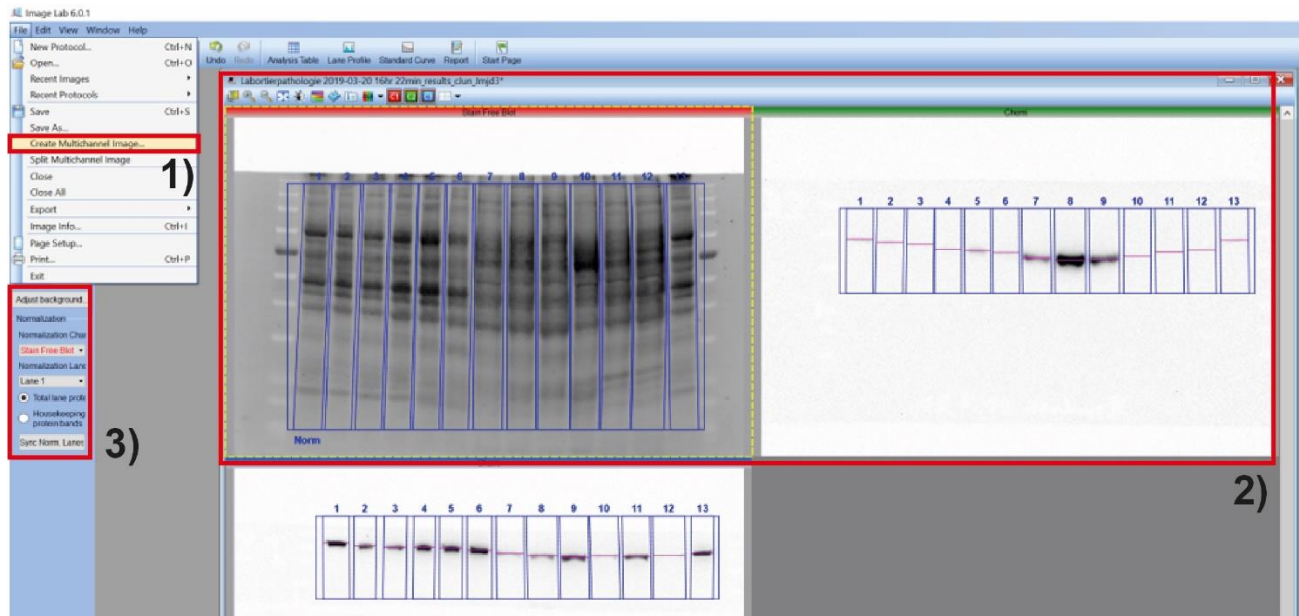


**Figure M6. Image Lab software for protein normalization.** Creation of a multichannel image allows for either total protein normalization or housekeeping protein normalization. This figure shows how multichannel images are created and the available normalization options for the 6.0.1 version of Image Lab. Highlighted are: 1) Option to create multichannel images via drag and drop window. 2) Example of a created multichannel image for total protein normalization. The first image is a stain free blot image. For all lanes a normalization factor is calculated by normalizing them to the total protein of the first lane. 3) Selection of normalization type, normalization image and lane. Available options and layout may vary depending on Image Lab software version.

### 2.8.3.2 Immunohistochemistry quantification

200 × magnification images were taken on an Olympus microscope (BX53; Olympus, JP) for quantitative analysis of c-Jun and Ki67 IHC sections. Three images were taken for each sample from three separate areas of prostate anterior lobe epithelium and up to three additional images were taken from areas of prostate lateral, ventral or dorsal lobe epithelium. Quantification was performed using the ImageJ software Fiji (version 1.52e; public domain).

The plug-ins used for quantification of AEC stained IHC samples were developed by Ursula Reichart, VetCORE, University of Veterinary Medicine Vienna. One plug-in allowed restriction of epithelial regions, stroma regions and excluded areas. Regions containing histological artifacts, cell-free lumen of glands or air bubbles were excluded. The second plug-in allowed for automated quantification. The plug-in characterizes cells by their size and RGB color intensity. Target protein positive cells were identified by the intensity of the brown-red staining which is characteristic for AEC IHC. The analysis only considered cell counts for epithelial cells. A mean target protein positive cell count and a mean total cell count was calculated for each replicate. A ratio of positive to total cells was calculated for each replicate and plotted. The mean ratio of the *Pten<sup>Δ/Δ</sup>* group was set to 1 to calculate relative expression levels. Statistical group comparison was performed by an unpaired t-test using GraphPad Prism 8.

CC3 IHC sections were analyzed semi-quantitatively. A relatively low expression of target protein did not allow for meaningful automated analysis. The epithelium layer of the entire sample area was semi-quantitatively evaluated by the pathologist Sandra Högler. All replicates were classified by one of five different target protein expression levels including no (0), occasional (1), low (2), mediate (3), and high (4) expression. Results were plotted according to genotype group of replicates. Statistical group comparison was performed by a Mann-Whitney-U-Test using GraphPad Prism 8.

### **2.8.3.3 C<sub>12</sub>FDG FACS Gating strategy and calculation**

By gating forward scatter height (FSC-H) versus forward scatter area (FSC-A), single cells were selected by size exclusion for further gating (Figure M7A). DAPI staining (pacific blue channel) specific to non-viable cells allowed for gating of the live cell fraction (Figure M7B). The leukocyte cell fraction was excluded by exclusion of CD45<sup>+</sup> (APC-A labeled) cells (Figure M7C). The epithelial cell fraction was selected for further analysis by gating for EpCAM<sup>+</sup> (PE-A labeled) cells (Figure M7D). This fraction was divided into C<sub>12</sub>FDG<sup>+</sup> (FITC-A labeled) and C<sub>12</sub>FDG<sup>-</sup> cells. For further calculations the percentage of C<sub>12</sub>FDG<sup>+</sup> cells to total epithelial cells for each replicate was plotted in GraphPad Prism 8. Statistical group comparison was performed by an unpaired t-test using GraphPad Prism 8.

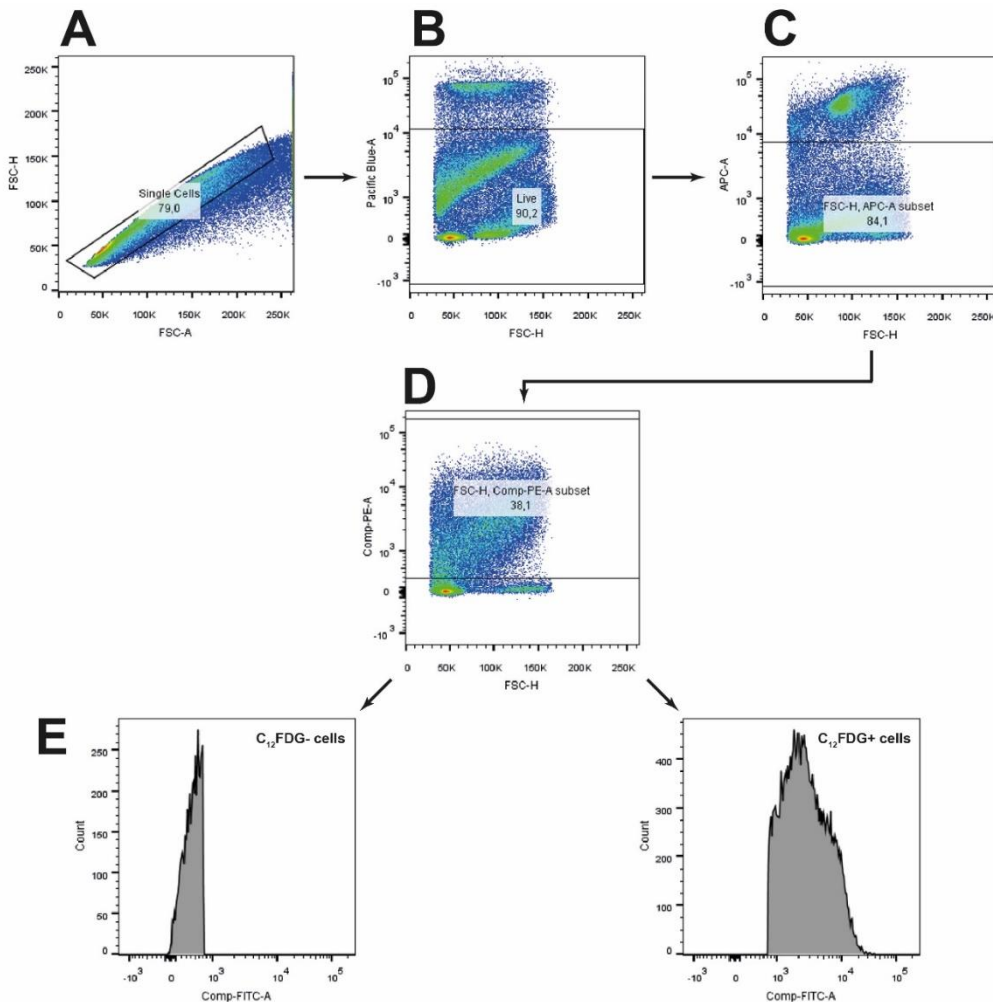


**Figure M7. Gating strategy for  $C_{12}$ FDG based senescence FACS.** (A) Single cell selection via FSC-H versus FSC-A. (B) Selection of live cell fraction via DAPI staining. (C) Selection of CD45 negative cell fraction to exclude leukocytes. (D) Selection of EpCAM positive cell fraction to specifically select epithelial cells. (E) Selection of  $C_{12}$ FDG+ and  $C_{12}$ FDG- cell fractions to distinguish between senescent and non-senescent cells.

## 2.8.4 Survival analysis on publicly available RNA-seq datasets and TMA data

### SurvExpress analysis

The SurvExpress web tool at “[www.bioinformatica.mty.itesm.mx:8080/Biomatec/SurvivaX.jsp](http://www.bioinformatica.mty.itesm.mx:8080/Biomatec/SurvivaX.jsp)” allows for survival analysis and risk assessment on publicly available cancer gene expression datasets (Aguirre-Gamboa et al. 2013). The datasets contain RNA-seq data of tissue biopsies and corresponding survival data of patients. The expression of one or multiple genes of interest is correlated with survival. Two or more risk groups with distinct gene of interest expression are defined by the web tool and Kaplan-Meier survival curves of the risk groups are plotted. A Log-rank test is used for statistical comparison of risk groups. For SurvExpress analysis the publicly available Taylor dataset was used (Taylor et al. 2010). The gene symbol “c-JUN” was entered into

the gene list of the query window (Figure M8A). “Prostate” was selected as tissue type and the database “Taylor MSKCC Prostate” was selected. All remaining selection options remained at default settings and the SurvExpress analysis was started. To correlate survival data with Gleason scores, the stratification method “CLASS:GLEASON” was selected at the result screen (Figure M8B).

**A**

(1) Genes: Symbol (TGFβ1) dropdown menu with 'c-JUN' selected and a count of 1.

(2) Tissue: Radio button selection for various tissues, with 'Prostate (8)' selected and a count of 2.

(3) Database: Table listing databases with columns for #, Database, Samples, Clinical data, and Source. 'Taylor MSKCC Prostate' is selected with 140 samples and source 'Taylor'.

(4) Options: (a) Duplicated genes: Average, Maximum average, Maximum variance, Show all. (b) Data: Original (Quantile-Normalized), Uniformized. (5) Send: 'SurvExpress Analysis' button highlighted.

**B**

SurvExpress - Web resource for Biomarker comparison and validation of Survival gene eXpression data.  
 Dataset: Taylor MSKCC Prostate (dup=mean, data=row)

Design: 2 Fields, Function: Biomarker: Cox Survival Analysis, Add

Feature List: Fields: 4, Columns: 1

General Options: Refresh All, Data, Header

Width: 640, Height: 480, Background: White, Generate PDF: No, Standardize: No, Quantize level: No quantization, NA Imputation: No imputation, Script File (.zip): No

Biomarker: Cox Survival Analysis

Censored: Select..., Risk Groups: 2

Maximize Risk Groups: No, Colors: 2,3,4,5,6,7,8,9

Train Set: [empty], Test Set: [empty]

Stratification: Select... (1), Stratas Separated: No

HeatMap: By Prognostic Index, HeatMap Color: green,black,red

HeatMap Colors: 15, Margins: 5,20

HeatMap Row: [empty], Fitting Information: No

Advanced: [empty], Attribute plot: No

Optional Weights: [empty], Network: None

Other Factors: [empty]

Go, Tutorial, Error/Feedback, No results yet.

2)

**Figure M8. SurvExpress web tool for validation of biomarkers.** (A-B) Overview on steps performed to validate *c-JUN* as a PCA biomarker using the SurvExpress web tool. (A) Query window of analysis tool. Highlighted options are: 1) selection of gene by gene symbol, 2) selection of tissue type 3) selection of RNA-seq databases of specified tissue type available for survival analysis, 4) button to send query. (B) Query result window allows exporting results in PDF format. Additional specifications to adjust generated plots, highlighted options are: 1) selection of a stratification method 2) button to reload results and adopt adjustments.

### **Tissue microarray survival analysis**

Tissue microarrays (TMA) were a gift from Merima Herac and originated from a cohort of patients treated at the Vienna General Hospital (unpublished). Raw data used for plotting of TMA data was provided by Olaf Merkel and Astrid Aufinger. Primary tumor biopsy samples of 63 PCa patients were included in the TMA set. TMAs were IHC stained to evaluate c-JUN protein expression. c-JUN expression was validated semi-quantitatively. Cytoplasm and nuclear expression were characterized by an expression level of 0 (no expression), 1 (low expression), 2 (mediate expression) or 3 (high expression). The individual expression level of cytoplasm and nucleus was added to obtain a c-JUN expression value. 31 samples with no measurable c-JUN expression and 32 samples with low to high expression levels were grouped. A survival curve was plotted for both groups and the groups were statistically compared by a Log-rank test.

#### **2.8.5 Other software**

Primers were designed using the web tool Primer3 at “[www.primer3.ut.ee](http://www.primer3.ut.ee)” (Untergasser et al. 2012; Koressaar and Remm 2007; Kõressaar et al. 2018). Specificity of primers was confirmed via PrimerBLAST at “[www.ncbi.nlm.nih.gov/tools/primer-blast](http://www.ncbi.nlm.nih.gov/tools/primer-blast)”. The NetPrimer webtool at “[www.premierbiosoft.com/netprimer](http://www.premierbiosoft.com/netprimer)” was used to determine if primer pairs form dimers and to exclude primers that form strong dimers. Representative images of IHC and macroscopic prostate images were brightness adjusted, resolution adjusted or cropped using Adobe Photoshop CC (version 20.0.6; Adobe, USA). Figures were created using Adobe Illustrator (version 23.0.6; Adobe).

## 3 Results

### 3.1 Low c-JUN expression correlates with bad prognosis in human PCa

Continued research on c-JUN suggested various tumor-suppressive properties of this AP-1 transcription factor (Eferl and Wagner 2003; Shaulian 2010). These findings are contrary to the common conception within literature of c-JUN being a proto-oncogene. The c-JUN activating c-JUN N-terminal kinase (JNK) has previously been identified as a potent tumor-suppressor in a murine PCa model (Hübner et al. 2012). The JUN family member JUNB which is also activated by JNK has been linked to growth limiting properties in PCa and activation of JUNB may explain the mechanism of JNKs tumor-suppression (Thomsen et al. 2015). However, the effects of c-JUN expression on PCa tumorigenesis have not been explored thoroughly yet.

We first analyzed *c-JUN* expression in human patients to investigate *c-JUN*'s role in PCa (Figure 1). For our first experiment we used a publicly available RNA-seq dataset (Taylor et al. 2011) to generate survival curves with the SurvExpress web tool. By using this tool we were able to classify patients into two risk groups with distinct expression of c-JUN (Figure 1A) (Aguirre-Gamboa et al. 2013). We found significantly decreased *c-JUN* mRNA expression in high-risk patients compared to low-risk patients. Our survival analysis showed a significantly decreased survival ratio of the low *c-JUN* mRNA group at a hazard ratio (HR) of 3.61 (Figure 1B). Gleason scores stratification was performed to determine whether *c-JUN* expression had different effects on high or low grade PCa. We measured significantly decreased survival of Gleason score 6 tumor patients at low *c-JUN* expression with a HR of 6.75 (Figure 1C). For Gleason score 7 tumor patients we observed a trend toward reduced survival in tumors with low *c-JUN* expression at a HR of 2.42, but these findings were not statistically significant (Figure 1D).

In addition to evaluation of transcriptomics data, we analyzed c-JUN protein expression levels in tissue microarrays (TMAs) of human PCa patients by immunohistochemistry (IHC) with a c-JUN antibody. We performed semi-quantitative evaluation of slides by assigning replicates to expression levels ranging from 0 for no expression to 3 for high expression. We proceeded by splitting the 60 patients equally into a high and a low c JUN expression group and correlated this data with survival data of the patients. With a median survival of 66.5 months, we observed a significantly decreased progression free survival within the low c-JUN expression group compared to the high c-JUN expression group which showed a median survival of 115 months (Figure 1E).

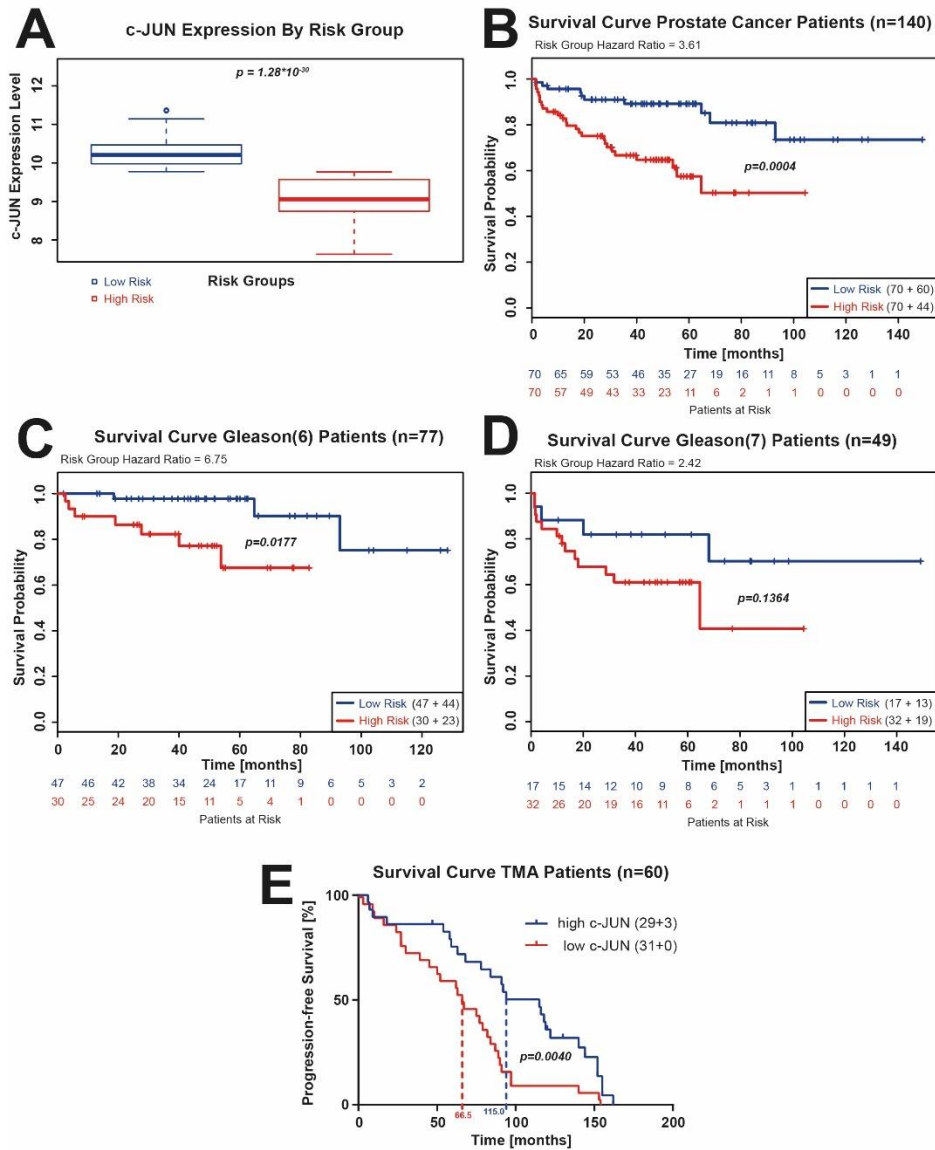


**Figure 1. Low *c-JUN* RNA and protein levels correlate with bad prognosis in human PCa patients.** (A-D) RNA-seq data from a publicly available dataset (Taylor et al. 2011) was analyzed with the SurvExpress web tool (Aguirre-Gamboa et al. 2013). (A) The algorithm classifies patients into two risk groups by high and low *c-JUN* mRNA expression levels. (B) Survival curves of risk groups including data from all patients who participated in the study. Number of total patients included and number of censored patients are displayed in the figure inset. Group comparison was performed via Log-Rank test. Numbers of patients at risk at given time points for both risk groups are listed below the survival curve graph. (C) Survival curves for patients with Gleason Score 6 tumors and patients with Gleason Score 7 tumors (D). (E) Survival curve of 60 PCa patients (data adapted from Olaf Merkel and Astrid Aufinger). Expression data was gained from semi-quantitative analysis of *c-JUN* IHC stained TMAs. Mean survival times are displayed in color. Statistical comparison of survival curves by Log-rank test.

In conclusion, our findings from analyses of publicly available RNA-seq data and TMAs suggest a correlation between low expression of *c-JUN* mRNA and protein with the reduced survival

probability of human PCa patients (Figure 1B-1E). This data suggests that c-JUN acts as a tumor-suppressor in human PCa.

### 3.2 Loss of c-Jun in a PCa *in-vivo* mouse model

Following our findings suggesting that c-JUN acts as a tumor-suppressor in human datasets, we next established an *in-vivo* model to further investigate putative tumor growth modulating properties of *c-Jun*. We therefore used a *Pten* knockout (KO) mouse model widely accepted in PCa research (S. Wang et al. 2003). Previous studies on *Pten* KO mice identified JNK as a tumor-suppressor (Hübner et al. 2012). A *c-Jun* KO in *Pten* KO mice may give insights whether c-Jun contributes to tumor-suppressive JNK signaling. We generated four genotypes of interest by crossbreeding *PB-Cre4* transgenic mice (Xiantuo Wu et al. 2001), animals with floxed *Pten*<sup>Ex4/Ex5</sup> alleles (Suzuki et al. 2001) and mice with floxed *c-Jun* alleles (Behrens et al. 2002). We bred *Control* mice not transgenic for *PB-Cre4* which resulted in wild type mice and the three homozygous KO genotypes *c-Jun*<sup>Δ/Δ</sup>, *Pten*<sup>Δ/Δ</sup> and *Pten*<sup>Δ/Δ</sup>;*c-Jun*<sup>Δ/Δ</sup> (Figure 2A). On the basis of preliminary survival data, we sacrificed animals at 19 weeks of age to ensure progressive tumor growth while minimalizing tumor burden.

To confirm successful KO of *Pten* and *c-Jun* in our mouse model, we used quantitative Real Time PCR (RT-qPCR) on whole prostate RNA extracts of 19-week-old males (Figure 2B-2C). We normalized expression of *Pten* and *c-Jun* to expression levels of the housekeeping genes *18s* rRNA and *Cyclophilin A* (*CypA*) (Figure 2B; left and right images). We calculated the relative expression by either setting the *Control* group or the *Pten*<sup>Δ/Δ</sup> mean to 1 in case the expression levels in the *Control* group were undetectable. Both groups *Control* and *c-Jun*<sup>Δ/Δ</sup> showed similar *Pten* levels whereas *Control* revealed significantly higher levels compared to *Pten*<sup>Δ/Δ</sup> and *Pten*<sup>Δ/Δ</sup>;*c-Jun*<sup>Δ/Δ</sup> thereby confirming deletion of *Pten* in the appropriate genotypes.

We did not detect significant differences in c-Jun expression between *Control* and *c-Jun*<sup>Δ/Δ</sup> while *Pten*<sup>Δ/Δ</sup> and *Pten*<sup>Δ/Δ</sup>;*c-Jun*<sup>Δ/Δ</sup> were significantly different. *Pten*<sup>Δ/Δ</sup>;*c-Jun*<sup>Δ/Δ</sup> showed significantly lower *c-Jun* levels than *Control* and *Pten*<sup>Δ/Δ</sup> confirming the *c-Jun* KO for this genotype. Interestingly, *c-Jun* expression seemed to be highly upregulated in *Pten*<sup>Δ/Δ</sup> prostates indicating that c-Jun may play an important regulative role in tumorigenesis of *Pten*-loss mediated PCa (Figure 2C).

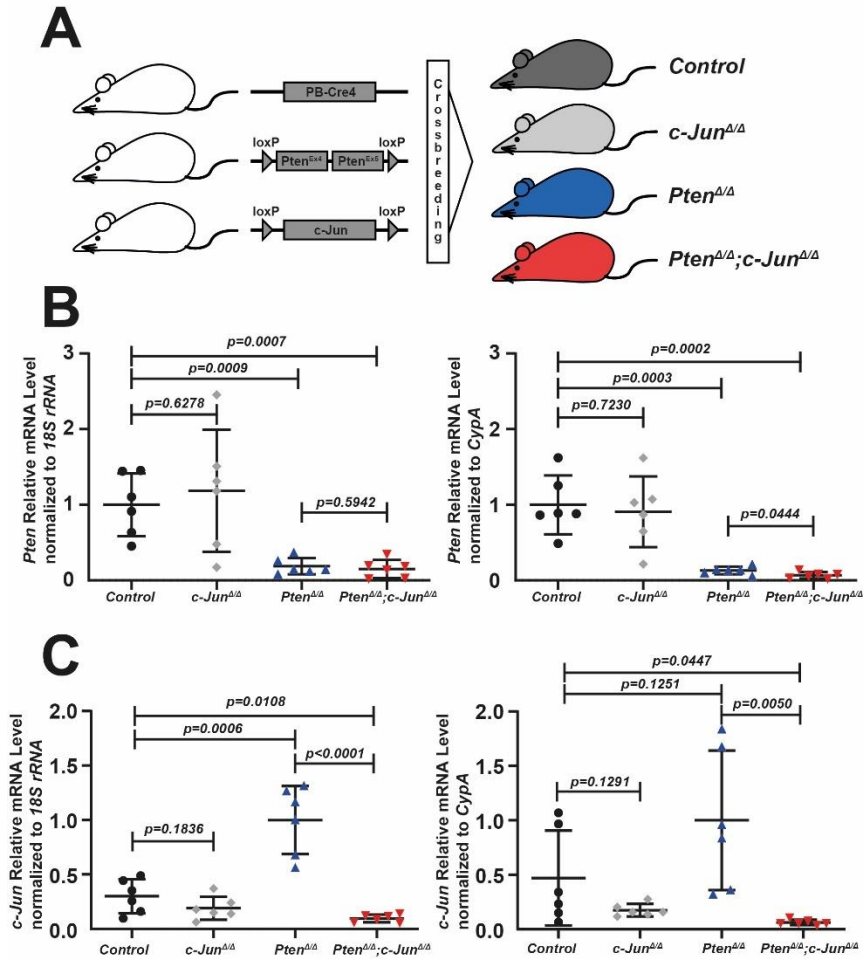


**Figure 2. Prostate specific prostate specific knockout of *Pten* and *c-Jun* by PB-Cre4.** (A) Breeding scheme for KO mouse. Genotypes of interest were generated by crossbreeding *PB-Cre4* transgenic mice (Xiantuo Wu et al. 2001), animals with floxed *Pten<sup>Ex4/Ex5</sup>* alleles (Suzuki et al. 2001) and mice with floxed *c-Jun* alleles (Behrens et al. 2002). This crossbreeding resulted in *PB-Cre4* negative wild type phenotype mice (*Control*) (dark grey), *c-Jun* KO (*c-Jun<sup>Δ/Δ</sup>*) (grey), *Pten* KO (*Pten<sup>Δ/Δ</sup>*) (blue) and *Pten/c-Jun* KO (*Pten<sup>Δ/Δ</sup>;c-Jun<sup>Δ/Δ</sup>*) (red) mice. (B-C) RT-qPCR on whole prostate RNA extracts of 19-week-old animals of the following genotypes: *Control* (n=6), *c-Jun<sup>Δ/Δ</sup>* (n=6), *Pten<sup>Δ/Δ</sup>* (n=6), *Pten<sup>Δ/Δ</sup>;c-Jun<sup>Δ/Δ</sup>* (n=6). *c-Jun* and *Pten* expression levels was normalized to house-keeping genes *18S* rRNA and *CypA*. Groups were statistically compared via two-sided unpaired t-test. (B) Relative expression of *Pten* was determined by setting the mean expression levels of the *Control* group to 1. (C) Relative expression of *c-Jun* was determined by setting the mean expression levels of the *Pten<sup>Δ/Δ</sup>* group to 1.

### 3.3 Mouse model confirmation at the protein level

In addition to KO confirmation of *Pten* and *c-Jun* on the mRNA level we next validated our mouse model on the protein level by Western blotting (WB). Because we did not obtain reliable antibodies for the detection of Pten, we indirectly measured Pten activity by analyzing the phosphorylation and expression status of protein kinase B (Akt) which is part of the pro-proliferative PI3K-Akt signaling pathway. Akt should be constitutively phosphorylated and activated upon loss of *Pten*

(M. S. Song, Salmena, and Pandolfi 2012). For quantification we normalized phospho-Akt (p-Akt) and Akt expression to total protein levels determined by the TGX technology.

We measured a significant increase of p-Akt and total Akt levels in *Pten*<sup>Δ/Δ</sup> and *Pten*<sup>Δ/Δ</sup>;*c-Jun*<sup>Δ/Δ</sup> mice compared to *Control* which indicates an efficient KO of *Pten* (Figure 3B). We performed c-Jun WB to confirm the KO of c-Jun on the protein level. For quantification we normalized phospho-c-Jun (p-c-Jun) and c-Jun expression to the total protein expression which was determined by TGX blotting. We found no significant difference in p-c-Jun nor c-Jun expression between *Control* and *c-Jun*<sup>Δ/Δ</sup> but significantly decreased levels between *Pten*<sup>Δ/Δ</sup>;*c-Jun*<sup>Δ/Δ</sup> and *Pten*<sup>Δ/Δ</sup> prostates (Figure 4A-4B). We measured highly increased p-c-Jun and c-Jun levels in *Pten*<sup>Δ/Δ</sup> compared to the other genotypes (Figure 4A-4B).

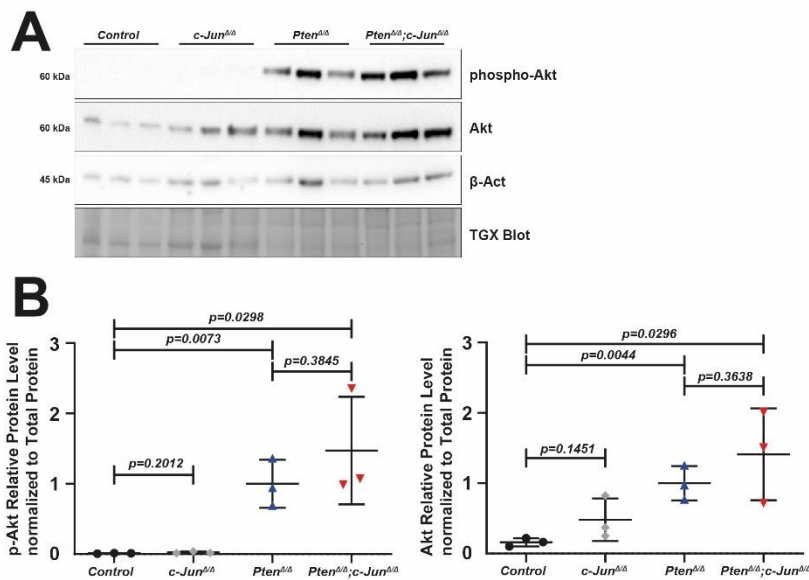


**Figure 3. *Pten* deficiency leads to increased phosphorylation of Akt.** (A-B) WB of whole prostate protein lysates of 19-week-old animals with antibodies against phospho-Akt (p-Akt), Akt and  $\beta$ -Act as a loading control. Genotypes: *Control* (n=3), *c-Jun*<sup>Δ/Δ</sup> (n=3), *Pten*<sup>Δ/Δ</sup> (n=3), *Pten*<sup>Δ/Δ</sup>;*c-Jun*<sup>Δ/Δ</sup> (n=3). Normalization was performed to total protein assessed by TGX blotting. Quantification of relative p-Akt and Akt expression was performed by setting the mean expression levels of the *Pten*<sup>Δ/Δ</sup> group to 1. Groups were statistically compared via two-sided unpaired t-test.

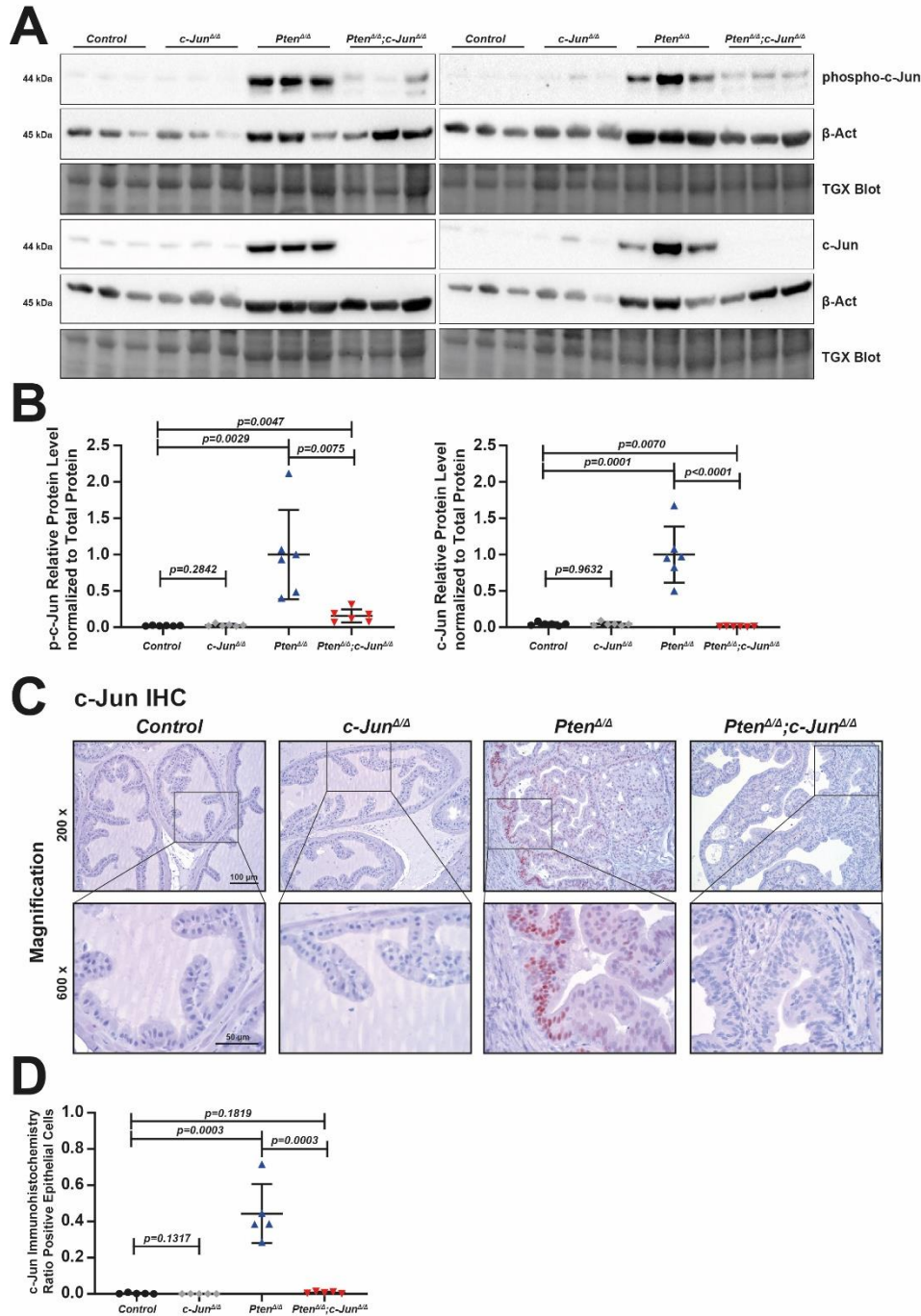


**Figure 4. *Pten* deficiency leads to increased levels of c-Jun.** (A-B) WB of whole prostate protein lysates of 19-week-old animals with antibodies against phospho-c-Jun (p-c-Jun), c-Jun and  $\beta$ -Act as a loading control. Genotypes: *Control* (n=6), *c-Jun* <sup>$\Delta/\Delta$</sup>  (n=6), *Pten* <sup>$\Delta/\Delta$</sup>  (n=6), *Pten* <sup>$\Delta/\Delta$</sup> ;*c-Jun* <sup>$\Delta/\Delta$</sup>  (n=6). Normalization was performed to total protein assessed by TGX blot. Quantification of relative phospho (p)-c-Jun and c-Jun expression was performed by setting the mean expression levels of the *Pten* <sup>$\Delta/\Delta$</sup>  group to 1. (C) c-Jun IHC of FFPE prostate samples from 19-week-old animals. Genotypes: *Control* (n=5), *c-Jun* <sup>$\Delta/\Delta$</sup>  (n=5), *Pten* <sup>$\Delta/\Delta$</sup>  (n=5), *Pten* <sup>$\Delta/\Delta$</sup> ;*c-Jun* <sup>$\Delta/\Delta$</sup>  (n=5). (D) Light microscopy images were quantified with an automated analysis tool measuring total cells and positive cells of the epithelium. Quantification was calculated by dividing positive epithelial cell count with total epithelial cell count. Group comparison was performed with a two-sided unpaired t-test.

We additionally performed c-Jun IHC on formalin fixed paraffin embedded (FFPE) prostates of 19-week-old animals as an additional KO validation. We took multiple representative images from each sample and then used an automated imaging software macro to measure the total amount of c-Jun positive cells in the prostate epithelium. As the anterior prostate lobe developed the largest tumor masses in our model and tumorigenic glands resembled the PCa typical cribriform pattern, we focused our analysis on the anterior lobe (Figure 4C) (Kryvenko and Epstein 2016; Epstein 2018). As already observed in RT-qPCR and WB analyses, IHC confirmed a low base level expression of c-Jun in *Control* non-malignant prostate (Figure 4C). As a result, we did not observe a significant decrease in *c-Jun*<sup>Δ/Δ</sup> (Figure 4C-4D). With notably pronounced c-Jun staining intensity we also reproduced our RT-qPCR and WB findings which indicated highly increased c-Jun expression in the *Pten*<sup>Δ/Δ</sup> group (Figure 4C). We measured significantly decreased c-Jun levels in the *Pten*<sup>Δ/Δ</sup>;*c-Jun*<sup>Δ/Δ</sup> genotype compared to *Pten*<sup>Δ/Δ</sup> which suggests an efficient *c-Jun* KO (Figure 4C-4D).

In conclusion, we confirmed efficient *Pten* and *c-Jun* KO in our PCa mouse model on the RNA and protein level. We additionally found that c-Jun levels were low in non-malignant prostate tissue but were upregulated upon oncogenic transformation in *Pten* KO animals.

### 3.4 c-Jun deficient PCa mice develop aggressive tumors

We continued our research on the murine model by assessing the effects of c-Jun deficiency on tumor burden and survival by morphological and survival analyses. After sacrificing 19-week-old animals of all four genotypes, we measured their body weight and then dissected the prostates. We carefully removed excess fat tissue, the connected bladder and seminal vesicle without disturbing the prostate tissue before measuring the prostate weight. Representative macroscopic images of prostates were taken according to mean prostate to body mass ratios. We did not measure a significant difference in prostate size and prostate to body mass ratio between the *c-Jun*<sup>Δ/Δ</sup> to *Control* genotypes indicating that both groups were protected from malignant transformation (Figure 5A-5B). With significantly increased prostate mass compared to *Control* we found clear tumor development in the *Pten*<sup>Δ/Δ</sup> and *Pten*<sup>Δ/Δ</sup>;*c-Jun*<sup>Δ/Δ</sup> group (Figure 5B). *Pten*<sup>Δ/Δ</sup>;*c-Jun*<sup>Δ/Δ</sup> tumors showed increased mass when compared to *Pten*<sup>Δ/Δ</sup> tumors (Figure 5A-5B). We next stained FFPE slides of prostates with hematoxylin and eosin (H&E) for histological assessment.

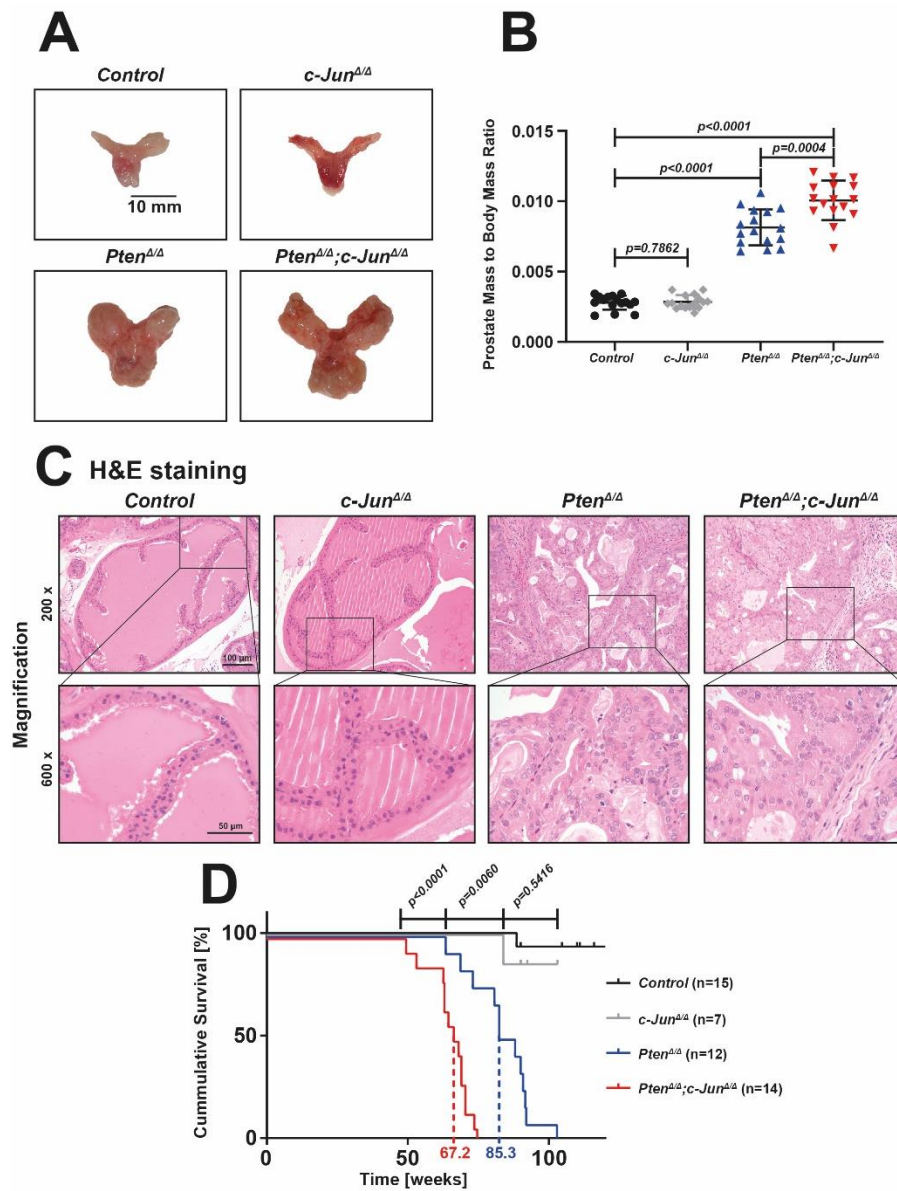


**Figure 5.** *c-Jun* deficiency leads to increased tumor mass and decreased survival in *Pten* KO mice. (A-C) Prostate samples from 19-week-old animals were used to produce representative macroscopic images, tumor mass to body mass plot and histological H&E staining. (A) Representative macroscopic images of prostate from ventral view with size indicator in mm. (B) Prostate mass to body mass ratio of the following genotypes: *Control* (n=16), *c-Jun*<sup>Δ/Δ</sup> (n=16), *Pten*<sup>Δ/Δ</sup> (n=16), *Pten*<sup>Δ/Δ</sup>;*c-Jun*<sup>Δ/Δ</sup> (n=16). Statistical group comparison was performed with a two-sided unpaired t-test. (C) Microscopic images of H&E stained FFPE prostate samples from 19-week-old animals. Representative images show anterior prostate lobe and were taken at magnifications of 200 × and 600 ×. Images were white balance adjusted using Photoshop. (D) Survival plot of Pca mouse model. Animals which died during the experiment are represented as a hit in cumulative survival and animals which were sacrificed past 100 weeks of age were right censored. Mean survival of tumor genotypes is shown at the x axis in color. Group comparison was performed via Log-Rank test.

We found inconspicuous epithelial monolayers in the prostate glands of *Control* and *c-Jun<sup>Δ/Δ</sup>* animals (Figure 5C) whereas both *Pten<sup>Δ/Δ</sup>* and *Pten<sup>Δ/Δ</sup>;c-Jun<sup>Δ/Δ</sup>* prostates contained hyperplastic cribriform glands and revealed clear histological signs of oncogenic transformation. Some of the glands appeared to be fused but overall, the glands remained well-circumscribed in both genotypes suggesting no clear histological difference between *Pten<sup>Δ/Δ</sup>* and *Pten<sup>Δ/Δ</sup>;c-Jun<sup>Δ/Δ</sup>* animals. We surveyed the overall survival in all four genotypes by Kaplan Meier survival analysis. Animals which participated in the survival experiment were maintained until their disease related death or were sacrificed after reaching a humane endpoint according to the guidelines of the 3R principle (Russell, Burch, and Welfare. 1992; Tannenbaum and Bennett 2015). We found no survival differences for the genotypes *Control* and *c-Jun<sup>Δ/Δ</sup>* (Figure 5D) whereas the *Pten<sup>Δ/Δ</sup>* group showed significantly decreased survival with a mean survival of 85.3 weeks compared to *Control*. With a mean survival of 67.2 weeks we measured significantly decreased survival of *Pten<sup>Δ/Δ</sup>;c-Jun<sup>Δ/Δ</sup>* animals when comparing them with *Pten<sup>Δ/Δ</sup>*. Our observations suggest that *c-Jun<sup>Δ/Δ</sup>* develop wild type prostates and that c-Jun deficiency in the *Pten* KO background leads to significantly increased tumor burden which results in significantly decreased survival (Figure 5). These findings support our observations on human data which suggested that c-JUN is a tumor-suppressor in PCa.

### 3.5 c-Jun deficiency does not affect proliferation in a murine PCa model

Our previous findings suggested that c-Jun expression suppresses murine prostate tumorigenesis and therefore our next goal was to determine which mechanisms may be involved in the tumor-suppressive properties of c-Jun (Figure 5). We based our further experiments on the hallmarks of cancer (Hanahan and Weinberg 2011) and investigated how c-Jun could regulate growth and survival of PCa cells. Previous studies suggested that c-Jun modulates hepatocellular tumorigenesis as an important regulator of cell cycle genes and c-Jun has been suggested as a coactivator and repressor of the prostate growth promoting androgen receptor (AR) (Eferl and Wagner 2003; Bubulya et al. 2001; Cai, Hsieh, and Shemshedini 2007). However, there is currently no *in-vivo* data on how c-Jun affects proliferation during prostate tumorigenesis. The regulative role of c-Jun on proliferation is controversial with both suppressive and promoting mechanisms being described in literature. We therefore investigated potential differences in proliferation in our four genotypes by staining for Ki67 which is continuously expressed in proliferating cells (Berney et al. 2009). In Ki67 IHC of FFPE prostates from 19-week-old-animals we detected a significantly increased number of positive cells in both tumor phenotypes *Pten<sup>Δ/Δ</sup>;c-Jun<sup>Δ/Δ</sup>* and *Pten<sup>Δ/Δ</sup>* compared

to *Control* and *c-Jun*<sup>Δ/Δ</sup> samples (Figure 6). We did not detect significant differences between the *Control* and *c-Jun*<sup>Δ/Δ</sup> group or the *Pten*<sup>Δ/Δ</sup>; *c-Jun*<sup>Δ/Δ</sup> and *Pten*<sup>Δ/Δ</sup> prostates. From these results, we conclude that changes in proliferation are not likely to affect the observed differences in survival between *Pten*<sup>Δ/Δ</sup>; *c-Jun*<sup>Δ/Δ</sup> and *Pten*<sup>Δ/Δ</sup> animals *in-vivo* (Figure 5D).

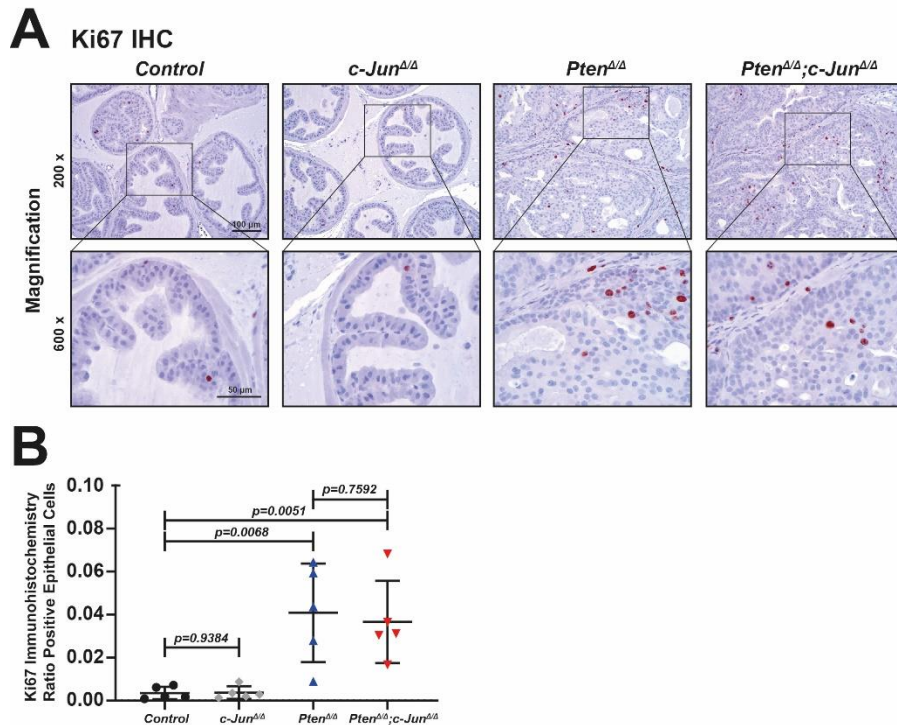


**Figure 6. *c-Jun* deficiency has no effect on proliferation in *Pten*-loss mediated prostate tumors.** (A-B) Ki67 IHC of FFPE prostate samples from 19-week-old animals of the following genotypes: *Control* (n=5), *c-Jun*<sup>Δ/Δ</sup> (n=5), *Pten*<sup>Δ/Δ</sup> (n=5), *Pten*<sup>Δ/Δ</sup>; *c-Jun*<sup>Δ/Δ</sup> (n=5). (A) Representative images of anterior prostate lobe were taken at magnification of 200 × and 600 × and images were white balance adjusted using Photoshop. (B) Quantification was performed by an automated analysis tool. Quantification was calculated by dividing positive epithelial cell count with total epithelial cell count. Group comparison was performed with a two-sided unpaired t-test.

### 3.6 *c-Jun* deficiency does not affect proliferation in a PCa *in-vitro* model

In addition to the *in-vivo* model we established an *in-vitro* CRISPR-Cas9 mediated KO model to study the effects of c-JUN expression in human prostate cancer cell lines. For this purpose we chose the PCa cell lines PC-3 and DU145 (Stone et al. 1978; Kaighn et al. 1979). WB experiments revealed that both cell lines expressed c-JUN protein to various levels but that PC-3 cells had diminished PTEN levels (Figure 7A). To delete c-JUN in the human cell lines, we designed three individual guide RNAs (sgRNAs) (G1, G12, G14) against the single exon of *c-JUN*, taking into consideration that different guide RNAs might produce varying KO efficiencies (Figure 7B). We

cloned the sgRNAs into the lentiCRISPRv2 one vector system (Sanjana, Shalem, and Zhang 2014; Shalem et al. 2014) and transfected HEK293 FT cell line with the vector.

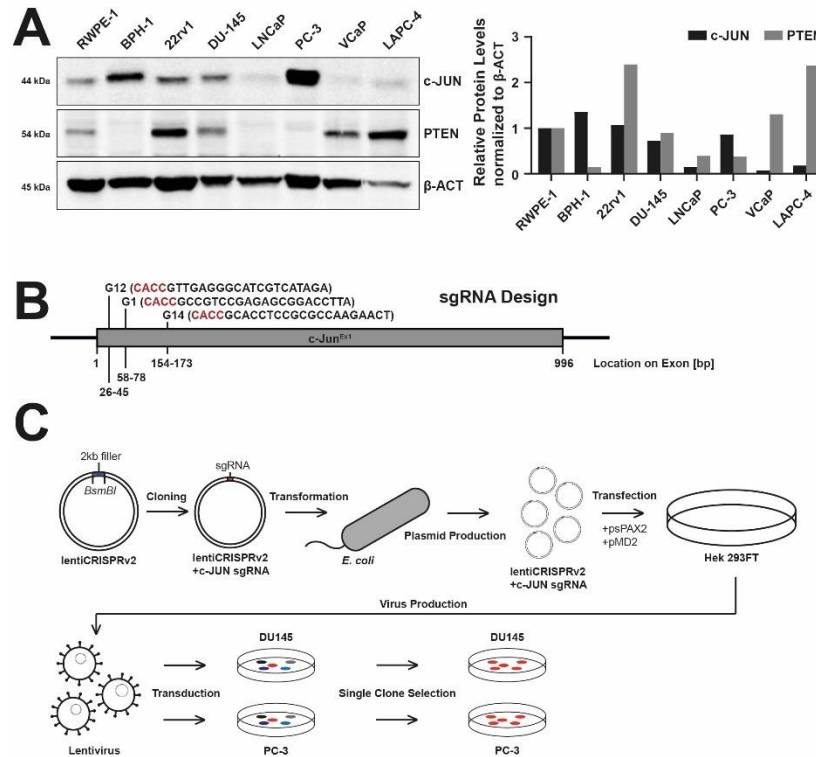


**Figure 7. Human PCa cell lines to study effects of *c-JUN* deficiency *in-vitro*.** (A) WB of lysates from human prostate cancer cell lines with antibodies against c-JUN, PTEN and  $\beta$ -ACT as a loading control. Right: quantification of WB normalized to  $\beta$ -ACT expression and relative to the expression in RWPE-1 cell line. (B) sgRNA design for *c-JUN* KO with accurate representation of sgRNA target locations on *c-JUN*<sup>Ex1</sup>. The sgRNAs G1, G12 and G14 were later introduced into the lentiCRISPRv2 vector. sgRNA sequence shown in brackets and overhangs for cloning highlighted in red. sgRNA target site location relative to 5'-end of *c-JUN*<sup>Ex1</sup> is indicated in base pairs (bp). (C) Schematic representation of *c-JUN* CRISPR KO workflow. sgRNAs were cloned into lentiCRISPR v2 vectors and transfected with the packaging plasmids psPAX2 and pMD2.G into HEK293 FT cell line to produce lentiviral particles for transduction. DU145 and PC-3 cell lines were transduced with virus carrying either original lentiCRISPR v2 or lentiCRISPR v2 cloned with either one of the three sgRNAs.

We confirmed that all cloned sgRNA vectors were able to target *c JUN* using the T7 endonuclease assay (Figure 8). After confirming the efficiency of the sgRNA vectors, we produced lentiviral particles in HEK293 FT cell line and transduced PC-3 and DU145 cells (Figure 7C). In addition to sgRNA vector carrying virus we also produced viruses harboring the original lentiCRISPRv2 vector as an empty vector control cell line (eV). We tested for potential reduction of c-JUN protein expression in lysates of G1, G12 and G14 transduced DU145 and PC-3 cell lines compared to empty vector controls (Figure 9A & 9C). All sgRNA transduced cell lines showed residual levels of c-JUN protein and only the bulk culture DU145 G1 showed near total depletion of the protein.

**Figure 8. sgRNA G1, G12 and G14 are able to target c-JUN.** (A) T7 endonuclease assay of DNA extracts from sgRNA lentiCRISPR v2 and lentiCRISPR v2 empty vector (eV) transfected HEK239 FT cell lines. G1, G12 and G14 were the sgRNAs clones into the lentiCRISPR v2 vector. (-) represents reactions without T7 endonuclease enzyme while (+) represents reactions using the enzyme. The intense bands at (-) show the undigested 961 bp product of the *c-JUN* allele amplified by PCR (blue indicator). Faint bands at (+) indicate digestion products of the amplicon (red indicators).

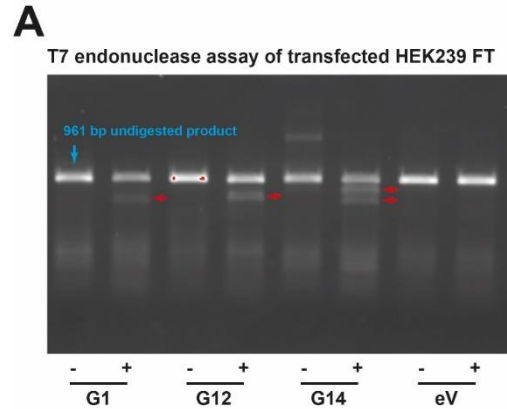
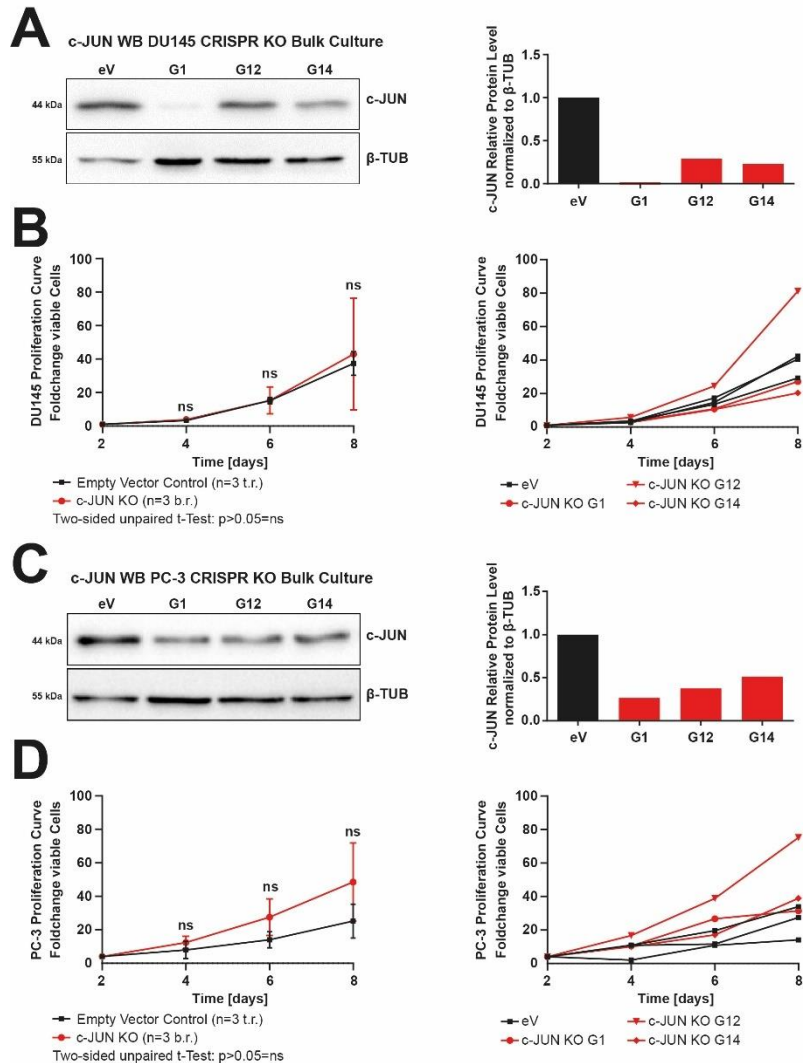


**Figure 9. In-vitro c-JUN KO in human cell lines by CRISPR-Cas9.** (A) c-JUN WB of lysates from transduced DU145 cell line bulk cultures and quantification (right) of proteins normalized to  $\beta$ -TUB expression. (B) Viable cell count-based proliferation curve of DU145 bulk cultures. Cell density of first measurement set to 1 and density measure on consecutive days calculated as fold-changes. Empty vector control included three technical replicates (t.r.) of DU145 transduced with lentiCRISPR v2. c-JUN KO included three biological replicates (b.r.) of DU145 G1, G12 and G14. Left-side image depicts combined values of three technical replicates for empty vector control and three biological replicates for *c-JUN* KO cell lines. Right-side image depicts values of each replicate. Two-sided unpaired t-test was used to determine differences between the two groups at any time point. (C-D) as in (A-B) but for the PC-3 transduced cell line.



A previous study in LNCaP cell lines suggested that *c-JUN* deficiency leads to reduced proliferation in PCa cells by (S. Y. Chen et al. 2006). These findings show a tumor-suppressive property of *c-JUN* which is contrary to the findings in our mouse model. We tested whether we were able to reproduce these results in our DU145 and PC-3 CRISPR cell lines.

We therefore performed a viable cell count-based proliferation analysis in the bulk cultures. We seeded cells of the transduced cell lines into 6-well plates and measured viable cell counts at consecutive days using an automated cell counting device. Three technical replicates of the eV transduced cell lines were regarded as the control group and compared with the three biological replicates G1, G12 and G14 as *c-JUN* deficient cell lines. We did not detect significant differences in proliferation of *c-JUN* deficient DU145 and PC-3 cell line bulk cultures compared to their empty vector controls (Figure 9B & 9D). However, the KO cell lines still showed residual expression of c-JUN (Figure 9A & 9C) and we therefore picked single clones to exclude potential effects of residual c-JUN expression. To pick single clones, we isolated single colonies which were seeded in a limiting dilution experiment.

For single clone validation, we determined the *c-JUN* KO efficiency by c-JUN WB. We indeed detected several single clones that had entirely lost c-JUN protein expression (DU145 G1.3, DU145 G12.1, DU145 G14.2, PC-3 G1.1, PC-3 G1.2, PC-3 G1.3 and PC-3 G14.3). The identified full *c-JUN* KO single clones were further validated by Sanger sequencing to guarantee origin from single cells (Figure 10A & 10C). We utilized the TIDE online web tool for this analysis (Brinkman et al. 2014). TIDE allows for the analysis of sequencing data from a mixed pool of samples and is therefore used to quantify occurring allele frequencies. The insertion-deletion (InDel) range of a true single clone should ideally indicate two alleles while bulk cultures have a broad InDel spectrum. We validated DU145 G1.3, DU145 G12.1, DU145 G14.2, PC-3 G1.1, PC-3 G1.2 and PC-3 G1.3 as true single clones and used these single clone cell lines for future experiments (Figure 10B & 10D). PC-3 G1.3 was identified as a triploid single clone with an InDel spectrum being divided into three peaks (Figure 10D). For further experiments we selected DU145 eV.1, DU145 eV.2, DU145 eV.3, PC-3 eV.1, PC-3 eV.2 and PC-3 eV.3.

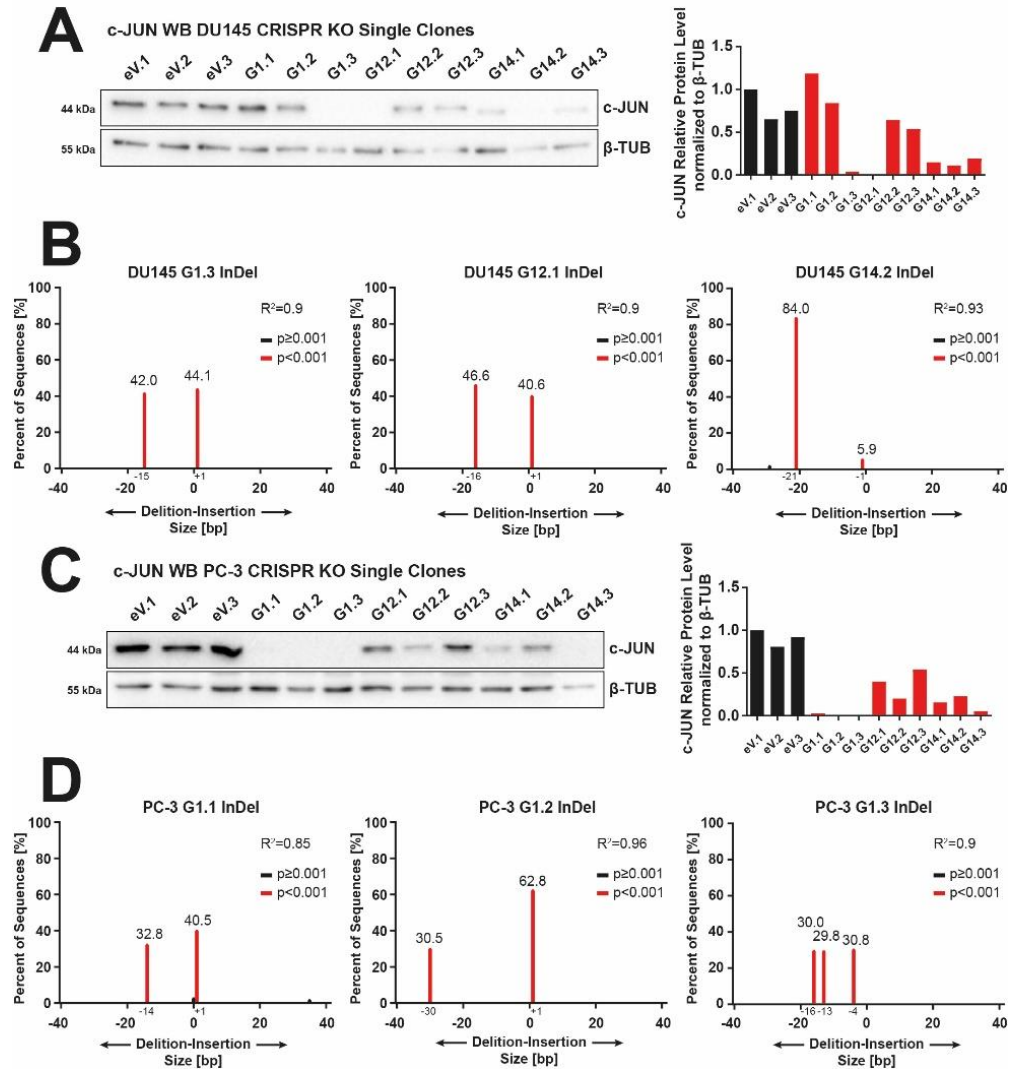


**Figure 10. TIDE analysis to verify clonality of single clones in human PCa cell lines.** (A) c-JUN WB of lysates from transduced DU145 cell line single clones. Right: quantification of proteins normalized to  $\beta$ -TUB expression. (B) Insertion-deletion (InDel) spectra of selected transduced DU145 single clones as measured by TIDE assay. DU145 single clones G1.3, G12.1 and G14.2 were identified as genetic single clones and used for further experiments. (C-D) as in (A-B) but for the PC-3 cell line single clones. PC-3 single clones G1.1 G1.2 and G1.3 were identified as genetic single clones and used for further experiments.

We next performed proliferation analysis based on viable cell count with three biological replicates for empty vector control and three biological replicates for *c-JUN* KO. As previously observed for the bulk cultures, we did not find any overall proliferative differences between single clones of empty vector control and *c-JUN* KO replicates in DU145 nor PC-3 cell lines (Figure 11A & 11C). At day two of the proliferation experiment we observed a significant increase of cell count in the DU145 *c-JUN* KO single clones, but consecutive time points did not confirm these differences (Figure 11A).

To increase the sensitivity of our proliferation assays and to measure potential subtle influences of *c-JUN* deficiency on proliferation, we performed a resazurin assay-based proliferation experiment. Resazurin is metabolized by viable cells and therefore cell density is directly proportional to the cellular metabolization rate (O'Brien et al. 2000). We seeded three technical replicates per time point for each biological replicate on a 96-well plate and conducted the first measurement at 12 hours after seeding. This first time point was regarded as day 0 and results of all consecutive time points were calculated as fold-changes over day 0. We measured the relative metabolization rates at days 2, 4 and 6 via fluorescence spectrometry after incubating cells for two hours with resazurin solution. Again, suggesting no changes in proliferation in *c-JUN* deficient DU145 and PC-3 SCs with the resazurin assay, we confirmed our results of the viable cell count-based proliferation curves (Figures 11B & 11D). In conclusion, our proliferation experiments in bulk cultures and single clones of DU145 and PC-3 *c-JUN* KO cell lines did not indicate any significant influence of *c-JUN* on the proliferation of PCa cell lines (Figure 8 & 10). These results from *in-vitro* experiments are in accordance with our observations in the *in-vivo* model, which did not show any proliferative differences between the tumor developing *Pten*<sup>ΔΔ</sup>;*c-Jun*<sup>ΔΔ</sup> and *Pten*<sup>Δ/Δ</sup> genotypes (see section 3.5).

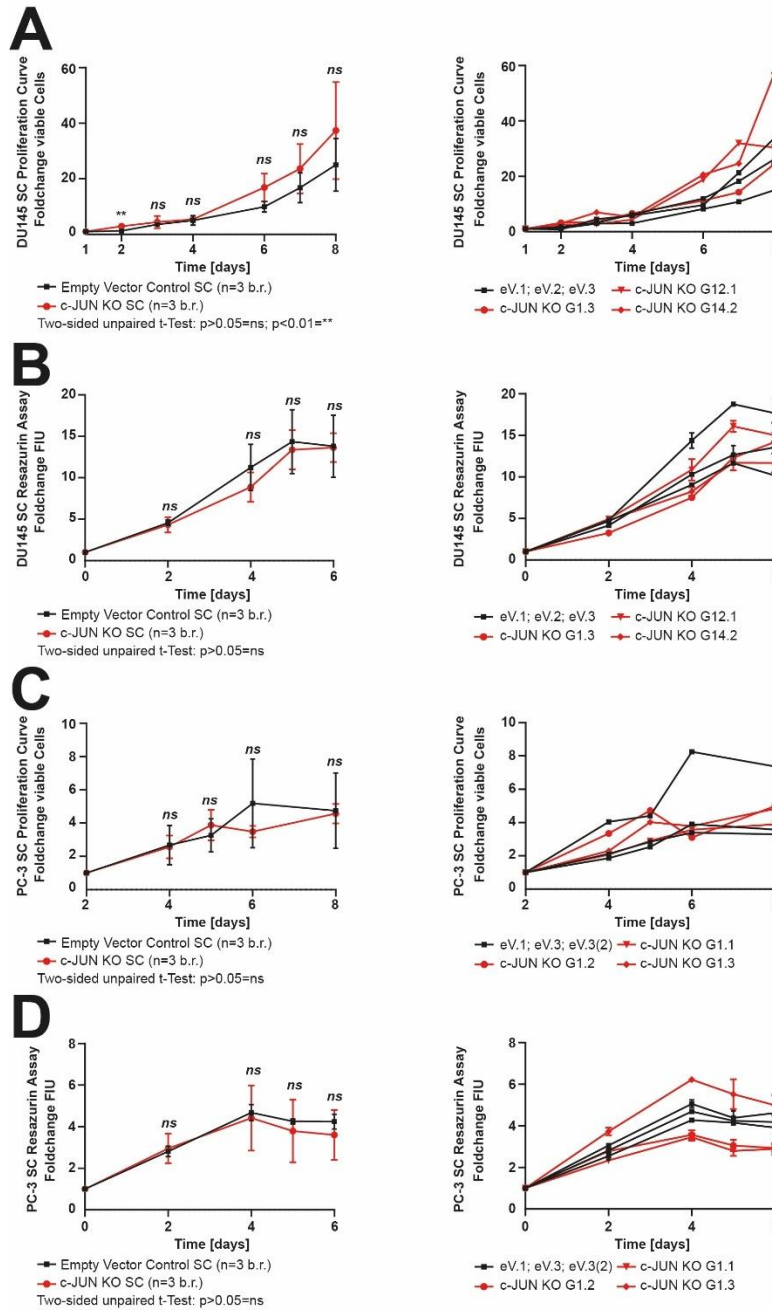


**Figure 11. *c-JUN* deficiency has no effects on proliferation in human PCa cell lines.** (A) Viable cell count-based proliferation curve of DU145 single clones (SC). Left side image depicts combined values of three biological replicates (b.r.) for empty vector control and three biological replicates for *c-JUN* KO cell lines. Right side image depicts values of separate biological replicates. Foldchanges were calculated by setting the viable cell count of the first time point as 1. Viable cell count foldchanges of empty vector control group and *c-JUN* KO group were compared for each time point using two-sided unpaired t-test. (B) Resazurin assay of DU145 SC. Left-side image depicts combined values of three biological replicates for empty vector control and three biological replicates for *c-JUN* KO cell lines. Right side image depicts values of separate biological replicate. For each biological replicate three technical replicates were included in the experiment. Foldchanges were calculated by setting the fluorescence intensity units (FIU) of the first time point as 1. FIU foldchanges of empty vector control group and *c-JUN* KO group were compared for each time point using two-sided unpaired t-test. (C-D) As in (A-B) but PC-3 single clone cell lines.

### 3.7 c-Jun deficiency does not affect CC3 mediated apoptosis in murine PCa model

c-JUN and JNK were previously suggested to regulate apoptosis of stressed cells (Shaulian et al. 2000; Hochedlinger, Wagner, and Sabapathy 2002). JNK has been reported to act pro-apoptotic in PCa cells, but it remains debatable whether c-JUN participates in these regulative properties in prostate tumorigenesis (Lorenzo and Saatcioglu 2008; Xu and Hu 2020). We therefore chose the cleaved-caspase 3 (CC3) as a marker to analyze apoptosis in our PCa *in-vivo* model (Blute et al. 2017). We observed by IHC that CC3 levels were generally low in all four genotypes of the PCa model. We performed semi-quantitative evaluation of expression to avoid the limited sensitivity of automated analysis. We assigned the expression levels 0 for no expression, 1 for scarce, 2 for low, 3 for medium and 4 for high expression to all sections.

For the *Control* and *c-Jun*<sup>Δ/Δ</sup> genotypes we observed occasional or no positive cells within the prostate epithelia (Figure 12A-12B). We found elevated CC3 expression in epithelial cells in the tumor genotypes *Pten*<sup>Δ/Δ</sup>;*c-Jun*<sup>Δ/Δ</sup> and *Pten*<sup>Δ/Δ</sup>, however we failed to detect overall significant differences in these two genotypes. We additionally observed excessive positive signal within the gland lumen of both tumor phenotypes (Figure 12A, black arrows). However, we cannot exclude the possibility that this positive signal is unspecific and results from secretions of the prostate gland. In summary, we were unable to detect differences between *Pten*<sup>Δ/Δ</sup>;*c-Jun*<sup>Δ/Δ</sup> and *Pten*<sup>Δ/Δ</sup> in CC3 mediated apoptosis, but we cannot exclude the possibility that *c-Jun* may regulate apoptotic pathways which are mediated by other executioner caspases. Future experiments, analyzing other caspases and alternate apoptotic signaling will further elucidate a potential contribution of c-Jun to apoptosis in the PCa *in-vivo* model.

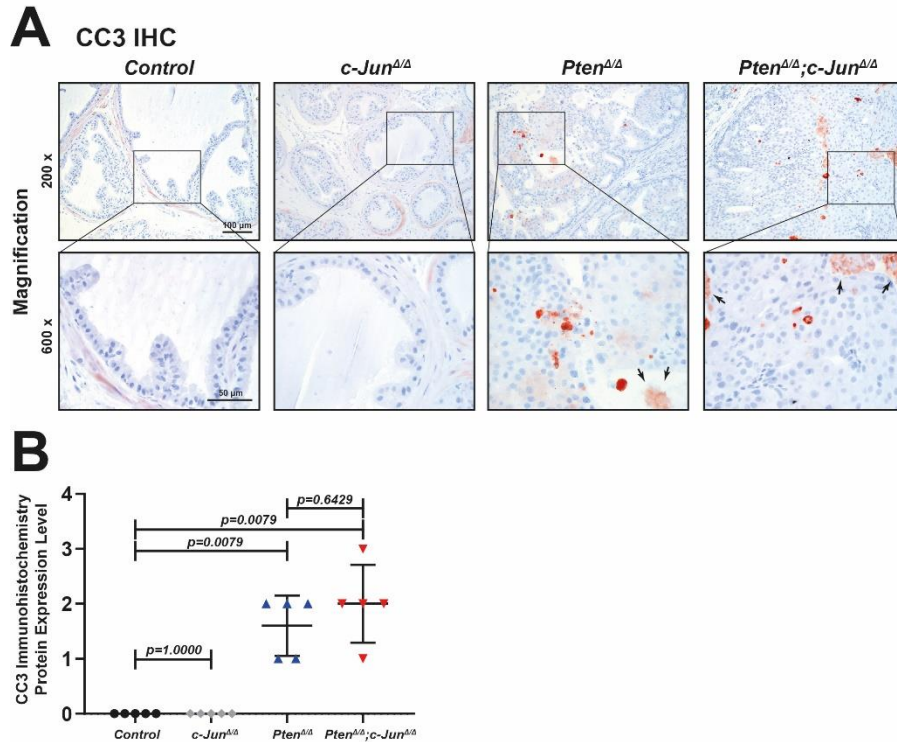


**Figure 12.** *c-JUN* deficiency has no effect on apoptosis in *Pten*-loss mediated prostate tumors. (A-B) Cleaved-caspase 3 (CC3) IHC of FFPE prostate samples from 19-week-old animals. Genotypes: Control (n=5), *c-Jun*<sup>Δ/Δ</sup> (n=5), *Pten*<sup>Δ/Δ</sup> (n=5), *Pten*<sup>Δ/Δ</sup>;*c-Jun*<sup>Δ/Δ</sup> (n=5). (A) Representative images of anterior prostate lobe taken at magnifications of 200 × and 600 × and images were white balance adjusted using Photoshop. Black arrows highlight positive intra-luminal staining. (B) Semi-quantitative evaluation of prostate CC3 expression. Classification into no (0), scarce (1), low (2), medium (3) and high (4) CC3 expression. Group comparison was performed by Mann-Whitney-U-test.

### 3.8 Trend of increased senescence in response to *c-Jun* deficiency in the murine PCa model

Deficiency of the tumor-suppressor gene *Pten* reportedly causes p53 mediated senescence in *Pten* KO mice (Jung et al. 2019; Z. Chen et al. 2005). This phenotype is called *Pten*-loss-induced cellular senescence (PICS) and is part of a senescence pathway which induces senescence in response to oncogenic signaling (Muñoz-Espín and Serrano 2014). We therefore assumed that a PICS phenotype is present in our PCa *in-vivo* model. A possible regulation of this phenotype by *c-Jun* may have significant influence on prostate tumorigenesis. *c-Jun* and JNK were previously suggested as negative regulators of senescence (Shaulian et al. 2000; Das et al. 2007; J. J. Lee et al. 2010). Senescence primarily suppresses cell growth and therefore acts as a tumor-suppressive mechanism (Gorgoulis et al. 2019; Schosserer, Grillari, and Breitenbach 2017). However, senescence is regulated by a multitude of different pathways and some forms of senescence shape the tumor microenvironment favorably toward tumor progression. We therefore tested whether

c-Jun regulates senescence in our PCa mouse model and which specific senescence pathways could be involved in such a regulation (Gorgoulis et al. 2019).

We tested the senescence markers  $\beta$ -galactosidase and p16<sup>INK4a</sup> which are universally overexpressed in senescent cells (B. Y. Lee et al. 2006; Muñoz-Espín and Serrano 2014). We started our investigation into a potential senescence-regulative mechanism of c-Jun by staining viable prostate epithelial cells isolated from 19-week-old animal prostates with the  $\beta$ -galactosidase substrate C<sub>12</sub>FDG (Cahu and Sola 2013). We used antibodies against the EpCAM cell surface protein in combination with C<sub>12</sub>FDG staining to isolate epithelial cells from the prostate cell population by FACS. We found similar levels of  $\beta$ -galactosidase activity in *Control* and *c-Jun* <sup>$\Delta/\Delta$</sup>  (Figure 12A). *Pten* <sup>$\Delta/\Delta$</sup>  and *Pten* <sup>$\Delta/\Delta$</sup> ;*c-Jun* <sup>$\Delta/\Delta$</sup>  had significantly elevated activity compared to control which suggests that the PCa mouse model does develop a senescence phenotype as it has been described in previous studies (Z. Chen et al. 2005). We observed no statistically significant difference between *Pten* <sup>$\Delta/\Delta$</sup>  and *Pten* <sup>$\Delta/\Delta$</sup> ;*c-Jun* <sup>$\Delta/\Delta$</sup> . However, the mean percentage of cells with  $\beta$ -galactosidase activity was slightly increased in the *Pten* <sup>$\Delta/\Delta$</sup> ;*c-Jun* <sup>$\Delta/\Delta$</sup>  genotype. As we were only able to measure three replicates for each genotype at the time of the experiment, an increase in replicate number in future experiments will elucidate the contribution of c-Jun in the regulation of senescence.

We next tested expression of the senescence marker p16<sup>INK4a</sup> which is the full-length transcription product of the *CDKN2A* gene locus by RT-qPCR and WB. RT-qPCR showed low levels of p16<sup>INK4a</sup> mRNA expression for *Control* and *c-Jun* <sup>$\Delta/\Delta$</sup>  (Figure 12B). We observed significantly increased p16<sup>INK4a</sup> mRNA levels for *Pten* <sup>$\Delta/\Delta$</sup>  and *Pten* <sup>$\Delta/\Delta$</sup> ;*c-Jun* <sup>$\Delta/\Delta$</sup>  which again points toward a senescent phenotype upon *Pten* deletion. p16<sup>INK4a</sup> expression normalized to *18S* rRNA expression was significantly increased *Pten* <sup>$\Delta/\Delta$</sup> ;*c-Jun* <sup>$\Delta/\Delta$</sup>  compared to *Pten* <sup>$\Delta/\Delta$</sup> . However, we did not observe this difference when normalizing to a second housekeeping gene *CypA*. On the protein level we reproduced our RT-qPCR results and measured no detectable p16<sup>INK4a</sup> expression in *Control* and *c-Jun* <sup>$\Delta/\Delta$</sup>  (Figures 12). We found increased p16<sup>INK4a</sup> expression in both tumor phenotypes but no significant difference between *Pten* <sup>$\Delta/\Delta$</sup> ;*c-Jun* <sup>$\Delta/\Delta$</sup>  and *Pten* <sup>$\Delta/\Delta$</sup>  prostates (Figure 12C-12D). In conclusion, our observations on  $\beta$  galactosidase activity and p16<sup>INK4a</sup> expression hint toward a mild increase in senescence upon *c-Jun* deficiency in *Pten*-loss mediated murine PCa. However, these findings were not statistically significant and further experiments will assess whether c-Jun regulates senescence in murine PCa.

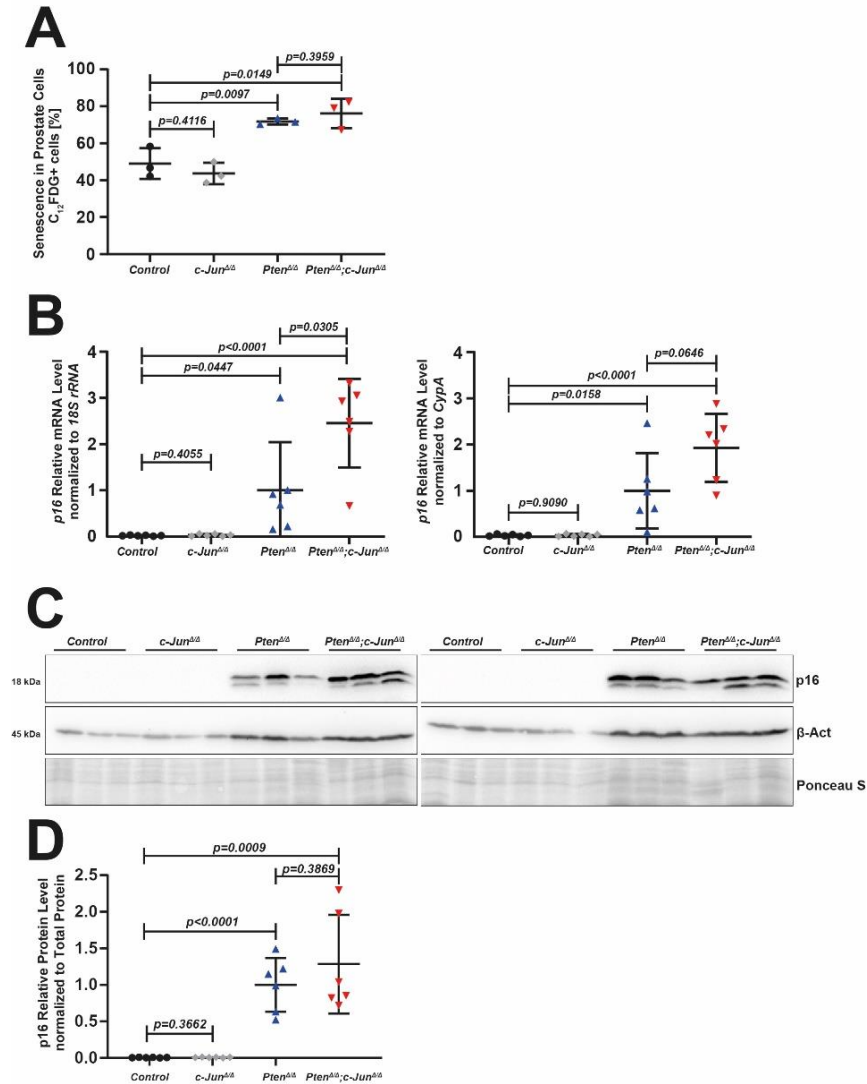


**Figure 13.** *c-JUN* deficiency may have an effect on senescence in *Pten*-loss mediated prostate tumors. (A) C<sub>12</sub>FDG staining for senescence FACS of prostate epithelial cell suspension from 19-week-old animals. Genotypes: *Control* (n=3), *c-Jun*<sup>Δ/Δ</sup> (n=3), *Pten*<sup>Δ/Δ</sup> (n=3), *Pten*<sup>Δ/Δ</sup>;*c-Jun*<sup>Δ/Δ</sup> (n=3). Percentage of senescent C<sub>12</sub>FDG+ epithelial cells to total epithelial cells are shown (data adapted from Christina Sternberg). Group comparison was performed with a two-sided unpaired t-test. (B) *p16*<sup>INK4a</sup> RT-qPCR of whole prostate RNA extracts of 19-week-old animals. Genotypes: *Control* (n=6), *c-Jun*<sup>Δ/Δ</sup> (n=6), *Pten*<sup>Δ/Δ</sup> (n=6), *Pten*<sup>Δ/Δ</sup>;*c-Jun*<sup>Δ/Δ</sup> (n=6). *p16*<sup>INK4a</sup> mRNA expression was normalized to *18S* rRNA or *CypA* mRNA expression and mean expression in the *Pten*<sup>Δ/Δ</sup> group was set to 1. Group comparison was performed with a two-sided unpaired t-test. (C) *p16*<sup>INK4a</sup> WB of whole prostate protein lysates of 19-week-old animals. Genotypes: *Control* (n=6), *c-Jun*<sup>Δ/Δ</sup> (n=6), *Pten*<sup>Δ/Δ</sup> (n=6), *Pten*<sup>Δ/Δ</sup>;*c-Jun*<sup>Δ/Δ</sup> (n=6). Exclusively the upper band was quantified as *p16*<sup>INK4a</sup> because the lower band represents C-terminal proteolytically cleaved *p16*<sup>INK4a</sup>. (D) *p16*<sup>INK4a</sup> protein levels were normalized to total protein levels as assessed by Ponceau S staining and *p16*<sup>INK4a</sup> level of *Pten*<sup>Δ/Δ</sup> group was set to 1. Group comparison was performed with a two-sided unpaired t-test.

### 3.9 RNA-seq suggests an influence of c-Jun on PCa immunology and inflammation

We continued to identify mechanisms which could explain tumorigenesis regulating properties of c-Jun by performing transcriptomic analysis via RNA-seq. For this experiment we prepared next-generation sequencing (NGS) libraries of five animals per group of: *Control*, *Pten<sup>Δ/Δ</sup>;c-Jun<sup>Δ/Δ</sup>* and *Pten<sup>Δ/Δ</sup>*. The *c-Jun<sup>Δ/Δ</sup>* genotype could unfortunately not be included due to an insufficient number of *c-Jun<sup>Δ/Δ</sup>* animals at the time of the experiment. We prepared RNA-seq libraries from EpCAM MACS sorted prostate epithelial cells of 19-week-old animals. We used DEseq2 and edgeR to perform differential gene expression analysis on the mapped sequencing data (Love, Huber, and Anders 2014; Robinson, McCarthy, and Smyth 2009). Using DEseq2 normalized data we plotted a principal component analysis (PCA) to investigate the association between genotypes. We produced a log ratio to mean average (MA) plot from DEseq2 data to compare *Pten<sup>Δ/Δ</sup>;c-Jun<sup>Δ/Δ</sup>* and *Pten<sup>Δ/Δ</sup>* for further exploratory data analysis.

We found clustering of individual replicates within the genotypes *Control*, *Pten<sup>Δ/Δ</sup>;c-Jun<sup>Δ/Δ</sup>* and *Pten<sup>Δ/Δ</sup>* which confirms that these genotypes exhibit a distinctively different transcription profile in PCA analysis (Figure 13A). In our analyses we also compared the genotypes *Pten<sup>Δ/Δ</sup>;c-Jun<sup>Δ/Δ</sup>* and *Pten<sup>Δ/Δ</sup>* with *Control* but for the scope of this thesis, we focused on differences between *Pten<sup>Δ/Δ</sup>;c-Jun<sup>Δ/Δ</sup>* and *Pten<sup>Δ/Δ</sup>* to explore the role of *c-Jun* deficiency in prostate tumorigenesis. We found a total of 1872 differentially expressed (DE) genes of which 1553 DE genes were down-regulated and 319 DE genes were up-regulated (Figure 14B-14C). Overall, deficiency of the transcription factor *c-Jun* appears to primarily lead to a downregulation of genes.

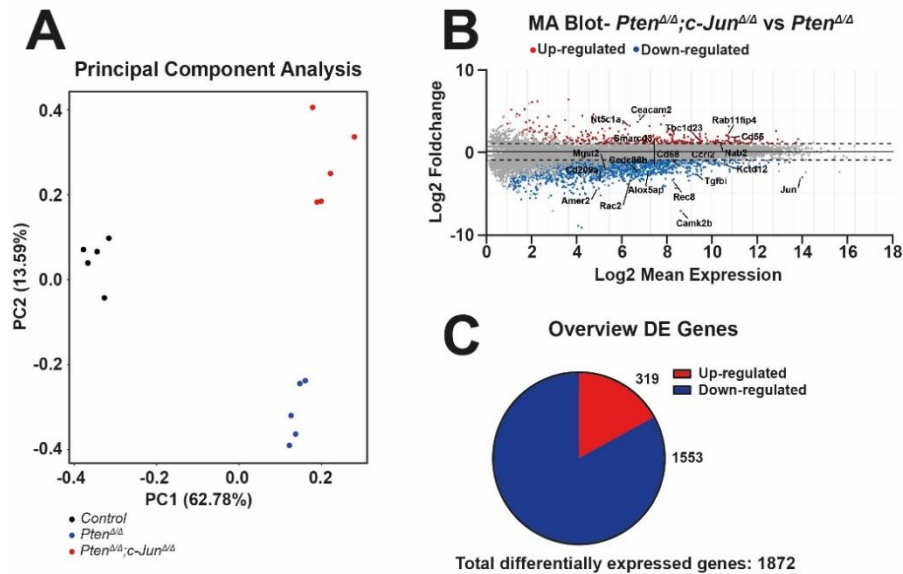


**Figure 14.** *c-JUN* deficiency changes the gene expression profile in *Pten*-loss mediated prostate tumors. Exploratory data analysis of the RNA-seq experiment. Sequencing libraries were generated from total RNA of EpCAM MACS sorted prostate epithelial cells of 19-week-old animals. Genotypes: *Control* (n=5), *Pten*<sup>Δ/Δ</sup> (n=5), *Pten*<sup>Δ/Δ</sup>;*c-Jun*<sup>Δ/Δ</sup> (n=5). Normalization to total reads and differential gene expression analysis was performed using DEseq2. (A) Principal component analysis (PCA) from DEseq2 normalized RNA-seq data. (B) Log ratio to mean average (MA) plot generated from DEseq2 differential gene expression data comparing *Pten*<sup>Δ/Δ</sup>;*c-Jun*<sup>Δ/Δ</sup> versus *Pten*<sup>Δ/Δ</sup> genotypes. The top-20 most differentially expressed genes are indicated on MA plot. (C) Pie chart showing the number of up- and down-regulated genes.

We performed gene set enrichment analysis (GSEA) on DEseq2 differentially expressed genes of *Pten*<sup>Δ/Δ</sup>;*c-Jun*<sup>Δ/Δ</sup> compared to *Pten*<sup>Δ/Δ</sup> in order to identify signaling pathways that rely on *c-Jun* expression in prostate tumorigenesis (Mootha et al. 2003; Subramanian et al. 2005). We investigated the gene set collections “Kegg” and “Hallmark” of the Molecular signature database (MSigDB) and set our significance cut-off at an adjusted p-value of <0.05 (Subramanian et al. 2005; Liberzon et al. 2011). With Kegg GSEA we found multiple immune response and inflammation related pathways to be down-regulated in the *Pten*<sup>Δ/Δ</sup>;*c-Jun*<sup>Δ/Δ</sup> genotype compared to *Pten*<sup>Δ/Δ</sup> (Figure 15A). These pathways included cytokine-cytokine receptor interaction, chemokine signaling, leukocyte trans-endothelial migration and natural killer (NK) cell mediated cytotoxicity all showing a negative normalized enrichment score (NES). Cell-cell interactions seemed to be affected in *Pten*<sup>Δ/Δ</sup>;*c-Jun*<sup>Δ/Δ</sup> as we observed a negative NES of the cell adhesion molecules (CAMs) data set. We found a positive NES from gene sets primarily associated with cellular metabolism including oxidative phosphorylation, citrate cycle, amino/nucleotide sugar metabolism and ubiquitin mediated proteolysis pathways. In Hallmark GSEA we observed a downregulation of the gene sets grouped within inflammatory response, complement activation and IL2-STAT5 signaling which further indicates an involvement of *c-Jun* in regulation of inflammation and immune

response (Figure 15B). The interferon alpha (IFN $\alpha$ ) response showed a positive NES in *Pten* $^{\Delta/\Delta};c-Jun$  $^{\Delta/\Delta}$ . Further pathways with a negative NES included IL6-Jak-STAT3 signaling, KRAS signaling, epithelial to mesenchymal transition (EMT) and TNF $\alpha$  signaling via NF- $\kappa$ B. We found an upregulation of the gene sets oxidative phosphorylation, protein secretion, cholesterol homeostasis, fatty acid metabolism and estrogen response. In summary, our results suggest that *c-Jun* may modulate inflammation, immune response and cell metabolism during prostate tumorigenesis.

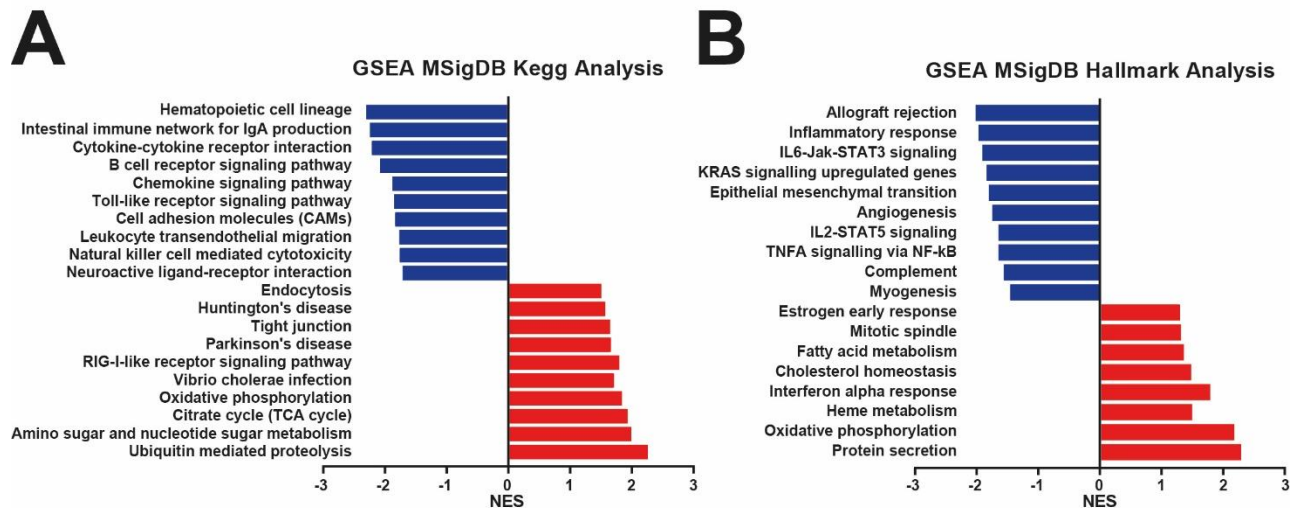


**Figure 15.** *c-Jun* deficiency leads to downregulation of multiple pathways of immunological relevance. Gene set enrichment analysis (GSEA) using the molecular signature database (MSigDB) gene set collections “Kegg” (A) and “Hallmark” (B). GSEA DEseq2 differential gene expression analysis comparing *Pten* $^{\Delta/\Delta};c-Jun$  $^{\Delta/\Delta}$  versus *Pten* $^{\Delta/\Delta}$  (data adapted from Monika Oberhuber). Significance cut-off was set at an adjusted p-value of  $\leq 0.05$ . Up to 20 top significantly deregulated pathways were plotted according to normalized enrichment score (NES) from lowest to highest.

### 3.10 *c-Jun* regulates mRNA expression and activity of other transcription factors

*c-Jun* is known to participate in complex signaling crosstalks of signaling transduction cascades (Meng and Xia 2011). *c-Jun* was reported to interact with other AP-1 transcription factors in an autocrine amplification loop in which *c-Jun* increases the activity of AP-1 transcription factors and vice versa *c-Jun* expression is promoted by AP-1 activity. *c-Jun* is also known to regulate other non-AP-1 transcriptions factors. For example, *c-Jun* was identified as a coactivator of AR (Bubulya et al. 2001; Cai, Hsieh, and Shemshedini 2007). Crosstalk between *c-Jun* and other transcription factors may play a role in the regulation of prostate tumorigenesis and we therefore explored the impact of *c-Jun* deficiency on the activity of other transcription factors. We used differential gene

expression analysis data of the RNA-seq experiment to analyze the mRNA expression of related AP-1 transcription factors. We plotted log<sub>2</sub>-foldchanges of the *Pten*<sup>Δ/Δ</sup>;*c-Jun*<sup>Δ/Δ</sup> to *Pten*<sup>Δ/Δ</sup> differentially expressed (DE) genes. *c-Jun* mRNA was significantly downregulated in *Pten*<sup>Δ/Δ</sup>;*c-Jun*<sup>Δ/Δ</sup> compared to *Pten*<sup>Δ/Δ</sup> which validates the differential gene expression data and serves as a control for the RNA-seq experiment. We observed similar expression of most AP-1 factors however *Batf* and *Batf3* showed significantly reduced expression in the *Pten*<sup>Δ/Δ</sup>;*c-Jun*<sup>Δ/Δ</sup> prostates (Figure 16A). These findings imply a transcriptional regulation of *Batf* and *Batf3* by c-Jun. However, we could not measure Batf protein expression in prostates which suggests that this regulation only has minor biological relevance on prostate tumorigenesis (Figure 16B). With GSEA of the “transcription factor target” MSigDB gene set collection we investigated whether c-Jun regulates the activity of non-AP-1 transcription factors (Yevshin et al. 2019). This form of GSEA determines activity of transcription factors by analyzing the mRNA expression of the genes which are activated by the transcription factor. We observed a downregulation of transcription factor target genes of Pbx1, Pu.1 and the core binding factor Runx1 (Aml) in *Pten*<sup>Δ/Δ</sup>;*c-Jun*<sup>Δ/Δ</sup> prostates (Figure 16C). Upregulated were target genes of Pax3, Nrf2 and Gabp. These findings suggest that c-Jun is capable of regulating the activity of multiple other

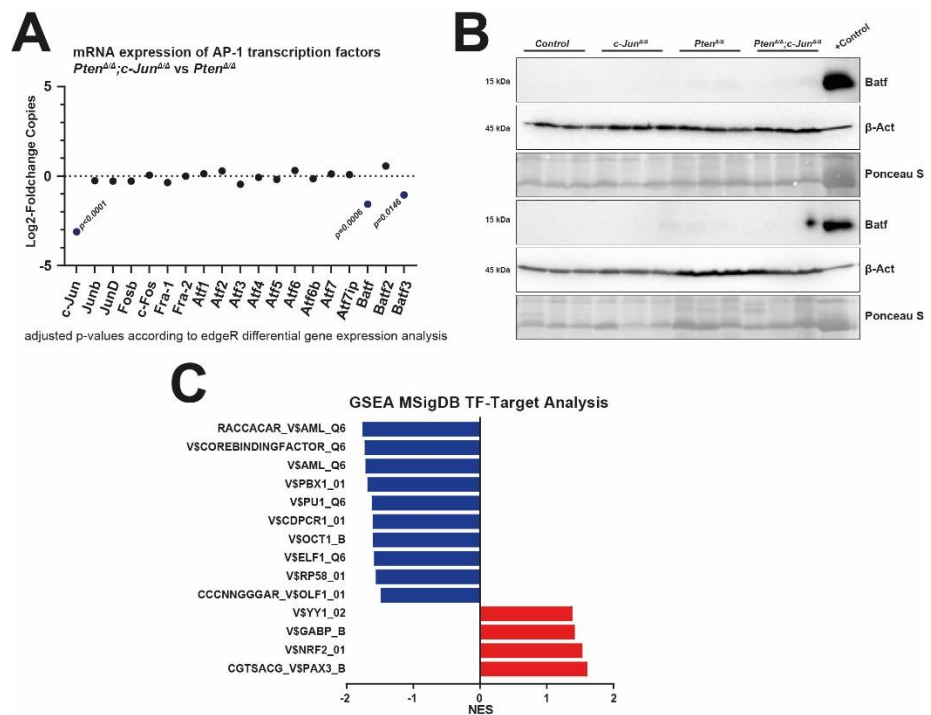


**Figure 16. *c-JUN* deficiency leads to deregulation of other transcription factors.**

(A) Log<sub>2</sub>-foldchanges of AP-1 transcription factors according to edgeR differential gene expression analysis comparing *Pten*<sup>Δ/Δ</sup>;*c-Jun*<sup>Δ/Δ</sup> versus *Pten*<sup>Δ/Δ</sup>. Color coding: downregulated genes (blue); upregulated genes (red). (B) Batf WB of whole prostate protein lysates of 19-week-old animals. Genotypes: *Control* (n=6), *c-Jun*<sup>Δ/Δ</sup> (n=6), *Pten*<sup>Δ/Δ</sup> (n=6), *Pten*<sup>Δ/Δ</sup>;*c-Jun*<sup>Δ/Δ</sup> (n=6). Lysate from Batf expressing cell line was used as positive control. (C) GSEA using the MSigDB gene set collection “transcription factor target” comparing *Pten*<sup>Δ/Δ</sup>;*c-Jun*<sup>Δ/Δ</sup> versus *Pten*<sup>Δ/Δ</sup> (data adapted from Monika Oberhuber). For GSEA DEseq2 differential gene expression analysis data was used. Significance cut-off was set at an adjusted p-value of ≤0.05.

transcription factors and the tumor-regulative effects of these transcription factors need to be considered to discern how c-Jun regulates prostate tumorigenesis.

### 3.11 Trend of deregulation of selected senescence related genes in response to c-Jun deficiency

Finally, we complemented our previous senescence experiment results (see section 3.8) with analysis of the RNA-seq data. We therefore analyzed the expression of selected genes which are associated with senescence (Muñoz-Espín and Serrano 2014). We observed a mostly equal expression of senescence associated genes between  $Pten^{\Delta/\Delta};c-Jun^{\Delta/\Delta}$  and  $Pten^{\Delta/\Delta}$  with only a few genes being DE (Figure 17).  $p38\beta$  and  $p16^{INK4a}$  expression were upregulated in the  $Pten^{\Delta/\Delta};c-Jun^{\Delta/\Delta}$  genotype. However, our previous RT-qPCR and WB experiments suggested that  $p16^{INK4a}$  expression is not or just mildly increased in the  $Pten^{\Delta/\Delta};c-Jun^{\Delta/\Delta}$  (Figure 13). For a conclusive validation of senescence in our mouse model we will test a broader array of senescence markers in the future (Gorgoulis et al. 2019).

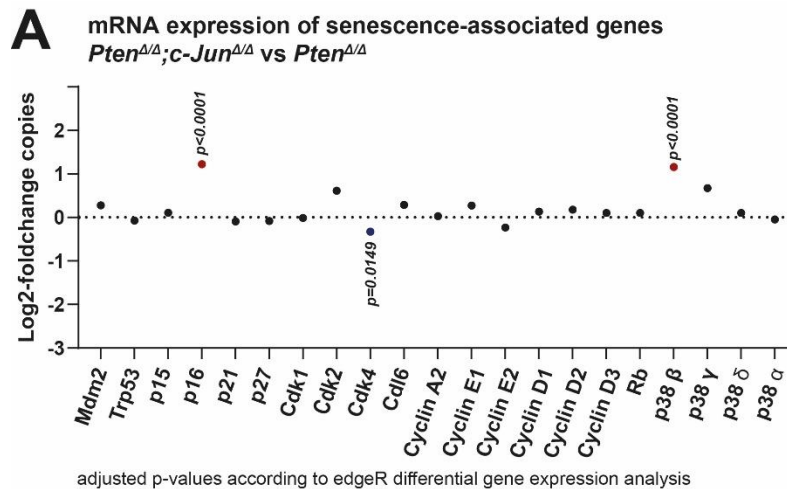


**Figure 17. c-JUN deficiency leads to increased  $p16^{INK4a}$  mRNA expression in  $Pten$ -loss mediated prostate tumors.**

(A) Log<sub>2</sub>-foldchanges of AP-1 transcription factors according to edgeR differential gene expression analysis of the genotypes  $Pten^{\Delta/\Delta};c-Jun^{\Delta/\Delta}$  versus  $Pten^{\Delta/\Delta}$ . Color coding: downregulated genes (blue); upregulated genes (red).

## 4 Discussion

### 4.1 c-JUN and its role in cancer

JUN transcription factors were first discovered as the oncoprotein v-Jun of the avian sarcoma virus 17 (Vogt 2001). The human gene c-JUN was later identified as a homolog of v-Jun (Wisdom, Johnson, and Moore 1999). c-JUN forms homo and heterodimers with other AP-1 transcription factors to establish an active transcription factor with direct DNA binding capacity. The basic function of c-JUN is the regulation of proliferation, differentiation, apoptosis and it is essential for embryogenesis (Jochum, Passequé, and Wagner 2001; Vogt 2001; Eferl et al. 2003). c-JUN promotes expression and activity of cell cycle promoters such as cyclin D1, epidermal growth factor receptor or granulocyte/macrophage colony-stimulating factor and furthermore downregulates cell cycle suppressors such as p53, p16<sup>INK4a</sup> or p21 (Mariani et al. 2007). The upregulation of c-JUN has been associated with multiple malignancies including breast cancer, liposarcoma, hepatocellular carcinomas and melanoma (Jiao et al. 2010; Mariani et al. 2007; Eferl et al. 2003; Kappelmann, Bosserhoff, and Kuphal 2014). These findings resulted in c-JUN being commonly classified as a proto-oncogene. However more recent findings suggest an ambiguous role of c-JUN in response to cellular stress (Eferl and Wagner 2003; Shaulian 2010). For example, c-JUN was suggested to promote apoptosis and DNA damage repair response (DDR) gene expression in UV damaged cells (Shaulian et al. 2000; Devary et al. 1991). Similarly ambiguous tumorigenesis regulative properties were reported for the c-JUN activating c-JUN N terminal kinase (JNK) (Leppä and Bohmann 1999; Tournier 2013; Bubici and Papa 2014). Interestingly in PCa, JNK and the JNK activated JUN family member JUNB were suggested as tumor-suppressors (Davis 2000; Thomsen et al. 2015; Hübner et al. 2012). Despite the fact that JUNB and c-JUN frequently form heterodimers, the influence of c-JUN on prostate tumorigenesis has not been investigated in dept by previous studies (Birner et al. 2015). Taken together, these findings implicate that c-JUN/JNK signaling might act tumor-suppressive or tumor-promoting, dependent on multiple variables such as cell type or upstream signaling. The aim of this project was to determine whether c-JUN acts as a tumor-suppressor or promoter in PCa.

## **4.2 Low c-JUN levels correlate with reduced progression free survival in human PCa patients**

To gain insights into the tumor-suppressive or promoting role of c-JUN in human PCa, we first analyzed publicly available mRNA-seq data of patients with the SurvExpress web tool. This open source software enables the validation of cancer biomarkers and correlation of gene expression to survival data (Aguirre-Gamboa et al. 2013). We used the PCa RNA-seq dataset of *Taylor et al.* which contains data from 218 tumors including 181 primary tumors and 37 metastases (Taylor et al. 2010). We identified two risk groups with significantly different survival curves (Figure 1A-1B). Patients with high levels of *c-JUN* mRNA expression showed significantly increased survival compared to patients with low mRNA expression. These results suggest a positive correlation between *c-JUN* mRNA levels and survival probability of PCa patients. Furthermore, we performed c-JUN IHC staining on prostate TMAs of 60 patients who underwent treatment at the Vienna General Hospital (Merima Herac, unpublished). We divided patients into two groups of which one was characterized by low c-JUN protein expression and one group with high expression. We measured reduced progression free survival of the low c-JUN group with a mean recurrence time of time of 67 months compared to the high c-JUN group with a mean recurrence time of 115 months (Figure 1E).

Our findings from survival analyses of human PCa patients imply that high levels of *c-JUN* mRNA (Figure 1A-D) and c-JUN protein (Figure 1E) correlate positively with progression free-survival. We therefore conclude that c-JUN acts as a tumor-suppressor in human prostate cancer. However, c-JUN was previously described as both tumor-suppressive and -promoting (Shaulian et al. 2000; Jiao et al. 2010). c-JUN expression may not have an effect on tumor growth if it acts equally suppressive and promoting, for example by promoting both proliferation and apoptosis. The correlation between c-JUN expression and enhanced survival could also be explained by parallel expression of c-JUN and a tumor-suppressor such as JUNB which is activated through the same pathways (Thomsen et al. 2015; Meng and Xia 2011). Considering this regulatory crosstalk, it is possible that c-JUN expression is simply a byproduct of tumor signaling but no effector.

### 4.3 c-Jun deficiency leads to increased PCa aggressiveness in mice

For *in-vivo* experiments we used an aggressive PCa mouse model harboring c-Jun wildtype or knockout alleles (Birbach et al. 2011). This mouse model utilizes PB-Cre4 for prostate epithelial cell specific KO of genes (Xiantuo Wu et al. 2001). We bred mice expressing *Pten* and *c-Jun* at wild type levels (*Control*), mice with *Pten* deletions (*Pten*<sup>ΔΔ</sup>), mice with *c-Jun* deletions (*c-Jun*<sup>ΔΔ</sup>) and mice with both *Pten* and *c-Jun* deletions (*Pten*<sup>ΔΔ</sup>;*c-Jun*<sup>ΔΔ</sup>) (Figure 2A). We chose 19-week-old and 38-week-old animals as experimental timepoints. As sample collection from 38-week-old animals was still ongoing, exclusively results from the 19-week-old timepoint are presented within the frame of this thesis. We assessed the effects of c-Jun on the aggressiveness of murine PCa by analysis of prostate to body mass ratio of 19-week-old animals and by a Kaplan Meier survival experiment. We did not find any differences in prostate to body mass ratio between the genotypes *Control* and *c-Jun*<sup>ΔΔ</sup> which suggests that *c-Jun* KO alone cannot drive malignant transformation (Figure 5B). However, we measured a significant increase in prostate mass when comparing *Pten*<sup>ΔΔ</sup>;*c-Jun*<sup>ΔΔ</sup> tumors to *Pten*<sup>ΔΔ</sup> tumors. This increased aggressiveness of *Pten*<sup>ΔΔ</sup>;*c-Jun*<sup>ΔΔ</sup> tumors was also reflected in decreased mean survival of 85 weeks in *Pten*<sup>ΔΔ</sup>;*c-Jun*<sup>ΔΔ</sup> compared to 67 weeks *Pten*<sup>ΔΔ</sup> animals (Figure 5D). We found no difference in survival of *Control* and *c-Jun*<sup>ΔΔ</sup> animals. On H&E sections of prostates we confirmed wild type morphology between *Control* and *c-Jun*<sup>ΔΔ</sup> prostates (Figure 5C) (Oliveira et al. 2016). *Pten*<sup>ΔΔ</sup> and *Pten*<sup>ΔΔ</sup>;*c-Jun*<sup>ΔΔ</sup> prostates were highly similar on a microscopic scale and both genotypes showed tumors with a PCa typical pattern of cribriform glands (Shappell et al. 2004; Kryvenko and Epstein 2016; Epstein 2018). *Pten*<sup>ΔΔ</sup> and *Pten*<sup>ΔΔ</sup>;*c-Jun*<sup>ΔΔ</sup> glands were similarly well circumscribed and showed no difference in differentiation of prostate epithelial cells. Due to this similarity, we cannot conclude that aggressiveness of the *Pten*<sup>ΔΔ</sup>;*c-Jun*<sup>ΔΔ</sup> genotype results from decreased differentiation and increased invasiveness of cancer cells. We therefore hypothesized that aggressiveness of the *Pten*<sup>ΔΔ</sup>;*c-Jun*<sup>ΔΔ</sup> genotype is primarily attributed to enhanced growth and survival of cancer cells.

Our findings on tumor formation and survival strongly implies *c-Jun* as tumor-suppressor for murine PCa formation (Figure 5). Interestingly, during validation of the *c-Jun* KO we measured a significant overexpression of *c-Jun* on mRNA and protein level in prostates of *Pten*<sup>ΔΔ</sup> animals. These findings suggest that c-Jun is upregulated in *Pten*-loss induced murine PCa and further supports the concept of c-Jun acting as a tumor-suppressor in prostate tumorigenesis. Furthermore, the *in-vivo* mouse model promotes our results from human patients indeed implying a

tumor-suppressive property of c-JUN in murine and human PCa (Figure 1). We hypothesized that c-Jun acts as a PCa tumor-suppressor through the same stress response mechanisms which lead to the tumor-suppressive properties of Jnk and JunB in PCa (Konishi et al. 2008; Hübner et al. 2012; Thomsen et al. 2015). However, further investigation to identify the exact pathway which facilitates the tumor-suppressive properties of c-Jun is required.

#### **4.4 c-JUN is not required for sustained proliferation of transformed prostate cells**

c-JUN has been described to promote cell proliferation by promoting growth factor signaling, increasing the expression of cell cycle members such as cyclin D1 and suppressing cell cycle inhibitors such as p53, p21 or p16<sup>INK4a</sup> (Eferl and Wagner 2003; Mariani et al. 2007). In murine cancer development c-Jun has primarily been described as a pro-proliferative oncogenic factor (Vogt 2001; Eferl et al. 2003; Gurzov et al. 2008). Furthermore, c-JUN has been described as a coactivator of the growth promoting AR in human PCa cell lines (Bubulya et al. 2001; Cai, Hsieh, and Shemshedini 2007). AR coactivation by c-JUN is required for sustained proliferation in LNCaP cell lines (S. Y. Chen et al. 2006). However, an overexpression of c-JUN also resulted in impaired growth of LNCaP cells which suggests that coactivity of AR and c-JUN is pro-proliferative but c-JUN activity acts anti-proliferative when it overshadows AR activity. Given these contradictory regulative properties of c-Jun, we next investigated the influence of *c-Jun* deficiency on proliferation in murine PCa cells by staining prostate sections of 19-week-old animals for the proliferation marker Ki67. Ki67 is a cell cycle regulator which is universally expressed in proliferating cells but not in resting G0 cells. We observed low proliferation in *Control* and *c-Jun*<sup>Δ/Δ</sup> prostates with only a small number of epithelial cells expressing Ki67 (Figure 6). We measured significantly increased Ki67 levels in *Pten*<sup>Δ/Δ</sup> and *Pten*<sup>Δ/Δ</sup>;*c-Jun*<sup>Δ/Δ</sup> prostates however we did not detect significant differences between the genotypes. Our findings suggest that *c-Jun* loss in murine PCa does not lead to inhibited proliferation of epithelial cells and that *c-Jun* activity is not required for sustained proliferation in the prostate. To validate our findings on proliferation from the *in-vivo* model, we established two human *c-JUN* KO PCa cell lines (brain metastasis derived DU145 and bone marrow metastasis derived PC-3 (Stone et al. 1978; Kaighn et al. 1979)) by CRISPR-Cas9 mediated deletion (Sanjana, Shalem, and Zhang 2014; Shalem et al. 2014). We used three different sgRNAs (G1, G12 and G14) targeting *c-JUN*<sup>Ex1</sup> to produce *c-JUN* KO cell lines and generated an empty vector cell line as *Control* (Figure 7). In proliferation assays, we did

not detect significant differences between *c-JUN* KO and *Control* bulk cultures of DU145 and PC-3. However, *c-JUN* KO bulk cultures still expressed residual c-JUN protein levels and therefore we picked single clones to obtain full *c-JUN* KO cell lines (Figure 9 & 10). In viable cell count base proliferation analysis of the single clones, we obtained results similar to those of bulk culture experiments and measured no proliferative difference between *c-JUN* KO and *Control*. We performed an additional resazurin proliferation assay to increase the sensitivity of our proliferation experiments. However, our resazurin assay mirrored the results of the cell-count-based proliferation curves showing no difference between *c-JUN* KO and *Control*. We therefore conclude that loss of *c-Jun* in an *in-vivo* model of PCa as well as in an *in-vitro* cell culture system did not result in significant changes in proliferation.

These findings contradict previous research on androgen-dependent and independent LNCaP cells which suggested that coactivation of AR by c-JUN is required for sustained proliferation (S. Y. Chen et al. 2006). This coactivation of AR target genes was described as independent from AR binding to its ligand and even androgen-independent cell lines such as DU145 and PC-3 should show impaired proliferation upon *c-JUN* deficiency. The previous study used short interference RNA (siRNA) to delete *c-JUN* in LNCaP cells and the discrepancy may be explained by methodological differences. In the future, we will address this difference by CRISPR-Cas9 deletion of *c-JUN* in LNCaP cells. Androgen-independent cell lines are the most similar *in-vitro* model to cancer cells of the aggressive PCa subtype castration resistant prostate cancer (CRPC) (Lonergan and Tindall 2011). Therefore, we will also investigate the coactivation of AR and c-JUN in androgen-independent cell lines in further experiments.

#### **4.5 c-Jun does not regulate caspase 3 mediated apoptosis in murine prostate tumorigenesis**

c-JUN and its activating kinase JNK were previously described to positively regulate apoptosis in mouse fibroblasts influenced by genotoxic stressors such as UV-irradiation (Shaulian et al. 2000; Hochedlinger, Wagner, and Sabapathy 2002). This mechanism was linked to c-JUN disrupting p53-p21 mediated growth arrest in favor of direct apoptosis in response to mitotic catastrophe. Furthermore, phosphorylation of c-JUN by JNK has been described to promote apoptosis in starved cells and in cells stressed by nitric oxide (NO) (L. Li, Feng, and Porter 2004). These mechanisms suggest that c-JUN and its activator JNK which is often referred to as the stress-activated protein kinase (SAPK) act as tumor-suppressors in response to cellular stress (Mehan et al. 2011). In stark

contrast, several studies showed anti-apoptotic effects of c-Jun in different settings. For example, c-Jun was reported to inhibit TNF- $\alpha$  mediated apoptosis in UV-damaged mouse fibroblasts (Wisdom, Johnson, and Moore 1999) and later a similar effect was observed for hepatocellular carcinomas (Eferl et al. 2003). The ambiguity of c-JUNs regulation of apoptosis appears to be dependent on cell type and the upstream signal inducing apoptosis (Leppä and Bohmann 1999). We hypothesized that c-Jun promotes apoptosis in the *Pten* <sup>$\Delta/\Delta$</sup>  mouse model which would explain the increased aggressiveness of the *Pten* <sup>$\Delta/\Delta$</sup> ;*c-Jun* <sup>$\Delta/\Delta$</sup>  phenotype. We therefore tested apoptosis by performing IHC of the commonly used apoptosis marker cleaved-caspase 3 (CC3) on prostate sections of 19-week-old animals. CC3 positive cells were absent in *Control* and *c-Jun* <sup>$\Delta/\Delta$</sup>  prostates whereas both tumor genotypes *Pten* <sup>$\Delta/\Delta$</sup>  and *Pten* <sup>$\Delta/\Delta$</sup> ;*c-Jun* <sup>$\Delta/\Delta$</sup>  revealed significantly increased numbers of CC3 expressing cells, however we did not observe a difference between the tumor genotypes (Figure 12). These findings suggest that c-Jun does not regulate CC3 mediated apoptosis. c-Jun activity may promote apoptosis to the same extent as it suppresses apoptosis during prostate tumorigenesis which leads to no detectable regulation of apoptosis (Shaulian et al. 2000; Wisdom, Johnson, and Moore 1999). However, we observed a highly CC3 positive staining within the gland lumen in the tumor genotypes (Figure 12A, black arrows). These glands showed a histological architecture reminiscent of intraluminal comedonecrosis which is repeatedly observed in human PCa (Kryvenko and Epstein 2016; Epstein 2018). Unspecific binding of antibody to prostate secretions could explain this staining, but the circumstance of this staining only appearing in the tumor genotypes suggests that the staining is indeed specific. The basophil granular within the intraluminal secrete may be nuclear residues of apoptotic cells which indicates that apoptotic cells are shed into the lumen and the overall rate of apoptosis may be higher than expected. A dUTP nick end labeling (TUNEL) assay may be able to clarify this observation by detection of fragmented DNA (Kyrylkova et al. 2012). Furthermore, preliminary experiments on another apoptotic marker cleaved-caspase 7 (CC7) showed reduced levels in *Pten* <sup>$\Delta/\Delta$</sup> ;*c-Jun* <sup>$\Delta/\Delta$</sup>  prostates (personal communication Desiree Lindner, Kenner lab). Activation of caspase 7 mediated apoptosis has been previously suggested as a potential therapeutic approach in treatment of human PCa cancer (Marcelli et al. 1998, 1999). In conclusion, our research suggested that CC3 mediated apoptosis is not affected upon *c-Jun*-loss *in-vivo*, but that CC7 mediated effects might be a plausible explanation for the tumor-suppressive properties of c-Jun.

## 4.6 c-Jun may be a weak regulator of senescence in murine prostate tumorigenesis

Senescence describes a permanent growth arrest of cells in response to cellular stressors and is associated with growth suppression in tumors (Muñoz-Espín and Serrano 2014; Shay and Wright 2000; Hayflick and Moorhead 1961). However, senescent cells often develop a senescence-associated secretory phenotype (SASP) which was repeatedly linked to tumor-promoting mechanisms (Kirkland and Tchkonja 2017; Muñoz-Espín and Serrano 2014). SASP promotes senescence in neighboring cells through paracrine signaling which can damage neighboring healthy tissue. Furthermore, SASP is characterized by release of pro-inflammatory chemokines and cytokines which shape a tumor-promoting microenvironment. Tumor cells which escaped senescence have been reported to adopt stem cell like features which increases their growth potential (S. Lee and Schmitt 2019; Milanovic et al. 2018). Multiple senescence marker need to be tested to determine whether an observed senescence phenotype suppresses or promotes tumor growth (Gorgoulis et al. 2019). Deficiency of the tumor-suppressor gene *PTEN* leads to the p53 mediated *PTEN*-loss induced cellular senescence (PICS) phenotype (Jung et al. 2019) and c-Jun was previously reported to suppress p53-p21 mediated senescence (Shaulian et al. 2000). We therefore hypothesized that c-Jun suppresses PICS in our PCa mouse model and we aimed to investigate the effects of this regulation in prostate tumorigenesis.

The most commonly used biomarker for senescence is  $\beta$ -galactosidase which is highly enriched in senescent cells (B. Y. Lee et al. 2006).  $\beta$ -galactosidase activity is usually tested on cryosections by measuring X-Gal metabolization rates. However, we were unable to establish a reliable staining protocol for mouse prostates due to issues with false positive and negative staining. We therefore chose an alternative  $\beta$ -galactosidase based method to measure senescence *in-vivo* by staining for the X-Gal substrate C<sub>12</sub>FDG in prostate epithelial cells of 19-week-old animals by flow cytometry (Cahu and Sola 2013). *Pten* <sup>$\Delta/\Delta$</sup>  and *Pten* <sup>$\Delta/\Delta$</sup> ;*c-Jun* <sup>$\Delta/\Delta$</sup>  prostates showed significantly increased numbers C<sub>12</sub>FDG<sup>+</sup> cells compared to *Control* which suggest that both genotypes do indeed develop a PICS phenotype (Figure 13A). Despite a mild trend toward increased senescence in *Pten* <sup>$\Delta/\Delta$</sup> ;*c-Jun* <sup>$\Delta/\Delta$</sup>  prostates, we did not observe significant differences compared to *Pten* <sup>$\Delta/\Delta$</sup>  animals. Further replicates will be necessary to obtain more conclusive results.

We also tested the senescence marker  $p16^{INK4a}$  on mRNA and protein level in prostates of 19-week-old animals to further assess the influence of c-Jun on senescence.  $Pten^{\Delta/\Delta}$  and  $Pten^{\Delta/\Delta};c-Jun^{\Delta/\Delta}$   $p16^{INK4a}$  mRNA levels were significantly different when normalized to *18s* rRNA expression (p-value of 0.0305) but were not significant when normalized to CypA (p-value of 0.0646) (Figure 13B-12D). In RNA-seq we again measured significantly increased  $p16^{INK4a}$  mRNA levels (Figure 17). However, we did not observe a difference between  $Pten^{\Delta/\Delta}$  and  $Pten^{\Delta/\Delta};c-Jun^{\Delta/\Delta}$  in  $p16^{INK4a}$  protein expression (Figure 13C-13D). Our contradictory observations on  $p16^{INK4a}$  mRNA and protein expression suggest that either c-Jun does not regulate senescence *in-vivo* or c-Jun has a mild suppressive effect on senescence. It is important to note, that RT-qPCR and WB experiments were performed using extracts of whole prostates while the RNA-seq experiment exclusively tested prostate epithelial cells. To detect minor differences in senescence through RT-qPCR and WB we would have to use extracts from epithelial cells for these experiments.

In conclusion, we propose that c-Jun has no effect on senescence or a weak suppressive effect on senescence in murine PCa. Previous studies in a *Pten/p53* deficient mouse model showed that the PICS phenotype primarily suppresses tumor growth in PCa which suggests that c-Jun acts as weak tumor-promoter by suppression of PICS (Z. Chen et al. 2005). However, expression of a SASP could result in an overall increased aggressiveness of senescent prostate tumors (Muñoz-Espín and Serrano 2014; Kirkland and Tchkonja 2017; Milanovic et al. 2018; S. Lee and Schmitt 2019; Gorgoulis et al. 2019). Testing of multiple senescence markers including SASP factors and stemness factors would be required to conclusively determine whether c-Jun actually suppresses senescence and whether this regulation promotes or suppresses tumorigenesis.

#### 4.7 c-Jun regulates immune response and inflammation

For transcriptome analysis we performed RNA-seq on prostate epithelial cells of 19-week-old animals of the genotypes *Control*,  $Pten^{\Delta/\Delta}$  and  $Pten^{\Delta/\Delta};c-Jun^{\Delta/\Delta}$ . We observed a total of 1553 DE genes being down-regulated and 319 DE genes being upregulated in  $Pten^{\Delta/\Delta};c-Jun^{\Delta/\Delta}$  compared to  $Pten^{\Delta/\Delta}$  (Figure 14B-14C). This predominant down-regulation of genes in response to *c-Jun* deficiency fits the description of c-Jun being a strong activator of gene transcription (Bakiri et al. 2002; Garces de Los Fayos Alonso et al. 2018). We investigated pathways potentially regulated by c-Jun through GSEA of the “Kegg” and “Hallmark” gene set collections of the MSigDB (Subramanian et al. 2005; Liberzon et al. 2011). We observed a down-regulation of multiple pathways associated with the development and functionality of immune cells in  $Pten^{\Delta/\Delta};c-Jun^{\Delta/\Delta}$ .

These pathways include B-cell receptor signaling, NK-cell mediated cytotoxicity and leukocyte trans-endothelial migration (Figure 15A). The importance of c-Jun and other AP-1 transcription factors for activation of leukocytes has been established previously (Foletta, Segal, and Cohen 1998; Atsaves et al. 2019). However, the RNA-seq experiment exclusively covered prostate epithelial cells. This raises the question how biologically relevant deregulation of immune cell pathways is for epithelial cells. Epithelial interaction with the innate and adaptive immune system is a well-documented mechanism which links epithelial cells with immune response (Schleimer et al. 2007). For example, epithelial cells facilitate transport of immune globulins, present antigens through pattern recognition receptors (PRR) and express factors which regulate immune cell activity and inflammation. We will review the gene sets in more detail to determine whether specific deregulated genes are also relevant for the interaction between epithelium and immune cells. The downregulation of Toll-like receptor (TLR) signaling in *Pten<sup>Δ/Δ</sup>;c-Jun<sup>Δ/Δ</sup>* indeed suggests that epithelial-immune cell interaction is impaired upon deficiency of *c-Jun* (Figure 15A). TLRs play an important role in the interaction between cancer and immune cells and can either promote anti-tumor immune response or promote tumorigenesis by facilitating inflammation (Shchebliakov et al. 2010). Furthermore, we observed a downregulation of cytokine and chemokine pathways which further hints toward an important role of c-Jun in regulation of PCa immunology and inflammation (Figure 15A). However, cytokine signaling in cancer is commonly associated with the formation of a tumor-progressive microenvironment which promotes cell growth, inflammation, and angiogenesis (Vindrieux, Escobar, and Lazennec 2009; J. Wang et al. 2005). Especially chemokines are known to promote tumor development by attracting inflammatory leukocytes and immune suppressive regulatory T-cells into the tumor microenvironment (Lien et al. 2017). In contrast, immune response promoting cytokines such as IL-2, IL-12, IL-18 and IFN- $\gamma$  act tumor-suppressive (Mocellin, Wang, and Marincola 2001; Dranoff 2004; Sheu et al. 2008). These cytokines promote the clearance of cancer cells by stimulating antigen presentation, cytotoxic T-cell activity and apoptosis. Our findings suggest that c-Jun regulates inflammation and immune response in PCa, but whether these regulatory effects promote or suppress prostate tumorigenesis is the subject of further investigation. Future experiments will focus on the status of inflammation and immune cell invasion in the PCa mouse model.

#### **4.8 c-JUN is a putative PCa biomarker with many faces**

In conclusion, our analysis of human data and experiments on the murine *c-Jun* KO model suggested that c-JUN acts as a tumor-suppressor in PCa development. Low c-JUN levels during PCa progression appear to be a risk factor for the survival of human patients. We therefore propose *c-JUN*-loss as a putative biomarker for PCa aggressiveness. We suggest that c-JUN, JNK and JUNB participate in a tumor-suppressive stress response in prostate tumorigenesis (Davis 2000; Eferl and Wagner 2003; Hübner et al. 2012; Kanno et al. 2012; Thomsen et al. 2015). Contradictive tumor-suppressive and tumor-promoting properties were described previously for all three factors, however in PCa the tumor-suppressive properties appear dominant. Our findings suggest that the pro-proliferative signaling of c-JUN has minor impact on sustained proliferation of PCa cells and *c-JUN*-loss does not lead to any proliferative impairments. We did not observe deregulation of CC3 mediated apoptosis upon *c-Jun*-loss, however preliminary results from our lab suggest impaired CC7 mediated apoptosis. Senescence appeared to be either unaffected or mildly upregulated upon *c-Jun*-loss. Furthermore, we observed a potential c-Jun mediated regulation of immune response and inflammation in murine prostate tumorigenesis. The tumor-suppressive properties of c-Jun could be attributed to one of these regulative effects or to a synergistic interaction between them and we will investigate the involved pathways in more detail. We suggest that c-JUN is foremost a tumor-modulator rather than proto-oncogene or tumor-suppressor. Cell type, tumorigenesis stage or origin of the primary activating signal may all have an influence on whether c-JUN promotes or suppresses tumor growth. We therefore propose that mere overexpression of c-JUN in any cancer type should not be regarded as compelling evidence to define c-JUN as a tumor-promoting factor and definition should be backed up by survival analyses.

## 5 References

- Aaronson, S A. 1991. "Growth Factors and Cancer." *Science* 254 (5035): 1146 LP–1153. <https://doi.org/10.1126/science.1659742>.
- Abida, Wassim, Joanna Cyrta, Glenn Heller, Davide Prandi, Joshua Armenia, Ilsa Coleman, Marcin Cieslik, et al. 2019. "Genomic Correlates of Clinical Outcome in Advanced Prostate Cancer." *Proceedings of the National Academy of Sciences of the United States of America* 166 (23): 11428–36. <https://doi.org/10.1073/pnas.1902651116>.
- Aguirre-Gamboa, Raul, Hugo Gomez-Rueda, Emmanuel Martínez-Ledesma, Antonio Martínez-Torteya, Rafael Chacolla-Huaringa, Alberto Rodriguez-Barrientos, José G. Tamez-Peña, and Victor Treviño. 2013. "SurvExpress: An Online Biomarker Validation Tool and Database for Cancer Gene Expression Data Using Survival Analysis." *PLoS ONE* 8 (9): 1–9. <https://doi.org/10.1371/journal.pone.0074250>.
- Albala, David M. 2017. "Imaging and Treatment Recommendations in Patients with Castrate-Resistant Prostate Cancer." *Reviews in Urology* 19 (3): 200–202. <https://doi.org/10.3909/riu193PracticeProfile>.
- Atsaves, Vasileios, Vasiliki Leventaki, George Z. Rassidakis, and Francois X. Claret. 2019. "AP-1 Transcription Factors as Regulators of Immune Responses in Cancer." *Cancers* 11 (7). <https://doi.org/10.3390/cancers11071037>.
- Bakiri, Latifa, Koichi Matsuo, Marta Wisniewska, Erwin F. Wagner, and Moshe Yaniv. 2002. "Promoter Specificity and Biological Activity of Tethered AP-1 Dimers." *Molecular and Cellular Biology* 22 (13): 4952–64. <https://doi.org/10.1128/mcb.22.13.4952-4964.2002>.
- Barnum, Kevin J, and Matthew J O'Connell. 2014. "Cell Cycle Regulation by Checkpoints." *Methods in Molecular Biology (Clifton, N.J.)* 1170: 29–40. [https://doi.org/10.1007/978-1-4939-0888-2\\_2](https://doi.org/10.1007/978-1-4939-0888-2_2).
- Bast, R. C., A. Berchuck, J. B. Weinberg, and R. C. Bast. 1993. "Tumor Necrosis Factor as an Autocrine and Paracrine Growth Factor for Ovarian Cancer: Monokine Induction of Tumor Cell Proliferation and Tumor Necrosis Factor Expression." *Cancer Research* 53 (8): 1939–44.
- Behrens, Axel, Maria Sibilía, Jean Pierre David, Uta Möhle-Steinlein, François Tronche, Günther Schütz, and Erwin F. Wagner. 2002. "Impaired Postnatal Hepatocyte Proliferation and Liver Regeneration in Mice Lacking C-Jun in the Liver." *EMBO Journal* 21 (7): 1782–90. <https://doi.org/10.1093/emboj/21.7.1782>.
- Behrens, Axel, Maria Sibilía, and Erwin F Wagner. 1999. "Amino-Terminal Phosphorylation of c-Jun Regulates Stress-Induced Apoptosis and Cellular Proliferation." *Nature Genetics* 21 (3): 326–29. <https://doi.org/10.1038/6854>.
- Berney, D. M., A. Gopalan, S. Kudahetti, G. Fisher, L. Ambroisine, C. S. Foster, V. Reuter, et al. 2009. "Ki-67 and Outcome in Clinically Localised Prostate Cancer: Analysis of Conservatively Treated Prostate Cancer Patients from the Trans-Atlantic Prostate Group Study." *British Journal of Cancer* 100 (6): 888–93. <https://doi.org/10.1038/sj.bjc.6604951>.
- Birbach, Andreas, David Eisenbarth, Nicolas Kozakowski, Eva Ladenhauf, Marc Schmidt-Supprian, and Johannes A. Schmid. 2011. "Persistent Inflammation Leads to Proliferative Neoplasia and Loss of Smooth Muscle Cells in a Prostate Tumor Model." *Neoplasia* 13 (8): 692–703. <https://doi.org/10.1593/neo.11524>.
- Birner, P., G. Egger, O. Merkel, and L. Kenner. 2015. "JunB and PTEN in Prostate Cancer: 'Loss Is Nothing Else than Change.'" *Cell Death and Differentiation* 22 (4): 522–23. <https://doi.org/10.1038/cdd.2014.232>.
- Blute, Michael L., Nathan Damaschke, Jennifer Wagner, Bing Yang, Martin Gleave, Ladan Fazli, Fangfang Shi, et al. 2017. "Persistence of Senescent Prostate Cancer Cells Following Prolonged Neoadjuvant Androgen Deprivation Therapy." *PLoS ONE* 12 (2): 1–11. <https://doi.org/10.1371/journal.pone.0172048>.
- Bratt, Ola, Linda Drevin, Olof Akre, Hans Garmo, and Pär Stattin. 2016. "Family History and Probability of Prostate Cancer, Differentiated by Risk Category: A Nationwide Population-Based Study." *Journal of the National Cancer Institute* 108 (10): 1–7. <https://doi.org/10.1093/jnci/djw110>.
- Brinkman, Eva K, Tao Chen, Mario Amendola, and Bas van Steensel. 2014. "Easy Quantitative Assessment of Genome Editing by Sequence Trace Decomposition." *Nucleic Acids Research* 42 (22): e168. <https://doi.org/10.1093/nar/gku936>.

- Bubici, Concetta, and Salvatore Papa. 2014. "JNK Signalling in Cancer: In Need of New, Smarter Therapeutic Targets." *British Journal of Pharmacology* 171 (1): 24–37. <https://doi.org/10.1111/bph.12432>.
- Bubulya, Athanasios, S Y Chen, C Fisher, Z Zheng, X Shen, and Lirim Shemshedini. 2001. "C-Jun Potentiates the Functional Interaction between the Amino and Carboxyl Termini of the Androgen Receptor." *The Journal of Biological Chemistry* 276 (December): 44704–11. <https://doi.org/10.1074/jbc.M107346200>.
- Budihardjo, Imawati, Holt Oliver, Michael Lutter, Xu Luo, and Xiaodong Wang. 1999. "Biochemical Pathways of Caspase Activation During Apoptosis." *Annual Review of Cell and Developmental Biology* 15 (1): 269–90. <https://doi.org/10.1146/annurev.cellbio.15.1.269>.
- Busuttill, Rita A., Miguel Rubio, Martijn E.T. Dollé, Judith Campisi, and Jan Vijg. 2003. "Oxygen Accelerates the Accumulation of Mutations during the Senescence and immortalization of Murine Cells in Culture." *Aging Cell* 2 (6): 287–94. <https://doi.org/10.1046/j.1474-9728.2003.00066.x>.
- Cahu, Julie, and Brigitte Sola. 2013. "A Sensitive Method to Quantify Senescent Cancer Cells." *Journal of Visualized Experiments : JoVE*, no. 78: 1–6. <https://doi.org/10.3791/50494>.
- Cai, Changmeng, Chen Lin Hsieh, and Lirim Shemshedini. 2007. "C-Jun Has Multiple Enhancing Activities in the Novel Cross Talk between the Androgen Receptor and Ets Variant Gene 1 in Prostate Cancer." *Molecular Cancer Research* 5 (7): 725–35. <https://doi.org/10.1158/1541-7786.MCR-06-0430>.
- Carnero, Amancio, and Jesus M. Paramio. 2014. "The PTEN/PI3K/AKT Pathway in Vivo, Cancer Mouse Models." *Frontiers in Oncology* 4 (September): 1–10. <https://doi.org/10.3389/fonc.2014.00252>.
- Chen, S. Y., C. Cai, C. J. Fisher, Z. Zheng, J. Omwancha, C. L. Hsieh, and L. Shemshedini. 2006. "C-Jun Enhancement of Androgen Receptor Transactivation Is Associated with Prostate Cancer Cell Proliferation." *Oncogene* 25 (54): 7212–23. <https://doi.org/10.1038/sj.onc.1209705>.
- Chen, Zhenbang, Lloyd C. Trotman, David Shaffer, Hui Kuan Lin, Zohar A. Dotan, Masaru Niki, Jason A. Koutcher, et al. 2005. "Crucial Role of P53-Dependent Cellular Senescence in Suppression of Pten-Deficient Tumorigenesis." *Nature* 436 (7051): 725–30. <https://doi.org/10.1038/nature03918>.
- Crawford, E David, Daniel Petrylak, and Oliver Sartor. 2017. "Navigating the Evolving Therapeutic Landscape in Advanced Prostate Cancer." *Urologic Oncology* 35S (May): S1–13. <https://doi.org/10.1016/j.urolonc.2017.01.020>.
- Cristofano, A Di, B Pesce, C Cordon-Cardo, and P P Pandolfi. 1998. "Pten Is Essential for Embryonic Development and Tumour Suppression." *Nature Genetics* 19 (4): 348–55. <https://doi.org/10.1038/1235>.
- Cunningham, David, and Zongbing You. 2015. "In Vitro and in Vivo Model Systems Used in Prostate Cancer Research." *Journal of Biological Methods* 2 (1): e17. <https://doi.org/10.14440/jbm.2015.63>.
- Dam, Hans Van, and Marc Castellazzi. 2001. "Distinct Roles of Jun:Fos and Jun:ATF Dimers in Oncogenesis." *Oncogene* 20 (19 REV. ISS. 2): 2453–64. <https://doi.org/10.1038/sj.onc.1204239>.
- Das, Madhumita, Feng Jiang, Hayla K. Sluss, Chao Zhang, Kevan M. Shokat, Richard A. Flavell, and Roger J. Davis. 2007. "Suppression of P53-Dependent Senescence by the JNK Signal Transduction Pathway." *Proceedings of the National Academy of Sciences of the United States of America* 104 (40): 15759–64. <https://doi.org/10.1073/pnas.0707782104>.
- Davies, Clare, and Cathy Tournier. 2012. "Exploring the Function of the JNK (c-Jun N-Terminal Kinase) Signalling Pathway in Physiological and Pathological Processes to Design Novel Therapeutic Strategies." *Biochemical Society Transactions* 40 (1): 85–89. <https://doi.org/10.1042/BST20110641>.
- Davis, Roger J. 2000. "Signal Transduction by the JNK Group of MAP Kinases." *Cell* 103 (2): 239–52. [https://doi.org/10.1016/S0092-8674\(00\)00116-1](https://doi.org/10.1016/S0092-8674(00)00116-1).
- Devary, Y, R A Gottlieb, L F Lau, and M Karin. 1991. "Rapid and Preferential Activation of the C-Jun Gene during the Mammalian UV Response." *Molecular and Cellular Biology* 11 (5): 2804–11. <https://doi.org/10.1128/mcb.11.5.2804>.
- Dong, Jin Tang. 2006. "Prevalent Mutations in Prostate Cancer." *Journal of Cellular Biochemistry* 97 (3): 433–47.

- <https://doi.org/10.1002/jcb.20696>.
- Dranoff, Glenn. 2004. "Cytokines in Cancer Pathogenesis and Cancer Therapy." *Nature Reviews Cancer* 4 (1): 11–22. <https://doi.org/10.1038/nrc1252>.
- DuBridge, R B, P Tang, H C Hsia, P M Leong, J H Miller, and M P Calos. 1987. "Analysis of Mutation in Human Cells by Using an Epstein-Barr Virus Shuttle System." *Molecular and Cellular Biology* 7 (1): 379–87. <https://doi.org/10.1128/mcb.7.1.379>.
- Eferl, Robert, Romeo Ricci, Lukas Kenner, Rainer Zenz, Jean Pierre David, Martina Rath, and Erwin F. Wagner. 2003. "Liver Tumor Development: C-Jun Antagonizes the Proapoptotic Activity of P53." *Cell* 112 (2): 181–92. [https://doi.org/10.1016/S0092-8674\(03\)00042-4](https://doi.org/10.1016/S0092-8674(03)00042-4).
- Eferl, Robert, and Erwin F Wagner. 2003. "AP-1: A Double-Edged Sword in Tumorigenesis." *Nature Reviews Cancer* 3 (11): 859–68. <https://doi.org/10.1038/nrc1209>.
- Elmore, Susan. 2007. "Apoptosis: A Review of Programmed Cell Death." *Toxicologic Pathology* 35 (4): 495–516. <https://doi.org/10.1080/01926230701320337>.
- Epstein, Jonathan I. 2018. "Prostate Cancer Grading: A Decade after the 2005 Modified System." *Modern Pathology: An Official Journal of the United States and Canadian Academy of Pathology, Inc* 31 (S1): S47–63. <https://doi.org/10.1038/modpathol.2017.133>.
- Esserman, Laura J, Ian M Thompson, Brian Reid, Peter Nelson, David F Ransohoff, H Gilbert Welch, Shelley Hwang, et al. 2014. "Addressing Overdiagnosis and Overtreatment in Cancer: A Prescription for Change." *The Lancet. Oncology* 15 (6): e234–42. [https://doi.org/10.1016/S1470-2045\(13\)70598-9](https://doi.org/10.1016/S1470-2045(13)70598-9).
- Fan, Meiyun, Mary E. Goodwin, Michael J. Birrer, and Timothy C. Chambers. 2001. "The C-Jun NH2-Terminal Protein Kinase/AP-1 Pathway Is Required for Efficient Apoptosis Induced by Vinblastine." *Cancer Research* 61 (11): 4450–58.
- Ferlay, Jacques, Isabelle Soerjomataram, Rajesh Dikshit, Sultan Eser, Colin Mathers, Marise Rebelo, Donald Maxwell Parkin, David Forman, and Freddie Bray. 2015. "Cancer Incidence and Mortality Worldwide: Sources, Methods and Major Patterns in GLOBOCAN 2012." *International Journal of Cancer* 136 (5): E359–86. <https://doi.org/10.1002/ijc.29210>.
- Ferrís-I-Tortajada, J, O Berbel-Tornero, J Garcia-I-Castell, J A López-Andreu, E Sobrino-Najul, and J A Ortega-García. 2011. "Non dietetic environmental risk factors in prostate cancer TT - Factores de riesgo ambientales no dietéticos en el cáncer de próstata." *Actas urológicas españolas* 35 (5): 289–95. <https://doi.org/10.1016/j.acuro.2010.12.010>.
- Foletta, Victoria C., David H. Segal, and Donna R. Cohen. 1998. "Transcriptional Regulation in the Immune System: All Roads Lead to AP-1." *Journal of Leukocyte Biology* 63 (2): 139–52. <https://doi.org/10.1002/jlb.63.2.139>.
- Fujita, Kazutoshi, and Norio Nonomura. 2019. "Role of Androgen Receptor in Prostate Cancer: A Review." *The World Journal of Men's Health* 37 (3): 288. <https://doi.org/10.5534/wjmh.180040>.
- Gaddipati, Jaya P, David G McLeod, Howard B Heidenberg, Isabell A Sesterhenn, Michael J Finger, Judd W Moul, and Shiv Srivastava. 1994. "Frequent Detection of Codon 877 Mutation in the Androgen Receptor Gene in Advanced Prostate Cancers." *Cancer Research* 54 (11): 2861 LP – 2864. <http://cancerres.aacrjournals.org/content/54/11/2861.abstract>.
- Gandaglia, Giorgio, Firas Abdollah, Jonas Schiffmann, Vincent Trudeau, Shahrokh F Shariat, Simon P Kim, Paul Perrotte, et al. 2014. "Distribution of Metastatic Sites in Patients with Prostate Cancer: A Population-Based Analysis." *The Prostate* 74 (2): 210–16. <https://doi.org/10.1002/pros.22742>.
- Gann, Peter H. 2002. "Risk Factors for Prostate Cancer." *Reviews in Urology* 4 Suppl 5 (Suppl 5): S3–10. <https://www.ncbi.nlm.nih.gov/pubmed/16986064>.
- Garces de Los Fayos Alonso, Ines, Huan Chang Liang, Suzanne D. Turner, Sabine Lagger, Olaf Merkel, and Lukas Kenner. 2018. "The Role of Activator Protein-1 (AP-1) Family Members in CD30-Positive Lymphomas." *Cancers* 10 (4): 1–22. <https://doi.org/10.3390/cancers10040093>.
- Gazon, Hélène, Benoit Barbeau, Jean Michel Mesnard, and Jean Marie Peloponese. 2018. "Hijacking of the AP-1 Signaling Pathway during Development of ATL." *Frontiers in Microbiology* 8 (JAN): 1–13. <https://doi.org/10.3389/fmicb.2017.02686>.

- George, Nicholas J R. 2010. "CHAPTER 86 - The Prostate." In , edited by Howard M Fillit, Kenneth Rockwood, and Kenneth B T - Brocklehurst's Textbook of Geriatric Medicine and Gerontology (Seventh Edition) Woodhouse, 701–15. Philadelphia: W.B. Saunders. <https://doi.org/https://doi.org/10.1016/B978-1-4160-6231-8.10086-8>.
- Gleason, D F. 1966. "Classification of Prostatic Carcinomas." *Cancer Chemotherapy Reports* 50 (3): 125–28.
- Gorgoulis, Vassilis, Peter D. Adams, Andrea Alimonti, Dorothy C. Bennett, Oliver Bischof, Cleo Bishop, Judith Campisi, et al. 2019. "Cellular Senescence: Defining a Path Forward." *Cell* 179 (4): 813–27. <https://doi.org/10.1016/j.cell.2019.10.005>.
- Gurzov, E. N., L. Bakiri, J. M. Alfaro, E. F. Wagner, and M. Izquierdo. 2008. "Targeting C-Jun and JunB Proteins as Potential Anticancer Cell Therapy." *Oncogene* 27 (5): 641–52. <https://doi.org/10.1038/sj.onc.1210690>.
- Guy, Michelle, Zsofia Kote-Jarai, Graham G. Giles, Ali Amin Al Olama, Sarah K. Jugurnauth, Shani Mulholland, Daniel A. Leongamornlert, et al. 2009. "Identification of New Genetic Risk Factors for Prostate Cancer." *Asian Journal of Andrology* 11 (1): 49–55. <https://doi.org/10.1038/aja.2008.18>.
- Hanahan, Douglas, and Robert A. Weinberg. 2011. "Hallmarks of Cancer: The next Generation." *Cell* 144 (5): 646–74. <https://doi.org/10.1016/j.cell.2011.02.013>.
- Hanahan, Douglas, and Robert A Weinberg. 2000. "The Hallmarks of Cancer." *Cell* 100 (1): 57–70. [https://doi.org/10.1016/S0092-8674\(00\)81683-9](https://doi.org/10.1016/S0092-8674(00)81683-9).
- Hasselblatt, P., L. Gresh, H. Kudo, J. Guinea-Viniegra, and E. F. Wagner. 2008. "The Role of the Transcription Factor AP-1 in Colitis-Associated and  $\beta$ -Catenin-Dependent Intestinal Tumorigenesis in Mice." *Oncogene* 27 (47): 6102–9. <https://doi.org/10.1038/onc.2008.211>.
- Hayakawa, Jun, Shalu Mittal, Yipeng Wang, Kemal S. Korkmaz, Eileen Adamson, Christopher English, Masahide Omichi, Michael McClelland, and Dan Mercola. 2004. "Identification of Promoters Bound by C-Jun/ATF2 during Rapid Large-Scale Gene Activation Following Genotoxic Stress." *Molecular Cell* 16 (4): 521–35. <https://doi.org/10.1016/j.molcel.2004.10.024>.
- Hayflick, L, and P S Moorhead. 1961. "The Serial Cultivation of Human Diploid Cell Strains." *Experimental Cell Research* 25 (3): 585–621. [https://doi.org/https://doi.org/10.1016/0014-4827\(61\)90192-6](https://doi.org/https://doi.org/10.1016/0014-4827(61)90192-6).
- Hegarty, Nicholas J., and Paul K. Hegarty. 2013. "Natural History of Prostate Cancer." *Prostate Cancer: A Comprehensive Perspective* 23 (1): 311–16. [https://doi.org/10.1007/978-1-4471-2864-9\\_25](https://doi.org/10.1007/978-1-4471-2864-9_25).
- Hess, Jochen, Peter Angel, and Marina Schorpp-Kistner. 2004. "AP-1 Subunits: Quarrel and Harmony among Siblings." *Journal of Cell Science* 117 (25): 5965–73. <https://doi.org/10.1242/jcs.01589>.
- Hilberg, Frank, Adriano Aguzzi, Norma Howells, and Erwin F Wagner. 1993. "C-Jun Is Essential for Normal Mouse Development and Hepatogenesis." *Nature* 365 (6442): 179–81. <https://doi.org/10.1038/365179a0>.
- Hill, Reginald, Yurong Song, Robert D Cardiff, and Terry Van Dyke. 2005. "Selective Evolution of Stromal Mesenchyme with P53 Loss in Response to Epithelial Tumorigenesis." *Cell* 123 (6): 1001–11. <https://doi.org/https://doi.org/10.1016/j.cell.2005.09.030>.
- Hochedlinger, Konrad, Erwin F. Wagner, and Kanaga Sabapathy. 2002. "Differential Effects of JNK1 and JNK2 on Signal Specific Induction of Apoptosis." *Oncogene* 21 (15): 2441–45. <https://doi.org/10.1038/sj.onc.1205348>.
- Hoof, Pamela, Ginger Tsai-Nguyen, Scott Paulson, Almas Syed, and Adam Mora Jr. 2016. "Neuroendocrine Carcinoma of the Prostate Gland." *Proceedings (Baylor University Medical Center)* 29 (1): 68–69. <https://doi.org/10.1080/08998280.2016.11929365>.
- Horoszewicz, J S, S S Leong, T M Chu, Z L Wajzman, M Friedman, L Papsidero, U Kim, et al. 1980. "The LNCaP Cell Line--a New Model for Studies on Human Prostatic Carcinoma." *Progress in Clinical and Biological Research* 37: 115–32.
- Hsu, Chih Chao, and Chang Deng Hu. 2013. "Transcriptional Activity of C-Jun Is Critical for the Suppression of AR Function." *Molecular and Cellular Endocrinology* 372 (1–2): 12–22. <https://doi.org/10.1016/j.mce.2013.03.004>.
- Hübner, Anette, David J Mulholland, Claire L Standen, Maria Karasarides, Julie Cavanagh-Kyros, Tamera Barrett, Hongbo Chi, et al. 2012. "JNK and PTEN Cooperatively Control the Development of Invasive Adenocarcinoma of the Prostate."

- Proceedings of the National Academy of Sciences* 109 (30): 12046 LP – 12051. <https://doi.org/10.1073/pnas.1209660109>.
- Hui, Lijian, Latifa Bakiri, Andreas Mairhorfer, Norbert Schweifer, Christian Haslinger, Lukas Kenner, Vukoslav Komnenovic, Harald Scheuch, Hartmut Beug, and Erwin F Wagner. 2007. “P38 $\alpha$  Suppresses Normal and Cancer Cell Proliferation by Antagonizing the JNK–c-Jun Pathway.” *Nature Genetics* 39 (6): 741–49. <https://doi.org/10.1038/ng2033>.
- Ilic, D, M M Neuberger, M Djulbegovic, and P Dahm. 2013. “Screening for Prostate Cancer.” *Cochrane Database of Systematic Reviews*, no. 1. <https://doi.org/10.1002/14651858.CD004720.pub3>.
- Ivanov, Vladimir N, Mikhail Krasilnikov, and Ze’ev Ronai. 2002. “Regulation of Fas Expression by STAT3 and C-Jun Is Mediated by Phosphatidylinositol 3-Kinase-AKT Signaling.” *The Journal of Biological Chemistry* 277 (7): 4932–44. <https://doi.org/10.1074/jbc.M108233200>.
- Jahn, Jaquelyn L., Edward L. Giovannucci, and Meir J. Stampfer. 2015. “The High Prevalence of Undiagnosed Prostate Cancer at Autopsy: Implications for Epidemiology and Treatment of Prostate Cancer in the Prostate-Specific Antigen-Era.” *International Journal of Cancer* 137 (12): 2795–2802. <https://doi.org/10.1002/ijc.29408>.
- Jiao, Xuanmao, Sanjay Katiyar, Nicole E. Willmarth, Manran Liu, Xiaojing Ma, Neal Flomenberg, Michael P. Lisanti, and Richard G. Pestell. 2010. “C-Jun Induces Mammary Epithelial Cellular Invasion and Breast Cancer Stem Cell Expansion.” *Journal of Biological Chemistry* 285 (11): 8218–26. <https://doi.org/10.1074/jbc.M110.100792>.
- Jochum, Wolfram, Emmanuelle Passequé, and Erwin F. Wagner. 2001. “AP-1 in Mouse Development and Tumorigenesis.” *Oncogene* 20 (19 REV. ISS. 2): 2401–12. <https://doi.org/10.1038/sj.onc.1204389>.
- Jung, Seung Hee, Hyun Jung Hwang, Donghee Kang, Hyun A. Park, Hyung Chul Lee, Daecheol Jeong, Keunwook Lee, Heon Joo Park, Young Gyu Ko, and Jae Seon Lee. 2019. “MTOR Kinase Leads to PTEN-Loss-Induced Cellular Senescence by Phosphorylating P53.” *Oncogene* 38 (10): 1639–50. <https://doi.org/10.1038/s41388-018-0521-8>.
- Kaighn, M E, K S Narayan, Y Ohnuki, J F Lechner, and L W Jones. 1979. “Establishment and Characterization of a Human Prostatic Carcinoma Cell Line (PC-3).” *Investigative Urology* 17 (1): 16–23.
- Kanno, T, T Kamba, T Yamasaki, N Shibasaki, R Saito, N Terada, Y Toda, et al. 2012. “JunB Promotes Cell Invasion and Angiogenesis in VHL-Defective Renal Cell Carcinoma.” *Oncogene* 31 (25): 3098–3110. <https://doi.org/10.1038/onc.2011.475>.
- Kappelmann, Melanie, Anja Bosserhoff, and Silke Kuphal. 2014. “AP-1/c-Jun Transcription Factors: Regulation and Function in Malignant Melanoma.” *European Journal of Cell Biology* 93 (1–2): 76–81. <https://doi.org/10.1016/j.ejcb.2013.10.003>.
- Karin, Michael. 1996. “The Regulation of AP-1 Activity by Mitogen-Activated Protein Kinases.” *Philosophical Transactions of the Royal Society B: Biological Sciences*. <https://doi.org/10.1098/rstb.1996.0008>.
- Kasibhatla, Shailaja, and Ben Tseng. 2003. “Why Target Apoptosis in Cancer Treatment?” *Molecular Cancer Therapeutics* 2 (6): 573–80.
- Kirkland, James L., and Tamara Tchkonina. 2017. “Cellular Senescence: A Translational Perspective.” *EBioMedicine* 21: 21–28. <https://doi.org/10.1016/j.ebiom.2017.04.013>.
- Konishi, Noboru, Keiji Shimada, Mitsutoshi Nakamura, Eiwa Ishida, Ichiro Ota, Nobumichi Tanaka, and Kiyohide Fujimoto. 2008. “Function of JunB in Transient Amplifying Cell Senescence and Progression of Human Prostate Cancer.” *Clinical Cancer Research* 14 (14): 4408–16. <https://doi.org/10.1158/1078-0432.CCR-07-4120>.
- Kõressaar, Triinu, Maarja Lepamets, Lauris Kaplinski, Kairi Raime, Reidar Andreson, and Mairo Remm. 2018. “Primer3\_masker: Integrating Masking of Template Sequence with Primer Design Software.” *Bioinformatics (Oxford, England)* 34 (11): 1937–38. <https://doi.org/10.1093/bioinformatics/bty036>.
- Koressaar, Triinu, and Mairo Remm. 2007. “Enhancements and Modifications of Primer Design Program Primer3.” *Bioinformatics (Oxford, England)* 23 (10): 1289–91. <https://doi.org/10.1093/bioinformatics/btm091>.
- Kryvenko, Oleksandr N., and Jonathan I. Epstein. 2016. “Prostate Cancer Grading: A Decade after the 2005 Modified Gleason Grading System.” *Archives of Pathology and Laboratory Medicine* 140 (10): 1153–56. <https://doi.org/10.5858/arpa.2015->

0487-SA.

- Kyrylkova, Kateryna, Sergiy Kyryachenko, Mark Leid, and Chrissa Kioussi. 2012. "Detection of Apoptosis by TUNEL Assay." In *Odontogenesis: Methods and Protocols*, edited by Chrissa Kioussi, 41–47. Totowa, NJ: Humana Press. [https://doi.org/10.1007/978-1-61779-860-3\\_5](https://doi.org/10.1007/978-1-61779-860-3_5).
- Lange, Tobias, Sebastian Ullrich, Imke Müller, Michael F. Nentwich, Katrin Stübke, Susanne Feldhaus, Christine Knies, et al. 2012. "Human Prostate Cancer in a Clinically Relevant Xenograft Mouse Model: Identification of b(1,6)-Branched Oligosaccharides as a Marker of Tumor Progression." *Clinical Cancer Research* 18 (5): 1364–73. <https://doi.org/10.1158/1078-0432.CCR-11-2900>.
- Le, Siyuan, Thomas J. Connors, and Anna C. Maroney. 2001. "C-Jun N-Terminal Kinase Specifically Phosphorylates P66ShcA at Serine 36 in Response to Ultraviolet Irradiation." *Journal of Biological Chemistry* 276 (51): 48332–36. <https://doi.org/10.1074/jbc.M106612200>.
- Lee, Bo Yun, Jung A. Han, Jun Sub Im, Amelia Morrone, Kimberly Johung, Edward C. Goodwin, Wim J. Kleijer, Daniel DiMaio, and Eun Seong Hwang. 2006. "Senescence-Associated  $\beta$ -Galactosidase Is Lysosomal  $\beta$ -Galactosidase." *Aging Cell* 5 (2): 187–95. <https://doi.org/10.1111/j.1474-9726.2006.00199.x>.
- Lee, J. J., J. H. Lee, Y. G. Ko, S. I. Hong, and J. S. Lee. 2010. "Prevention of Premature Senescence Requires JNK Regulation of Bcl-2 and Reactive Oxygen Species." *Oncogene* 29 (4): 561–75. <https://doi.org/10.1038/onc.2009.355>.
- Lee, Soyoung, and Clemens A. Schmitt. 2019. "The Dynamic Nature of Senescence in Cancer." *Nature Cell Biology* 21 (1): 94–101. <https://doi.org/10.1038/s41556-018-0249-2>.
- Leppä, Sirpa, and Dirk Bohmann. 1999. "Diverse Functions of JNK Signaling and C-Jun in Stress Response and Apoptosis." *Oncogene* 18 (45): 6158–62. <https://doi.org/10.1038/sj.onc.1203173>.
- Li, Lei, Zhiwei Feng, and Alan G. Porter. 2004. "JNK-Dependent Phosphorylation of c-Jun on Serine 63 Mediates Nitric Oxide-Induced Apoptosis of Neuroblastoma Cells." *Journal of Biological Chemistry* 279 (6): 4058–65. <https://doi.org/10.1074/jbc.M310415200>.
- Li, Wenhua, Chin Lee Wu, Phillip G. Febbo, and Aria F. Olumi. 2007. "Stromally Expressed C-Jun Regulates Proliferation of Prostate Epithelial Cells." *American Journal of Pathology* 171 (4): 1189–98. <https://doi.org/10.2353/ajpath.2007.070285>.
- Liberzon, Arthur, Chet Birger, Helga Thorvaldsdóttir, Mahmoud Ghandi, Jill P Mesirov, and Pablo Tamayo. 2015. "The Molecular Signatures Database (MSigDB) Hallmark Gene Set Collection." *Cell Systems* 1 (6): 417–25. <https://doi.org/10.1016/j.cels.2015.12.004>.
- Liberzon, Arthur, Aravind Subramanian, Reid Pinchback, Helga Thorvaldsdóttir, Pablo Tamayo, and Jill P. Mesirov. 2011. "Molecular Signatures Database (MSigDB) 3.0." *Bioinformatics* 27 (12): 1739–40. <https://doi.org/10.1093/bioinformatics/btr260>.
- Lien, Ming Yu, Chiao Wen Lin, Hsiao Chi Tsai, Yng Tay Chen, Ming Hsui Tsai, Chun Hung Hua, Shun Fa Yang, and Chih Hsin Tang. 2017. "Impact of CCL4 Gene Polymorphisms and Environmental Factors on Oral Cancer Development and Clinical Characteristics." *Oncotarget* 8 (19): 31424–34. <https://doi.org/10.18632/oncotarget.15615>.
- Litwin, Mark S., and Hung Jui Tan. 2017. "The Diagnosis and Treatment of Prostate Cancer: A Review." *JAMA - Journal of the American Medical Association* 317 (24): 2532–42. <https://doi.org/10.1001/jama.2017.7248>.
- Lone, Bilal Ahmad, Shibendra Kumar Lal Karna, Faiz Ahmad, Nerina Shahi, and Yuba Raj Pokharel. 2018. "CRISPR/Cas9 System: A Bacterial Tailor for Genomic Engineering." *Genetics Research International* 2018. <https://doi.org/10.1155/2018/3797214>.
- Lonergan, Peter, and Donald Tindall. 2011. "Androgen Receptor Signaling in Prostate Cancer Development and Progression." *Journal of Carcinogenesis* 10: 1–21. <https://doi.org/10.4103/1477-3163.83937>.
- Lorenzo, Petra Isabel, and Fahri Saatcioglu. 2008. "Inhibition of Apoptosis in Prostate Cancer Cells by Androgens Is Mediated through Downregulation of C-Jun N-Terminal Kinase Activation." *Neoplasia* 10 (5): 418–28. <https://doi.org/10.1593/neo.07985>.

- Love, Michael I., Wolfgang Huber, and Simon Anders. 2014. "Moderated Estimation of Fold Change and Dispersion for RNA-Seq Data with DESeq2." *Genome Biology* 15 (12): 1–21. <https://doi.org/10.1186/s13059-014-0550-8>.
- Madan, Raghav, Mustafa Deebajah, Shaheen Alanee, Nilesh S Gupta, Shannon Carskadon, Nallasivam Palanisamy, and Sean R Williamson. 2019. "Prostate Cancer with Comedonecrosis Is Frequently, but Not Exclusively, Intraductal Carcinoma: A Need for Reappraisal of Grading Criteria." *Histopathology* 74 (7): 1081–87. <https://doi.org/10.1111/his.13833>.
- Marcelli, Marco, Glenn R. Cunningham, S. Joe Haidacher, Sebastian J. Padayatty, Lydia Sturgis, Carolina Kagan, and Larry Denner. 1998. "Caspase-7 Is Activated during Lovastatin-Induced Apoptosis of the Prostate Cancer Cell Line LNCaP." *Cancer Research* 58 (1): 76–83.
- Marcelli, Marco, Glenn R. Cunningham, Margaret Walkup, Zening He, Lydia Sturgis, Carolina Kagan, Roberta Mannucci, Ildo Nicoletti, Ba Bie Teng, and Larry Denner. 1999. "Signaling Pathway Activated during Apoptosis of the Prostate Cancer Cell Line LNCaP: Overexpression of Caspase-7 as a New Gene Therapy Strategy for Prostate Cancer." *Cancer Research* 59 (2): 382–90.
- Mariani, Odette, Caroline Brennetot, Jean Michel Coindre, Nadège Gruel, Carine Ganem, Olivier Delattre, Marc Henri Stern, and Alain Aurias. 2007. "JUN Oncogene Amplification and Overexpression Block Adipocytic Differentiation in Highly Aggressive Sarcomas." *Cancer Cell* 11 (4): 361–74. <https://doi.org/10.1016/j.ccr.2007.02.007>.
- Mehan, Sidharth, Harikesh Meena, Deepak Sharma, and Rameshwar Sankhla. 2011. "JNK: A Stress-Activated Protein Kinase Therapeutic Strategies and Involvement in Alzheimer's and Various Neurodegenerative Abnormalities." *Journal of Molecular Neuroscience* 43 (3): 376–90. <https://doi.org/10.1007/s12031-010-9454-6>.
- Meng, Qinghang, and Ying Xia. 2011. "C-Jun, at the Crossroad of the Signaling Network." *Protein and Cell* 2 (11): 889–98. <https://doi.org/10.1007/s13238-011-1113-3>.
- Milanovic, Maja, Dorothy N Y Fan, Dimitri Belenki, J Henry M Däbritz, Zhen Zhao, Yong Yu, Jan R Dörr, et al. 2018. "Senescence-Associated Reprogramming Promotes Cancer Stemness." *Nature* 553 (7686): 96–100. <https://doi.org/10.1038/nature25167>.
- Mocellin, Simone, Ena Wang, and Francesco Maria Marincola. 2001. "Cytokines and Immune Response in the Tumor Microenvironment." *Journal of Immunotherapy* 24 (5). [https://journals.lww.com/immunotherapy-journal/Fulltext/2001/09000/Cytokines\\_and\\_Immune\\_Response\\_in\\_the\\_Tumor.2.aspx](https://journals.lww.com/immunotherapy-journal/Fulltext/2001/09000/Cytokines_and_Immune_Response_in_the_Tumor.2.aspx).
- Mootha, Vamsi K, Cecilia M Lindgren, Karl-Fredrik Eriksson, Aravind Subramanian, Smita Sihag, Joseph Lehar, Pere Puigserver, et al. 2003. "PGC-1 $\alpha$ -Responsive Genes Involved in Oxidative Phosphorylation Are Coordinately Downregulated in Human Diabetes." *Nature Genetics* 34 (3): 267–73. <https://doi.org/10.1038/ng1180>.
- Muñoz-Espín, Daniel, and Manuel Serrano. 2014. "Cellular Senescence: From Physiology to Pathology." *Nature Reviews Molecular Cell Biology* 15 (7): 482–96. <https://doi.org/10.1038/nrm3823>.
- Nateri, Abdolrahman S, Bradley Spencer-Dene, and Axel Behrens. 2005. "Interaction of Phosphorylated C-Jun with TCF4 Regulates Intestinal Cancer Development." *Nature* 437 (7056): 281–85. <https://doi.org/10.1038/nature03914>.
- Nguyen, Bastien, Jose Mauricio Mota, Subhiksha Nandakumar, Konrad H Stopsack, Emily Weg, Dana Rathkopf, Michael J Morris, et al. 2020. "Pan-Cancer Analysis of *CDK12* Alterations Identifies a Subset of Prostate Cancers with Distinct Genomic and Clinical Characteristics." *European Urology*, June. <https://doi.org/10.1016/j.eururo.2020.03.024>.
- O'Brien, John, Ian Wilson, Terry Orton, and François Pognan. 2000. "Investigation of the Alamar Blue (Resazurin) Fluorescent Dye for the Assessment of Mammalian Cell Cytotoxicity." *European Journal of Biochemistry* 267 (17): 5421–26. <https://doi.org/10.1046/j.1432-1327.2000.01606.x>.
- Oberholzer, Patrick A., Damien Kee, Piotr Dziunycz, Antje Sucker, Nyam Kamsukom, Robert Jones, Christine Roden, et al. 2012. "RAS Mutations Are Associated with the Development of Cutaneous Squamous Cell Tumors in Patients Treated with RAF Inhibitors." *Journal of Clinical Oncology* 30 (3): 316–21. <https://doi.org/10.1200/JCO.2011.36.7680>.
- Oliveira, Daniel S.M., Sijana Dzinic, Alan I. Bonfil, Allen D. Saliganan, Shijie Sheng, and R. Daniel Bonfil. 2016. "The Mouse Prostate: A Basic Anatomical and Histological Guideline." *Bosnian Journal of Basic Medical Sciences* 16 (1): 8–13.

- <https://doi.org/10.17305/bjbms.2016.917>.
- Parker, C., S. Gillissen, A. Heidenreich, and A. Horwich. 2015. "Cancer of the Prostate: ESMO Clinical Practice Guidelines for Diagnosis, Treatment and Follow-Up." *Annals of Oncology* 26 (February 2002): v69–77. <https://doi.org/10.1093/annonc/mdv222>.
- Philip, Joe, Subhajit Dutta Roy, Mohammed Ballal, Christopher S. Foster, and Pradip Javlé. 2005. "Is a Digital Rectal Examination Necessary in the Diagnosis and Clinical Staging of Early Prostate Cancer?" *BJU International* 95 (7): 969–71. <https://doi.org/10.1111/j.1464-410X.2005.05449.x>.
- Picco, Vincent, and Gilles Pagès. 2013. "Linking JNK Activity to the DNA Damage Response." *Genes and Cancer* 4 (9–10): 360–68. <https://doi.org/10.1177/1947601913486347>.
- Pilić, Patrick G., Anna M. Johnson, Kristen L. Hanson, Megan E. Dayno, Ashley L. Kapron, Elena M. Stoffel, and Kathleen A. Cooney. 2017. "Germline Genetic Variants in Men with Prostate Cancer and One or More Additional Cancers." *Cancer* 123 (20): 3925–32. <https://doi.org/10.1002/cncr.30817>.
- Potapova, O., M. Gorospe, R. H. Dougherty, N. M. Dean, W. A. Gaarde, and N. J. Holbrook. 2000. "Inhibition of C-Jun N-Terminal Kinase 2 Expression Suppresses Growth and Induces Apoptosis of Human Tumor Cells in a P53-Dependent Manner." *Molecular and Cellular Biology* 20 (5): 1713–22. <https://doi.org/10.1128/mcb.20.5.1713-1722.2000>.
- Rawla, Prashanth. 2019. "Epidemiology of Prostate Cancer." *World Journal of Oncology* 10 (2): 63–89. <https://doi.org/10.14740/wjon1191>.
- Robinson, Mark D., Davis J. McCarthy, and Gordon K. Smyth. 2009. "EdgeR: A Bioconductor Package for Differential Expression Analysis of Digital Gene Expression Data." *Bioinformatics* 26 (1): 139–40. <https://doi.org/10.1093/bioinformatics/btp616>.
- Russell, W M S, R L Burch, and Universities Federation for Animal Welfare. 1992. *The Principles of Humane Experimental Technique*. Wheathampstead: Universities Federation for Animal Welfare.
- Ryseck, Rolf-peter, and Rodrigo Bravo. 2014. "C-JUN , JUN B , and JUN D Differ in Their Binding Affinities to AP-1 and CRE Consensus Sequences : Effect of FOS Proteins c-JUN , JUN B , and JUN D Differ in Their Binding Affinities to AP-1 and CRE Consensus Sequences : Effect of FOS Proteins," no. May.
- Sagiv, A., A. Biran, M. Yon, J. Simon, S. W. Lowe, and V. Krizhanovsky. 2013. "Granule Exocytosis Mediates Immune Surveillance of Senescent Cells." *Oncogene* 32 (15): 1971–77. <https://doi.org/10.1038/onc.2012.206>.
- Sanjana, Neville E, Ophir Shalem, and Feng Zhang. 2014. "Improved Vectors and Genome-Wide Libraries for CRISPR Screening." *Nature Methods* 11 (8): 783–84. <https://doi.org/10.1038/nmeth.3047>.
- Schleimer, Robert P, Atsushi Kato, Robert Kern, Douglas Kuperman, and Pedro C Avila. 2007. "Epithelium: At the Interface of Innate and Adaptive Immune Responses." *The Journal of Allergy and Clinical Immunology* 120 (6): 1279–84. <https://doi.org/10.1016/j.jaci.2007.08.046>.
- Schossere, Markus, Johannes Grillari, and Michael Breitenbach. 2017. "The Dual Role of Cellular Senescence in Developing Tumors and Their Response to Cancer Therapy." *Frontiers in Oncology* 7 (NOV). <https://doi.org/10.3389/fonc.2017.00278>.
- Schreiber, Martin, Andrea Kolbus, Fabrice Piu, Axel Szabowski, Uta Möhle-Steinlein, Jianmin Tian, Michael Karin, Peter Angel, and Erwin F. Wagner. 1999. "Control of Cell Cycle Progression by C-Jun Is P53 Dependent." *Genes and Development* 13 (5): 607–19. <https://doi.org/10.1101/gad.13.5.607>.
- Shalem, Ophir, Neville E Sanjana, Ella Hartenian, Xi Shi, David A Scott, Tarjei Mikkelsen, Dirk Heckl, et al. 2014. "Genome-Scale CRISPR-Cas9 Knockout Screening in Human Cells." *Science (New York, N.Y.)* 343 (6166): 84–87. <https://doi.org/10.1126/science.1247005>.
- Shappell, Scott B., George V. Thomas, Richard L. Roberts, Ron Herbert, Michael M. Ittmann, Mark A. Rubin, Peter A. Humphrey, et al. 2004. "Prostate Pathology of Genetically Engineered Mice: Definitions and Classification. The Consensus Report from the Bar Harbor Meeting of the Mouse Models of Human Cancer Consortium Prostate Pathology Committee." *Cancer Research* 64 (6): 2270–2305. <https://doi.org/10.1158/0008-5472.CAN-03-0946>.

- Shaulian, Eitan. 2010. "AP-1 - The Jun Proteins: Oncogenes or Tumor Suppressors in Disguise?" *Cellular Signalling* 22 (6): 894–99. <https://doi.org/10.1016/j.cellsig.2009.12.008>.
- Shaulian, Eitan, Martin Schreiber, Fabrice Piu, Michelle Beeche, Erwin F Wagner, and Michael Karin. 2000. "The Mammalian UV Response: C-Jun Induction Is Required for Exit from P53-Imposed Growth Arrest." *Cell* 103 (6): 897–907. [https://doi.org/10.1016/S0092-8674\(00\)00193-8](https://doi.org/10.1016/S0092-8674(00)00193-8).
- Shay, J W, and W E Wright. 2000. "Hayflick, His Limit, and Cellular Ageing." *Nature Reviews. Molecular Cell Biology* 1 (1): 72–76. <https://doi.org/10.1038/35036093>.
- Shchebliakov, D V, D Y Logunov, A I Tikhvatulin, M M Shmarov, B S Naroditsky, and A L Ginzburg. 2010. "Toll-Like Receptors (TLRs): The Role in Tumor Progression." *Acta Naturae* 2 (3): 21–29. <https://doi.org/10.32607/20758251-2010-2-3-21-29>.
- Shen, Michael M, and Cory Abate-Shen. 2010. "Molecular Genetics of Prostate Cancer: New Prospects for Old Challenges." *Genes & Development* 24 (18): 1967–2000. <https://doi.org/10.1101/gad.1965810>.
- Sheu, Bor-Ching, Wen-Chun Chang, Chieh-Yang Cheng, Ho-Hsiung Lin, Daw-Yuan Chang, and Su-Cheng Huang. 2008. "Cytokine Regulation Networks in the Cancer Microenvironment." *Frontiers in Bioscience: A Journal and Virtual Library*. Department of Obstetrics and Gynecology, National Taiwan University Hospital, 7 Chung-Shan South Road, Taipei, 100, Taiwan. [bcsheu@ntu.edu.tw](mailto:bcsheu@ntu.edu.tw). <https://doi.org/10.2741/3152>.
- Song, Allisa J, and Richard D Palmiter. 2018. "Detecting and Avoiding Problems When Using the Cre-Lox System." *Trends in Genetics: TIG* 34 (5): 333–40. <https://doi.org/10.1016/j.tig.2017.12.008>.
- Song, Min Sup, Leonardo Salmena, and Pier Paolo Pandolfi. 2012. "The Functions and Regulation of the PTEN Tumour Suppressor." *Nature Reviews Molecular Cell Biology* 13 (5): 283–96. <https://doi.org/10.1038/nrm3330>.
- Stewart, Sheila A, Derek M Dykxhoorn, Deborah Palliser, Hana Mizuno, Evan Y Yu, Dong Sung An, David M Sabatini, et al. 2003. "Lentivirus-Delivered Stable Gene Silencing by RNAi in Primary Cells." *RNA (New York, N.Y.)* 9 (4): 493–501. <https://doi.org/10.1261/rna.2192803>.
- Stone, Kenneth R, Don D Mickey, Heidi Wunderli, George H Mickey, and David F Paulson. 1978. "Isolation of a Human Prostate Carcinoma Cell Line (DU 145)." *International Journal of Cancer* 21 (3): 274–81. <https://doi.org/10.1002/ijc.2910210305>.
- Subramanian, Aravind, Pablo Tamayo, Vamsi K. Mootha, Sayan Mukherjee, Benjamin L. Ebert, Michael A. Gillette, Amanda Paulovich, et al. 2005. "Gene Set Enrichment Analysis: A Knowledge-Based Approach for Interpreting Genome-Wide Expression Profiles." *Proceedings of the National Academy of Sciences of the United States of America* 102 (43): 15545–50. <https://doi.org/10.1073/pnas.0506580102>.
- Suzuki, Akira, Manae Tsukio Yamaguchi, Toshiaki Ohteki, Takehiko Sasaki, Tsuneyasu Kaisho, Yuki Kimura, Ritsuko Yoshida, Andrew Wakeham, Tetsuya Higuchi, and Manabu Fukumoto. 2001. "T Cell-Specific Loss of Pten Leads to Defects in Central and Peripheral Tolerance Fied in Many Human Sporadic Cancers and in Hereditary Disorders Such as Cowden Disease and Bannayan- Riley-Ruvalcaba Syndrome, Which Are Characterized by Multiple Hamartomas." *Immunity* 14: 523–34.
- Switlyk, Marta D, Unn Beate Salberg, Oliver M Geier, Ljiljana Vlatkovic, Wolfgang Lilleby, Heidi Lyng, and Therese Seierstad. 2019. "PTEN Expression in Prostate Cancer: Relationship With Clinicopathologic Features and Multiparametric MRI Findings." *American Journal of Roentgenology* 212 (6): 1206–14. <https://doi.org/10.2214/AJR.18.20743>.
- Szabowski, Axel, Nicole Maas-Szabowski, Sven Andrecht, Andrea Kolbus, Marina Schorpp-Kistner, Norbert E. Fusenig, and Peter Angel. 2000. "C-Jun and JunB Antagonistically Control Cytokine-Regulated Mesenchymal-Epidermal Interaction in Skin." *Cell* 103 (5): 745–55. [https://doi.org/10.1016/S0092-8674\(00\)00178-1](https://doi.org/10.1016/S0092-8674(00)00178-1).
- Takayama, Hitoshi, Tetsuya Takakuwa, Yuichi Tsujimoto, Yoichi Tani, Norio Nonomura, Akihiko Okuyama, Shigekazu Nagata, and Katsuyuki Aozasa. 2002. "Frequent Fas Gene Mutations in Testicular Germ Cell Tumors." *American Journal of Pathology* 161 (2): 635–41. [https://doi.org/10.1016/S0002-9440\(10\)64219-8](https://doi.org/10.1016/S0002-9440(10)64219-8).
- Tan, Mh Eileen, Jun Li, H. Eric Xu, Karsten Melcher, and Eu Leong Yong. 2015. "Androgen Receptor: Structure, Role in Prostate Cancer and Drug Discovery." *Acta Pharmacologica Sinica* 36 (1): 3–23. <https://doi.org/10.1038/aps.2014.18>.

- Tannenbaum, Jerrold, and B. Taylor Bennett. 2015. "Russell and Burch's 3Rs Then and Now: The Need for Clarity in Definition and Purpose." *Journal of the American Association for Laboratory Animal Science* 54 (2): 120–32.
- Taylor, Barry S, Nikolaus Schultz, Haley Hieronymus, Anuradha Gopalan, Yonghong Xiao, Brett S Carver, Vivek K Arora, et al. 2010. "Integrative Genomic Profiling of Human Prostate Cancer." *Cancer Cell* 18 (1): 11–22. <https://doi.org/10.1016/j.ccr.2010.05.026>.
- . 2011. "Integrative Genomic Profiling of Human Prostate Cancer" 18 (1): 11–22. <https://doi.org/10.1016/j.ccr.2010.05.026>. Integrative.
- Thomsen, M. K., L. Bakiri, S. C. Hasenfuss, H. Wu, M. Morente, and E. F. Wagner. 2015. "Loss of JUNB/AP-1 Promotes Invasive Prostate Cancer." *Cell Death and Differentiation* 22 (4): 574–82. <https://doi.org/10.1038/cdd.2014.213>.
- Tournier, Cathy. 2013. "The 2 Faces of JNK Signaling in Cancer." *Genes and Cancer* 4 (9–10): 397–400. <https://doi.org/10.1177/1947601913486349>.
- Untergasser, Andreas, Ioana Cutcutache, Triinu Koressaar, Jian Ye, Brant C Faircloth, Maido Remm, and Steven G Rozen. 2012. "Primer3--New Capabilities and Interfaces." *Nucleic Acids Research* 40 (15): e115–e115. <https://doi.org/10.1093/nar/gks596>.
- Vermeulen, Katrien, Dirk R. Van Bockstaele, and Zwi N. Berneman. 2003. "The Cell Cycle: A Review of Regulation, Deregulation and Therapeutic Targets in Cancer." *Cell Proliferation* 36 (3): 131–49. <https://doi.org/10.1046/j.1365-2184.2003.00266.x>.
- Vinall, Ruth L., Jane Q. Chen, Neil E. Hubbard, Shola S. Sulaimon, Michael M. Shen, Ralph W. DeVere White, and Alexander D. Borowsky. 2012. "Initiation of Prostate Cancer in Mice by Tp53R270H: Evidence for an Alternative Molecular Progression." *DMM Disease Models and Mechanisms* 5 (6): 914–20. <https://doi.org/10.1242/dmm.008995>.
- Vindrieux, David, Pauline Escobar, and Gwendal Lazennec. 2009. "Emerging Roles of Chemokines in Prostate Cancer." *Endocrine-Related Cancer* 16 (3): 663–73. <https://doi.org/10.1677/ERC-09-0109>.
- Vleugel, Marije M, Astrid E Greijer, Reinhard Bos, Elsken van der Wall, and Paul J van Diest. 2006. "C-Jun Activation Is Associated with Proliferation and Angiogenesis in Invasive Breast Cancer." *Human Pathology* 37 (6): 668–74. <https://doi.org/https://doi.org/10.1016/j.humpath.2006.01.022>.
- Vogt, P. K. 2001. "Jun, the Oncoprotein." *Oncogene* 20 (19 REV. ISS. 2): 2365–77. <https://doi.org/10.1038/sj.onc.1204443>.
- Wada, Teiji, Nicholas Joza, Hai-ying M Cheng, Takehiko Sasaki, Ivona Kozieradzki, Kurt Bachmaier, Toshiaki Katada, et al. 2004. "MKK7 Couples Stress Signalling to G2/M Cell-Cycle Progression and Cellular Senescence." *Nature Cell Biology* 6 (3): 215–26. <https://doi.org/10.1038/ncb1098>.
- Wang, Jianhua, Jincheng Wang, Yanxi Sun, Wenying Song, Jacques E Nor, Cun Yu Wang, and Russell S Taichman. 2005. "Diverse Signaling Pathways through the SDF-1/CXCR4 Chemokine Axis in Prostate Cancer Cell Lines Leads to Altered Patterns of Cytokine Secretion and Angiogenesis." *Cellular Signalling* 17 (12): 1578–92. <https://doi.org/https://doi.org/10.1016/j.cellsig.2005.03.022>.
- Wang, Shunyou, Jing Gao, Qunying Lei, Nora Rozengurt, Colin Pritchard, Jing Jiao, George V. Thomas, et al. 2003. "Prostate-Specific Deletion of the Murine Pten Tumor Suppressor Gene Leads to Metastatic Prostate Cancer." *Cancer Cell* 4 (3): 209–21. [https://doi.org/10.1016/S1535-6108\(03\)00215-0](https://doi.org/10.1016/S1535-6108(03)00215-0).
- Wisdom, Ron, Randall S. Johnson, and Connie Moore. 1999. "C-Jun Regulates Cell Cycle Progression and Apoptosis by Distinct Mechanisms." *EMBO Journal* 18 (1): 188–97. <https://doi.org/10.1093/emboj/18.1.188>.
- Wong, Martin C.S., William B. Goggins, Harry H.X. Wang, Franklin D.H. Fung, Colette Leung, Samuel Y.S. Wong, Chi Fai Ng, and Joseph J.Y. Sung. 2016. "Global Incidence and Mortality for Prostate Cancer: Analysis of Temporal Patterns and Trends in 36 Countries." *European Urology* 70 (5): 862–74. <https://doi.org/10.1016/j.eururo.2016.05.043>.
- Wu, Xiantuo, Jian Wu, Jiapeng Huang, William C. Powell, Jian Feng Zhang, Robert J. Matusik, Frank O. Sangiorgi, Robert E. Maxson, Henry M. Sucov, and Pradip Roy-Burman. 2001. "Generation of a Prostate Epithelial Cell-Specific Cre Transgenic Mouse Model for Tissue-Specific Gene Ablation." *Mechanisms of Development* 101 (1–2): 61–69.

[https://doi.org/10.1016/S0925-4773\(00\)00551-7](https://doi.org/10.1016/S0925-4773(00)00551-7).

- Wu, Xinyu, Shiaoqing Gong, Pradip Roy-Burman, Peng Lee, and Zoran Culig. 2013. "Current Mouse and Cell Models in Prostate Cancer Research." *Endocrine-Related Cancer* 20 (4): 1–26. <https://doi.org/10.1530/ERC-12-0285>.
- Xu, Ruiyuan, and Jieping Hu. 2020. "The Role of JNK in Prostate Cancer Progression and Therapeutic Strategies." *Biomedicine and Pharmacotherapy* 121 (July 2019): 109679. <https://doi.org/10.1016/j.biopha.2019.109679>.
- Yatani, R, I Kusano, T Shiraishi, T Hayashi, and G N Stemmermann. 1989. "Latent Prostatic Carcinoma: Pathological and Epidemiological Aspects." *Japanese Journal of Clinical Oncology* 19 (4): 319–326. <http://europepmc.org/abstract/MED/2691730>.
- Yevshin, Ivan, Ruslan Sharipov, Semyon Kolmykov, Yury Kondrakhin, and Fedor Kolpakov. 2019. "GTRD: A Database on Gene Transcription Regulation - 2019 Update." *Nucleic Acids Research* 47 (D1): D100–105. <https://doi.org/10.1093/nar/gky1128>.
- Zeke, András, Mariya Misheva, Attila Reményi, and Marie A. Bogoyevitch. 2016. "JNK Signaling: Regulation and Functions Based on Complex Protein-Protein Partnerships." *Microbiology and Molecular Biology Reviews* 80 (3): 793–835. <https://doi.org/10.1128/membr.00043-14>.
- Zhao, Chunyan, Yichun Qiao, Philip Jonsson, Jian Wang, Li Xu, and Pegah Rouhi. 2014. *Genome-Wide Profiling of AP-1 Regulated Transcription Provides Insights into the Invasiveness of Triple-Negative Breast Cancer*. <https://doi.org/10.1158/0008-5472.CAN-13-3396>.
- Zhao, Hua Fu, Jing Wang, and Shing Shun Tony To. 2015. "The Phosphatidylinositol 3-Kinase/Akt and c-Jun N-Terminal Kinase Signaling in Cancer: Alliance or Contradiction? (Review)." *International Journal of Oncology* 47 (2): 429–36. <https://doi.org/10.3892/ijo.2015.3052>.
- Zimmermann, K. C., and D. R. Green. 2001. "How Cells Die: Apoptosis Pathways." *Journal of Allergy and Clinical Immunology* 108 (4 SUPPL.): 0–4. <https://doi.org/10.1067/mai.2001.117819>.